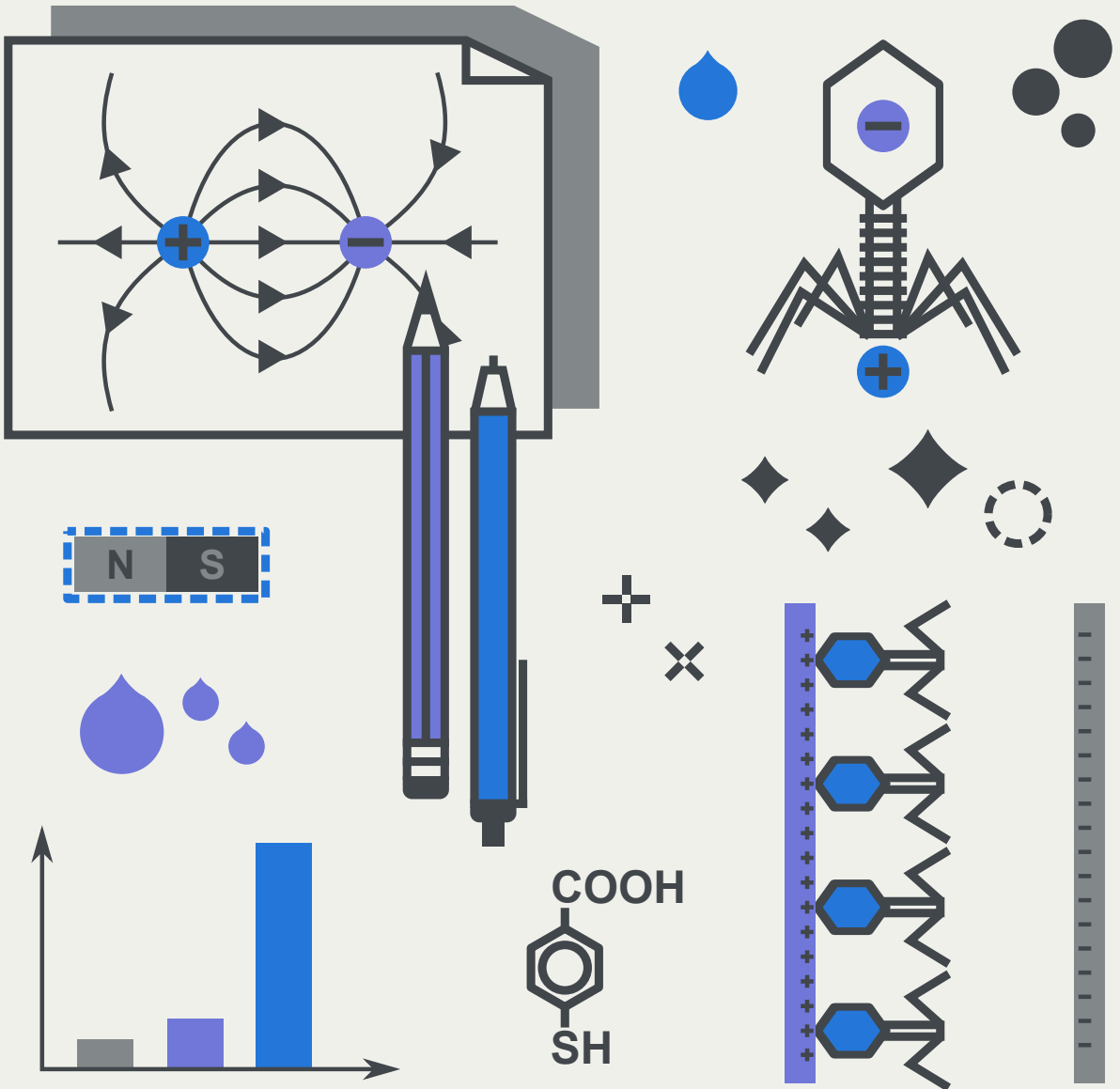


PhD Thesis

APPLICATION OF THE ELECTRIC AND MAGNETIC FIELDS IN SENSORS AND BIOSENSORS



Łukasz Richter

<http://rcin.org.pl>



Application of the electric and magnetic fields in sensors and biosensors

Łukasz Richter

Advisor: prof. dr hab. Robert Hołyst

Auxiliary advisor: dr Jan Paczesny

The dissertation was prepared within
the International Doctoral Studies at the

Institute of Physical Chemistry of the Polish Academy of Sciences

Kasprzaka 44/52, 01-224 Warsaw

A - 21 - 7
A - 21 - 3
K - 8 - 160

K - 8 - 161
K - 8 - 185
K - 8 - 216
H - 68

Biblioteka Instytutu Chemii Fizycznej PAN

F-B.510/19



50000000202584

Warsaw, June 2019

<http://rcin.org.pl>



B. 510/19

Acknowledgements

Moim Rodzicom, za to że nieustannie odkrywali przede mną nowe horyzonty, krzewili ciekawość i umożliwiali poznawanie świata.

Prof. Robert Holyst, for sharing his wide knowledge, spreading the unstoppable joy of science and having always open doors. As they say, *my success is his success*.

Dr Jan Paczesny, for being a Friend and a Mentor, teaching me with great patience, and hundreds of hours of discussions not only about science.

Kinga Matuła and Krzysztof Bielec, for their invaluable help during long hours spent together in the biolab.

I gracefully acknowledge all my other co-workers who were involved in the work described herein: **prof. Marcin Łoś, prof. Carlos Drummond, Monika Księżopolska-Gocalska, Pawel Albrycht, dr Krzysztof Sozański, dr Tomasz Kalwarczyk, dr Marcin Hołdyński, dr Witold Adamkiewicz, prof. Jerzy Kawiak, dr Grażyna Hoser, dr hab. Ewa Poboży, dr Adam Leśniewski, dr Robert Bachliński, dr Volodymyr Sashuk**.

All members of Team 10, for amazing atmosphere and making time of my PhD studies really joyful and great period in my life.

Last, but not the least, **my beloved Wife**, for her love, patience and constant support, even in the darkest hour.

This work was supported by
the National Science Centre

within the Preludium Grant 2017/27/N/ST4/02353

and within the Sonata Grant 2012/07/D/ST5/02240



NATIONAL SCIENCE CENTRE
POLAND

Table of contents

Acknowledgements	III
Table of contents	V
List of abbreviations	VIII
Abstract	X
Streszczenie	XI
CHAPTER 1 General introduction	1
1.1. Electrokinetics	2
1.1.1. The classic theory of the electrical double layer	2
1.1.2. Electrokinetic phenomena	4
1.2. Manipulation of matter by the electric field	7
1.2.1. AC electrokinetics in biodetection	8
1.2.2. Electrophoretic deposition.....	10
1.3. Aim of the research and outline of this thesis.....	14
1.4. References.....	16
CHAPTER 2 Fluctuations of ions in the alternating electric field	21
2.1. Introduction.....	22
2.1.1. Surface forces apparatus.....	24
2.2. Results and discussion	25
2.2.1. Effect of repulsion between oppositely charged surfaces	25
2.2.2. Selected compounds	26
2.2.3. Influence of applied voltage	27
2.2.4. Influence of mobilities of ions.....	28
2.2.5. Influence of concentration of ions.....	29
2.2.6. Influence of distance between electrodes	31
2.2.7. Influence of frequency of applied alternating voltage.....	33
2.2.8. Time scales of the observed effect	34
2.2.9. Long-time measurements	35
2.2.10. Proposed explanation of the observed phenomenon	36
2.3. Conclusions.....	37
2.4. Materials and methods.....	37
2.4.1. Materials.....	37
2.4.2. Surface forces apparatus.....	38
2.4.3. Calculation of the force	38
2.4.4. Calculation of typically reported time scales	39
2.4.5. Calculation of diffusion of water in the studied system	40

2.5. References.....	42
CHAPTER 3 Deposition of the analytes in the electric field for SERS technique	45
3.1. Introduction.....	46
3.1.1. Surface-enhanced Raman spectroscopy	46
3.2. Results and discussion	50
3.2.1. Process of deposition of analytes in the electric field	50
3.2.2. Time of deposition.....	53
3.2.3. Influence of applied voltage	53
3.2.4. Influence of the electric field on homogeneity of results	54
3.2.5. Influence of frequency of applied voltage.....	55
3.2.6. Deposition of various analytes	56
3.2.7. Electrophoretic mobility of deposited compounds.....	61
3.2.8. Influence of polarization of the applied voltage	62
3.2.9. Confocal microscopy analysis of deposited ATTO-647N	63
3.3. Conclusions.....	63
3.4. Materials and methods.....	64
3.4.1. Materials.....	64
3.4.2. Deposition of analytes in the electric field.....	66
3.4.3. SERS measurement	66
3.4.4. Measurement of electrophoretic mobility	66
3.4.5. Additional instrumentation.....	68
3.5. References.....	69
CHAPTER 4 Layers of phages ordered in the electric field for bacteria detection	73
4.1. Introduction.....	74
4.2. Results and discussion	79
4.2.1. Preparation of the deposition cell.....	79
4.2.2. Deposition of phages in the constant electric field.....	81
4.2.3. Deposition of phages in the alternating applied voltage.....	84
4.2.4. Preparation of the phage-based layers by combining chemical modification and the alternating electric field.....	87
4.3. Conclusions.....	93
4.4. Materials and methods.....	93
4.4.1. Materials.....	93
4.4.2. Phage preparation and bacteria culturing	94
4.4.3. Setup for deposition of phages in the electric field	95
4.4.4. Solid substrates for sensing layers.....	95
4.4.5. Modifications with DTSP or with cysteamine and glutaraldehyde.....	96
4.4.6. Protocol for preparation of biosensors	96

4.4.7.	Analysis of number of deposited phages and phage deactivation	96
4.4.8.	Protocol for analysis of sensitivity of studied biosensors.....	97
4.4.9.	Calculations of time constant τ in the system.....	97
4.4.10.	Additional instrumentation.....	99
4.5.	References.....	100
CHAPTER 5	Magnetic-fluorescent bacteriophage-based bioconjugates	
	for bacteria detection	105
5.1.	Introduction.....	106
5.2.	Results and discussion	108
5.2.1.	Preparation and characterization of phage-based bioconjugates	108
5.2.2.	Analysis of capture efficiency of prepared bioconjugates.....	112
5.2.3.	Detection of bacteria <i>E. coli</i> with phage-based bioconjugates	113
5.3.	Conclusions.....	115
5.4.	Materials and methods.....	116
5.4.1.	Materials.....	116
5.4.2.	Phage preparation and bacteria culturing	116
5.4.3.	Determination of number of active phages and bacteria	117
5.4.4.	Preparation of fluorescently labeled phages and bacteria	117
5.4.5.	Preparation of phage-based bioconjugates	117
5.4.6.	Efficiency of bacteria capture.....	118
5.4.7.	Flow cytometry.....	118
5.4.8.	Additional instrumentation.....	118
5.5.	References.....	119
CHAPTER 6	Conclusions and future perspectives	121
6.1.	Summary.....	122
6.2.	Future perspectives	123
6.3.	References.....	126

List of abbreviations

AC EPD	alternating current electrophoretic deposition
ACEK	alternating current electric field induced electrokinetics
ACEO	alternating current electroosmosis
ACEOF	alternating current electroosmotic flow
ACETF	alternating current electrothermal flow
AFM	atomic force microscopy
CA	cysteamine
CE	capture efficiency
CFU	colony forming unit
DC EPD	direct current electrophoretic deposition
DCEO	direct current electroosmosis
DEP	dielectrophoresis
DMSO	dimethyl sulfoxide
DTSP	dithiobis(succinimidyl propionate)
EDC	1-ethyl-3-(3-dimethylaminopropyl)carbodiimide
EDL	electrical double layer
EDTA	ethylenediaminetetraacetic acid
EOF	electroosmotic flow
EPD	electrophoretic deposition
FECO	fringes of equal chromatic order
GA	glutaraldehyde
GFP	green fluorescence protein
IgG	immunoglobulin G
IHP	inner Helmholtz plane
IPTG	isopropyl β -D-1-thiogalactopyranoside
ITO	indium tin oxide
LB	lysogeny broth

LOD	limit of detection
MALDI-MS	matrix-assisted laser desorption/ionization mass spectrometry
MBI	multiple beam interferometry
OHP	outer Helmholtz plane
PCR	polymerase chain reaction
PDC	pulse-direct current electrophoresis deposition
PFU	plaque forming unit
PMBA	para-mercaptobenzoic acid
PTFE	polytetrafluoroethylene
RBP	receptor binding protein
SEM	scanning electron microscopy
SERS	surface-enhanced Raman spectroscopy
SFA	surface forces apparatus
SP	slip plane or shear plane
TH-PVP	3',4'-tetramethylene- α -pyrrolidinovalerophenone
TRIS	tris(hydroxymethyl)aminomethane
α -PVT	α -pyrrolidinopentiothiophenone

Abstract

For over two centuries electric and magnetic fields remain among the most important effects used for controlled movement of objects, molecules and ions. Their utilization revolutionized myriads of branches of science and industry and technologies based on them are commonly used in various aspects of our everyday life. Main goal of this thesis is to make a contribution in this field and create important solutions that aid various sensing and biosensing technologies. Presented research concerns three practical applications complemented with basic research of unusual electrokinetic phenomena.

First part of my thesis consists of basic research focused on analysis of interaction upon application of alternating electric field. As a result, novel electrokinetic phenomenon of non-trivial characteristics was analyzed. Namely, long-range repulsion between oppositely charged surface was described. Created system was in fact a capacitor filled with electrolyte consisting of ions of unequal mobilities. Strength, range and time scale of the observed effect exceeded all previously reported electrokinetic phenomena.

Next part is focused on utilization of the electric field for improvement of various detection methods. First improved technology was surface enhanced Raman spectroscopy (SERS). Application of the alternating electric field allowed for deposition of wide range of tested analytes, from small organic molecules, through dyes and drugs, to biomolecules, such as DNA and proteins, on SERS substrates. Moreover, practical dependency between electrophoretic mobilities of deposited analytes and frequency of applied voltage was described.

Second application of the electric field concerned phage-based method of bacteria detection. Layers of phages oriented in the electric fields were utilized for fast and sensitive detection of bacteria. Proper orientation of bacteriophages allowed to overcome the problem of sterical hindrances of virions. Combination of developed solution with chemical modification of the surface allowed for creation of densely packed layers of properly ordered phages. This resulted in 64-fold increase of sensitivity of prepared sensing layers. Detection step took only 15 min and obtained limit of detection was less than 100 CFU/ml.

As the last part of performed research I used magnetic field for improvement of another phage-based method for bacteria detection. Bioconjugates prepared for this purpose were composed of sub-micron fluorescent-magnetic particles covered with bacteriophages. For preparation of bioconjugates only simple and accessible components were used. Moreover, created detection technology was based on flow cytometer – equipment common in hospitals and diagnostic laboratories. All of this resulted in technology that can be easily adapted and implemented, not only in highly-equipped research facilities.

Finally, I summarized all described achievements and proposed paths of further development of designed technologies and described effects.

Streszczenie

Od ponad dwóch stuleci oddziaływania elektryczne i magnetyczne stanowią jedne z najważniejszych metod wykorzystywanych do precyzyjnego manipulowania obiektami, molekułami i jonami. Ich wykorzystanie zrewolucjonizowało wiele dziedzin nie tylko nauki, ale również przemysłu. Rozwiązania oparte o pola magnetyczne i elektryczne stanowią obecnie istotną część naszego codziennego życia. Głównym celem badań opisanych w niniejszej pracy było stworzenie technologii, których wykorzystanie przyczyni się do dalszego rozwój tej dziedziny i usprawni metody wykorzystywane w detekcji.

Pierwsza część mojej pracy doktorskiej stanowi opis badań podstawowych skupionych na analizie oddziaływań pod wpływem zmiennego pola elektrycznego. W efekcie zostało zaobserwowane nowe zjawisko elektrokinetyczne dalekozasięgowego odpychania pomiędzy dwoma przeciwnie naładowanymi okładkami kondensatora. Kondensator wypełniony był elektrolitem zawierającym jony o różnych ruchliwościach elektroforetycznych. Siła, zasięg oraz skala czasowa analizowanych oddziaływań przekraczały zakresy wszystkich opisanych wcześniej zjawisk elektrokinetycznych.

Kolejny fragment niniejszej pracy opisuje wykorzystanie pola elektrycznego do usprawniania różnych metod detekcji. Pierwszą ulepszoną techniką była powierzchniowo wzmacniana spektroskopia Ramana. Zastosowanie zmiennego pola elektrycznego pozwoliło na osadzenie na podłożach metalicznych wielu różnych analitów, od małych cząstek organicznych, przez dopalacze, aż po duże biomolekuły, takie jak DNA czy białka. Dodatkowo, określona została zależność pomiędzy efektywną częstotliwością napięcia, a ruchliwością elektroforetyczną osadzanego związku chemicznego.

Drugi przykład wykorzystania pól elektrycznych dotyczy metody detekcji bakterii opartej o bakteriofagi. Przedstawiona tam technologia tworzenia warstw bakteriofagów zorientowanych w polu elektrycznym została wykorzystana do szybkiego i czułego wykrywania bakterii. Odpowiednia orientacja fagów na powierzchni czujnika umożliwiła wyeliminowanie problemu przestrzennego blokowania wirionów. W kolejnym etapie metoda ta została połączona z chemiczną modyfikacją powierzchni. Czułość tak przygotowanej gęstej warstwy odpowiednio ułożonych bakteriofagów wzrosła 64-krotnie. Wyłapywanie bakterii trwało 15 min, a osiągnięty limit detekcji wynosił 100 jtk/ml.

Ostatnia część również zawiera opis usprawnienia metod detekcji bakterii, lecz tym razem wykorzystane zostało w tym celu pole magnetyczne. Stworzone biokoniugaty składały się z fluorescencyjno-magnetycznych cząstek opłaszczonych bakteriofagami. Biokoniugaty przygotowano z tanich i łatwo dostępnych elementów, a wybrana metoda detekcji – cytometria przepływowa, jest powszechnie stosowana w szpitalach i laboratoriach diagnostycznych. Wszystkie te czynniki sprawiły, że opracowane rozwiązanie może być szeroko stosowane nie tylko w dobrze wyposażonych placówkach naukowych.

Ostatni rozdział stanowi podsumowanie wszystkich osiągnięć wraz ze spisem proponowanych oraz podjętych kierunków dalszego rozwoju opracowanych technologii i opisanych zjawisk.

Chapter 1

General introduction

1.1. Electrokinetics

The electric field is an intrinsic component of our world, that governs myriad of physical, chemical and even biological processes. Its omnipotent influence on almost every aspect of our lives cannot be overestimated. Over last two centuries, since discovery of movement of clay particles in the electric field made by Reuss in 1809 [1], we have been learning how to exploit the electric field to control movement of matter and develop ever newer technological advances. The field of science that was established that day in 1809 is called electrokinetics.

Electrokinetics includes wide range of contact-free techniques that allow to convert electrical energy into kinetic energy of particles or molecules suspended in fluids. For over a century it had been the foundation of many fundamental advances in colloid science. Currently, the electrokinetics is an independent branch of science that manifests its importance in spectacular applications in analysis of surface properties, separations, manipulation in colloidal materials, and movement of fluid in microchannels. For example, most common technique to separate biological molecules, such as proteins or nucleic acids, is electrophoresis [2]. Phenomena such as streaming potential [3] or electrophoretic mobility [4] are very important aspect of characterization of particles or surfaces in wide range of industrial applications. Water filtration and purification is almost exclusively connected with the idea of reverse osmosis [5]. All above examples are just a tip of the iceberg of diverse applications of electrokinetic manipulation of matter. Also theoretical understanding underlying electrokinetics has undergone remarkable improvement over a last century. Currently obtained knowledge creates rather complete and unified picture of electrokinetic phenomena. However, there are areas that are believed to be incomplete and sometimes even inaccurate.

1.1.1. The classic theory of the electrical double layer

If a solid surface is in contact with the electrolyte solution, it gains the surface charge [6]. This might be due to several effects. Among them, the most common are: selective adsorption of ions on the surface, ionization or disassociation of surface chemical groups, isomorphic substitution (replacement of one atom by another of similar size in a crystal lattice) and adsorption-desorption of lattice ions.

Nature always strives to maintain electroneutrality of given system. Thus, a layer of counterions, called the electrical double layer (EDL) has to be created on such surfaces to counterbalance the surface charge. Despite traditionally called “double”, such layer can be more complex and typically it consists of three or four layers of ions. Figure 1.1 schematically shows generally agreed model of the electrical double layer. In the presented case, the surface is positively charged and layer of anions (dark blue) in the solution specifically adsorbs directly onto the surface. This effect is caused mainly by chemical

affinity of ionic species to the surface and not by typical Coulombic interactions [6], [7]. Such model is known as Gouy-Chapman-Stern model. It consists of following regions:

- 1) The inner Helmholtz plane (IHP) consists of layer of ions adsorbed on the surface due to chemical affinity.
- 2) The outer Helmholtz plane (OHP) is composed of solvated counterions at their position of closest approach.
- 3) Stern layer spreads between solid surface and OHP. This layer of ions is often referred as compact part of the electrical double layer.
- 4) Region outside OHP is diffusive part of the electrical double layer. Concentration of ions in this region decreases continuously and eventually reaches the concentration of ions in the bulk solution.
- 5) Slip plane (or shear plane, SP) is located in diffusive part of the electrical double layer, in close proximity to OHP. Its potential, called zeta potential (ζ), is often considered as effective potential in interactions with other charged objects, is potential between this plane and bulk solution. In general, the outer Helmholtz plane and slip plane are not collocated. However, in many cases is it convenient to approximate that they are the same plane and in such case potential of slip plane (Ψ_d) equals ζ .

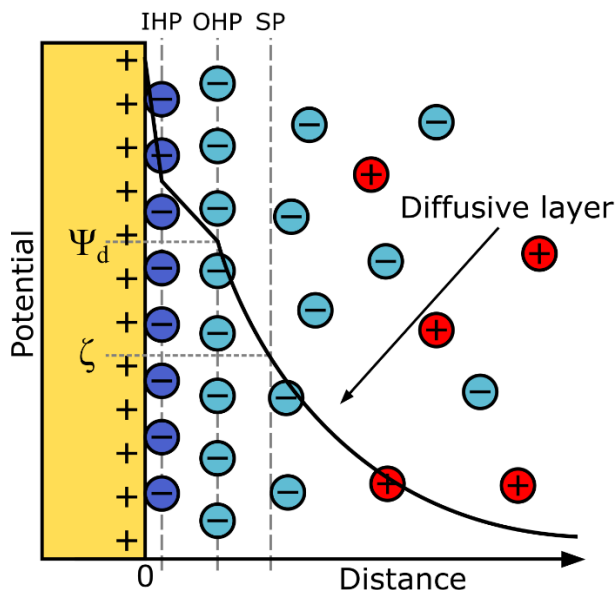


Figure 1.1 Schematic representation of commonly accepted Gouy-Chapman-Stern model of the electrical double layer (EDL) composed of Stern (compact) and Gouy-Chapman (diffusive) layers of counterions.

In practice, two charged objects in electrolyte solution can interact electrostatically only if their electrical double layers overlap. When the distance is larger the surface charges of both objects are completely screened and objects act as neutral for each other. Thus,

important parameter is thickness of the electrical double layers, which is called Debye length. Debye length (denoted as λ_D or κ^{-1}) is a measure how far the electrostatic effect of charged surface or object persist in solution and can be formulated as:

$$\lambda_D = \kappa^{-1} = \sqrt{\frac{\varepsilon_0 \varepsilon_r k_B T}{\sum_{i=1}^N e^2 z_i^2 n_i^0(\infty)}} \quad (1.1)$$

where ε_0 is vacuum permittivity, ε_r is relative permittivity of solution, k_B is Boltzmann constant, T is temperature, e is elementary charge, z_i is charge of a given ion, and $n_i^0(\infty)$ is concentration of given ions in bulk solution.

Second important aspect are dynamics of the electrolyte solution. Time-dependent effects of the electrolyte upon applied or induced electric potential have been exploited in such applications as desalination [8], manipulation of biological [9] and colloidal particles [10] and microfluidics [11]. Many characteristic screening time scales of formation of the electric double layer were reported in the literature [10]. In some cases $\tau = \lambda_D^2/D$ is reported as leading order time scale, where τ is time scale, λ_D is Debye length, and D is diffusion coefficient of ions [12]. In other cases response time of $\lambda_D L/D$ (where L is half of the distance separating electrodes) is considered [13]. The picture become even more complicated if nonlinearity is taken into account and additional time scales, such as L^2/D can significantly contribute in the process. On top of that, many different parameters influence the time of formation of EDLs, such as concentration of ions, type of solvent, presence of Faradaic currents, isolations on electrodes, geometry and dimensions of designed system [14].

1.1.2. Electrokinetic phenomena

Generally speaking, electrokinetics phenomena are the effect of interaction between the external electric field and the electrical double layers [15]. Due to complex nature of such interaction, many various types of electrokinetic phenomena can be distinguished. Most commonly used are schematically represented in Figure 1.2. In classical electrokinetics, the surface charges are determined only by the properties of charged object and surrounding solution. Therefore, surface charge for a given pair of surface and electrolyte is constant and independent from the applied electric field.

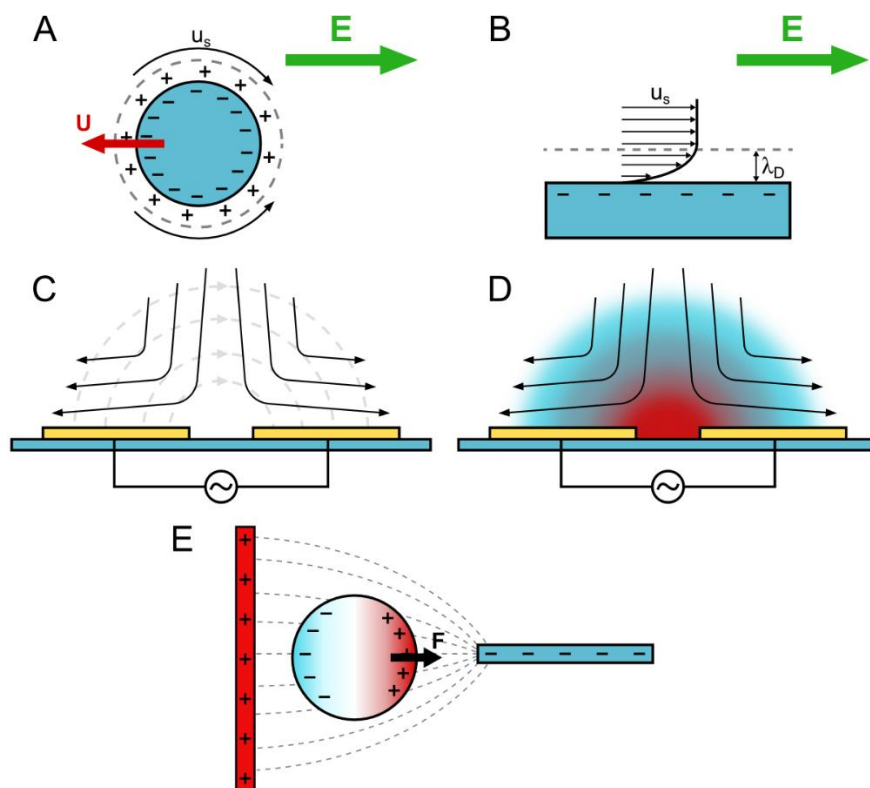


Figure 1.2 Scheme depicting various electrokinetic phenomena. (A) Electrophoresis is movement of charged object in the external electric field due to oppositely directed slip velocity of diffusive part of electrical double layer; (B) Electroosmosis is movement of diffusive part of the electrical double layer on solid surface in applied electric field; (C) AC electroosmosis of fluid above coplanar electrodes is generated by application of alternating voltage. Black arrows indicate direction of fluid movement; (D) AC electrothermal effect is obtained by Joule heating. Joule heating results in the gradient of temperature and subsequent flow indicated by arrows; (E) Dielectrophoresis is movement of polarizable object in gradient of the electric field. Movement towards or away from the highest electric field is dependent on difference between polarizabilities of particle and surrounding fluid.

Electrophoresis

When a particle is immersed in the electrolyte solution, it gains the given surface charge q . Then, due to electrostatic and chemical interactions, counterions are attracted and create the electrical double layer (EDL) that continuously screens the surface charges. This results in effective drop of the potential across the EDL and determine the effective potential of such particle, called zeta potential. If the external electric field is applied in such system, it cannot affect the particle directly, as its surface charges are counterbalanced by the electrical double layer. Instead, the electric field exerts the force on the diffusive part of the electrical double layer and drives the ions and fluid in motion according to the charges creating the EDL (Figure 1.2A). Velocity of such movement of ions in diffusive part of electric double layer is called slip velocity [13]. In case of particles freely suspended in electrolyte solution, slip velocity give a rise to movement of the particle in the direction opposite to the slip velocity.

This phenomenon is known as the electrophoresis. If the Debye length is small enough, electrophoretic velocity of particle U is described by the Smoluchowski equation:

$$U = \frac{\varepsilon_0 \varepsilon_r \zeta}{\eta} E_0 = \mu_{EP} E_0 \quad (1.2)$$

where ε_0 is vacuum permittivity, ε_r is relative permittivity of solution, ζ is zeta potential of the particle, E_0 is the strength of the electric field and η is the viscosity of the electrolyte. Parameter μ_{EP} is known as electrophoretic mobility of the particle. There is comprehensive literature describing both detailed theoretical analysis and many practical applications of this effect [16], [17]. Some of them will be discussed in details further in this chapter and later in chapter 3 of this thesis.

Electroosmosis

Another interesting case is application of the electric field tangential to the charged solid wall. Similarly as in case of the particle, the diffusive part of electrical double layer is driven in motion. This velocity is then transferred by viscous coupling to the bulk liquid near the EDL (Figure 1.2B). At the steady state the velocity of the moving liquid stabilizes. This velocity (denoted as u) of electroosmotic slip of the outer part of the electrical double layer is given by Helmholtz-Smoluchowski equation:

$$u = -\frac{\varepsilon_0 \varepsilon_r \zeta}{\eta} E_0 \quad (1.3)$$

where all symbols are as in the Equation 1.2.

Direct current electroosmosis (DCEO) was proven to be useful in numerous applications, especially in microfluidics, where velocity generated by the electroosmotic flow is independent from the size of the channels [15]. This is in stark difference from typically applied pressure-driven flow, where velocity strongly depends on the sizes of the channels. However, electroosmosis has also a few disadvantages, such as bubbles formation, electrochemical and electrolysis reactions on both electrodes and creation of gradient of pH [18], [19]. As an improvement, alternating current electroosmosis (ACEO), which is sometimes called also AC electroosmotic flow (ACEOF), was proposed [20].

ACEO is a steady flow of a fluid above electrodes generated by the alternating electric field (Figure 1.2C). Direction of movement of the electrolyte originates in interactions between the tangential generated electric field and the charge at the diffusive part of the electrical double layer [21]. The fluid flows on the surface of the electrodes to their opposite ends, irrespective of the polarity. As thickness of the electric double layer decreases with increasing concentration of ions in the solution (Equation 1.1), the effective ACEO requires utilization of solutions of relatively low conductivity ($\sigma < 8.4 \cdot 10^{-2}$ S/m) and low frequencies ($f < 100$ kHz) [22]. ACEO was proven to be effective in fluid manipulation in cases of both single electrode and many various arrays of electrodes as it will be shown later in this chapter.

AC electrothermal effect

Very similar to previously described ACEO is the phenomenon called AC electrothermal flow (ACETF). Also in this case application of non-uniform alternating electric field between two planar electrodes generates steady flow of fluid (Figure 1.2D). However, in ACETF highly conductive electrolyte has to be utilized and high frequencies have to be applied. In such case, Joule heating becomes more efficient than electroosmosis. Ions in the solution are accelerated but their kinetic energy is released as heat by the collision with surrounding molecules and ions. Uneven electric field results in uneven Joule heating of the electrolyte, which cause nonuniformities in conductivity and permittivity of the fluid [23]. Observed electrothermal flow is the effect of interaction between these inhomogeneities and the AC electric field. Interestingly, Joule heating can be generated by both application of the electric field [24] and usage of external heat source [25]. Similar to previously described phenomena, also ACETF was proven to be effective in fluid pumping and mixing in number of practical applications [26].

Dielectrophoresis

Dielectrophoretic (DEP) effect is generated when the polarizable object suspended in a fluid is subjected to the nonuniform electric field (Figure 1.2E). Such field can be generated by application of DC or AC voltage. The particle of higher polarizability than surrounding media is dragged towards higher electric fields. Such effect is called positive dielectrophoresis. Negative dielectrophoresis is when object has lower polarizability and it is pushed away into lower electric fields. Direction and force of DEP is not dependent on polarization of the electric field. The only important parameter is its gradient. DEP is broadly used in frequency dependent manipulation of cells, as their effective polarization is determined by their cellular structures and electrical properties [27]. Moreover, different modes, such as traveling-wave or electrorotation can be created by DEP, depending on the phase shift generated at the electrodes [28].

All above-mentioned effects do not exhaust the list of possible electrokinetic phenomena. However, the rest of them (such as recently mentioned electrorotation, traveling-wave dielectrophoresis or induced-charge electroosmosis) are modifications or variations of the basic phenomena described in this chapter.

1.2. Manipulation of matter by the electric field

The electrokinetic phenomena were found useful in numerous applications. Many research areas, such as colloidal materials [16], dynamic assembly and self-assembly processes [29], analytical chemistry [26], materials science [30] and microfluidics [31] took a great advantage of manipulation of molecules and particles by proper application of the electric fields. In this chapter I will focus on two areas of applications that are related to the research described in this thesis. First is utilization of the AC electrokinetic phenomena for improvement of biodetection methods. Secondly, electrophoretic deposition of molecules or particles is described.

1.2.1. AC electrokinetics in biodetection

AC electroosmosis

AC electroosmosis (ACEO) have been widely used to enhance movement of the proteins. Directed transport of these molecules towards sensing surfaces allowed for speeding up the binding process between antigen and macromolecule to be detected. This resulted in development of rapid and sensitive detection methods based on such techniques as capacitive immunosensing [32], surface-enhanced Raman spectroscopy [33], electrical impedance spectroscopy [33] and capillary-based technique [34]. For instance, improvement in heterogeneous immunoassays was possible due to combination of ACEO and dielectrophoresis (Figure 1.3A) [35]. Analysis of fluorescence intensity of fluorescein-labeled immunoglobulin G showed that upon application of optimal frequency of 100-200 Hz, 6.7-fold enhancement of fluorescence signal was obtained. Effect was the most pronounced on the edges of utilized electrodes, probably due to additional effect of dielectrophoresis. Hart et al. proved also that rotational fluid patterns generated in the AC electroosmosis can improve the capture of protein on specially modified quartz crystal microbalance [36]. The signal was enhanced by the factor of around 5.6. Moreover, combination of ACEO, positive dielectrophoresis and electrochemical impedance spectroscopy resulted in rapid, sensitive, and label-free immunodetection method [37]. After only 90 s of electrokinetic procedure, measured signal achieved plateau reaching limit of detection of 200 pg/ml of target protein A. AC electrokinetic impedance sensing method was used also for rapid detection of tuberculosis [38]. The limit of detection of IgG antibody was estimated to be better than 10 ng/ml.

ACEO is also attractive to concentrate DNA by orders of magnitude, which allows for bypassing typically utilized complicated and expensive enzyme-based amplification methods [39]. Martins et al. used electroosmotic flow to create microfluidic concentrator that effectively reduced incubation time from 16 h to 15 min and enabled detection of 1 nM of DNA within 15 min [40]. DC-biased AC electroosmosis stirring was also combined with the electrochemical impedance spectroscopy-based DNA biosensing chip (Figure 1.3B) [41]. Resulted method presented good linearity and repeatability in range of 1 aM –10 pM and had ultrasensitive limit of detection of 0.5 aM. Also detection of microorganisms was improved by ACEO. Liao et al. presented a method in which properly designed geometry of electrodes provided concentration of bacteria through ACEO and dielectrophoresis, whereas micro-Raman spectroscopy allowed for detection of bacteria *Escherichia coli* K12 with limit of detection of 10² CFU/ml (Figure 1.3CD) [42].

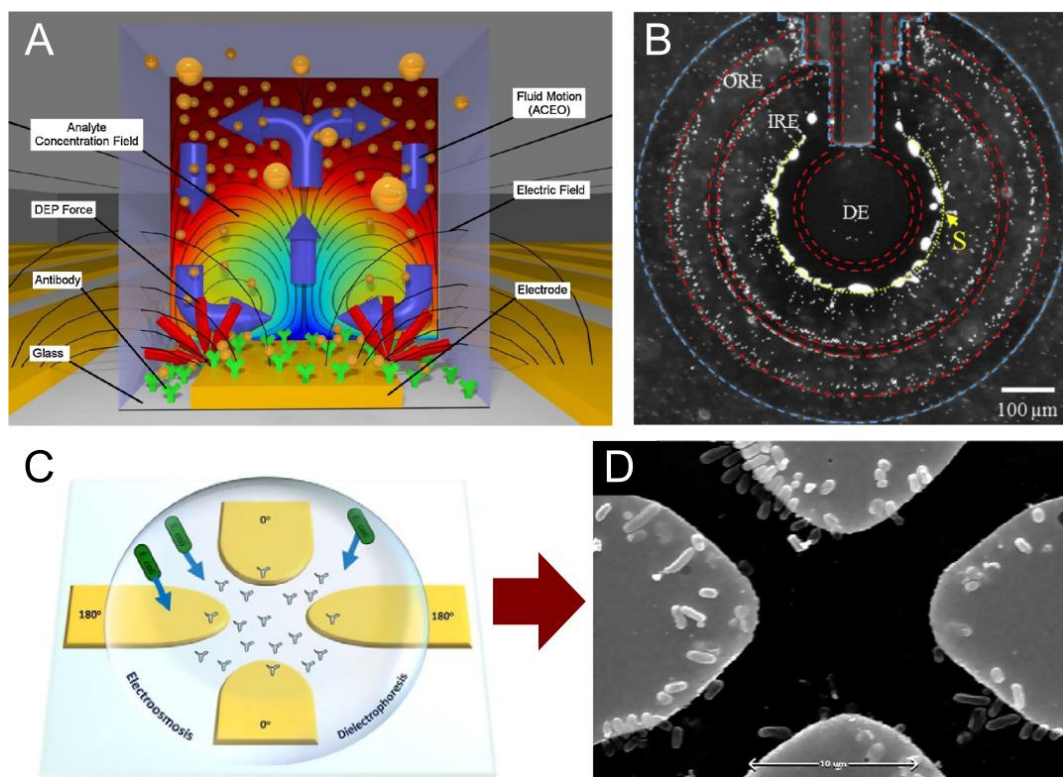


Figure 1.3 Exemplary applications of AC electroosmosis (ACEO) in biosensing. **(A)** Diagram of immunoassay performed with combination of AC electroosmosis and dielectrophoresis. Blue arrows indicate fluid motion, whereas movement of molecules of analyte is shown by red arrows [35]; **(B)** Image of fluorescent beads used as probes for analysis of bias-varied ACEO stirring. Red dashed, blue dashed, and yellow dotted lines represent edges of the electrodes and insulator, and the stagnation point (S), respectively [41]; **(C)** Schematic representation of accumulation of bacteria at the tips of the electrodes due to electroosmosis and dielectrophoresis [42]; **(D)** Scanning electron microscope image of bacteria captured at the microelectrode tips [42]. All figures have been reproduced with permission.

AC electrothermal effect

The effect of electrothermally generated motion of fluid has been widely described both theoretically and experimentally. Numerical and analytical analysis of ACET provided detailed description of acceleration of analytes transport towards sensing surfaces [23], [43], [44]. This knowledge was utilized in many practical applications, such as improvement of binding time in microfluidic immuno-sensor [45]. ACET was utilized to generate electrothermal flow in high conductivity buffer, which is especially desired in context of biologically relevant fluids. Moreover, ACET was proved to be useful in improving lab-on-a-chip immunoassay for rapid detection of molecular markers of pathogens [46]. Very similar approach was also combined with capacitive immunoassay [47]. The enhanced transport of analyte allowed for distinction between positive and negative pregnancy serum in 60 s. Combination of ACET and capacitive immunodetection was also used to detect molecules other than proteins. ACET enrichment allowed for detection of small molecule

bisphenol A [48] and phylogenetic biomarker – bacterial 16S rRNA [49]. Moreover, Rocha et al. utilized this technique for detection and quantification of naturally occurring microbes in both batch cultures and environmentally sourced seawater and groundwater systems [50].

Dielectrophoresis

DEP has many advantages, such as independency from strength and polarization of the electric field and simplicity of creating geometries that results in DEP forces. Therefore, this technique has been heavily utilized over last decades in many various applications. DEP improved manipulation of such biological molecules and objects as blood cells [51], stem cells [52], neurons [53], bacteria [54], viruses [55], proteins [56], [57], and nucleic acids [58].

1.2.2. Electrophoretic deposition

Electrophoretic deposition (EPD) is a process of deposition of particles or molecules onto solid surface under the influence of applied external electric field [30]. Particles with non-zero zeta potential, suspended or dispersed in fluids, move towards the electrode of opposite charge due to electrostatic forces described previously in this chapter. Two kinds of electrophoretic deposition can be distinguished. If the particles are negatively charged, they move to the positively charged electrode – the anode, and the process is called anodic EPD. On the other hand, positively charged particles travel towards negatively charged cathode, so such case is described as cathodic EPD.

EPD consist of two main steps. First, migration of particles according to applied electric field occurs. Second process is deposition of particles on the surface of the electrode. There is a number of parameters that can influence the process as well as the efficiency and quality of final coverage [59]. Among them, the most important are zeta potential of particles (which could be manipulated by careful control of the pH of the solution), particle size, conductivity and viscosity of the suspension and suspension stability. During the design of the process it is necessary to control and take into account all of these variables.

Due to the relatively simple mechanism, EDP is considered to be versatile and cost-effective. The first EDP experiment was carried out by Bose in 1740. Many years later, in 1807 Reuss described the movement of clay particles in an aqueous suspension in an electric field [1]. However, it took another 170 years to obtain first industrial application of EPD [60]. Nowadays, there are many different applications of EPD, including the processes of production of nanomaterials [61], biomaterials [62], ceramic composites [63] and biofilms [64].

Direct current EPD (often referred as DC EPD or simply EPD) is reported as the first and the most straightforward type of electrophoretic deposition. Because of the simple nature of the process, it is easy to simulate and to predict the parameters necessary for desired result. Basic EPD needs to be carried out in organic solvents, as water and water-based electrolytes decompose easily due to electrolysis. Utilization of organic solvents has

many benefits, such as low conductivity, chemical stability and lower contribution of Joule heating or electrochemical reactions. All these advantages lead to coatings of high quality. However, utilization of organic solvents causes many difficulties associated with environmental problems, high costs, toxicity or flammability. Moreover, organic solvents have low dielectric constant and high voltages are necessary for efficient deposition. This causes additional costs and dangerous conditions.

Usage of aqueous solvent is a must-have alternative for organic compounds, as it provides solutions for all of the previously mentioned drawbacks and it hugely extends applicability of the method. Additionally, high dielectric constant of water enables the usage of lower electric fields, and thus lower applied voltages. Unfortunately, the biggest problem associated with such an approach is the occurrence of phenomena of electrolysis of water. Water has low thermodynamic potentials of reduction and oxidation, and therefore even in case of low values of applied potentials electrochemical reaction appears and generates gases (H_2 at the cathode and O_2 at the anode). Bubbles of gases can be integrated into the deposited layer and cause poor quality of the coating. Moreover, number of ions decomposes at even lower values of applied potential. There were a few attempts to overcome this issue, among them utilization of membranes, keeping voltage below the thermodynamic values of water electrolysis, using palladium electrodes that absorb hydrogen or addition of chemicals seem most relevant [65]–[67].

Another interesting alternative for direct EDP of aqueous solutions, that enables deposition directly on the surface of the electrode, is using another type of voltage waveform. Application of the alternating field gives a rise for a wide range of possibilities, not only introducing frequency as an additional parameter, but also opening the chance of combination of DC and AC. All waveforms of the voltage that will be described in this chapter are considered to generate an alternating electric field as applied voltage changes over time (Figure 1.4). However, additional division into pulse electric field and typical alternating electric field will be introduced to avoid any ambiguities. It is also important to mention, that square voltage waveforms presented in Figure 1.4 are not the only shapes that can be utilized. Triangular and sinusoidal waveforms were also utilized in the same way [68]–[70].

Pulse DC Fields

Typical voltage waveform of Pulse-Direct Current Electrophoresis Deposition (PDC) is presented in Figure 1.4A. It was shown that PDC can be used for formation of layers of ceramic particles, polymers, carbon nanotubes or enzymes [59]. Main advantage of PDC over regular EDP is reduction of integration of bubbles into formed structures, and thus obtained layers are dense and uniform. Electrolysis of water is considered to be rather slow [60], and hence short pulses can prevent the formation of products of this reaction. Additionally, long gaps between pulses can give enough time for created bubbles to diffuse towards the bulk. Other advantages are reduction of aggregates between particles and preservation of the activity of deposited biomolecules. The latter effect is caused by small

changes of pH in the vicinity of the surface of the electrodes. In terms of disadvantages, utilization of PDC results in the decrease of the deposition yield. This, however, can be overcome by, for instance, longer time of deposition process.

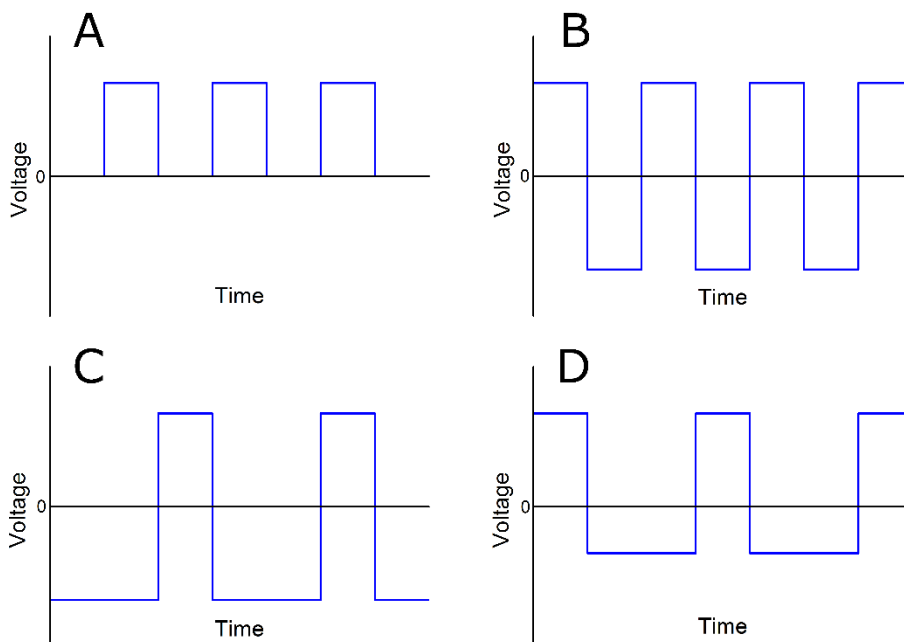


Figure 1.4 Different types of voltage waveforms used in electrophoretic deposition: **(A)** pulsed DC; **(B)** symmetrical AC; **(C)** asymmetrical AC with net DC; **(D)** asymmetrical AC without net DC.

Symmetrical AC EPD

Another option is electrophoretic deposition conducted in alternating field (AC EPD). In this case, the movement of electric charge periodically reverses direction between positive and negative. Thus, dynamics of particles are much more complicated in comparison with DC EDP. In contrast to DC, interactions of alternating field and suspended particles in AC EPD cause number of phenomena and forces that influence the process. Some of them are already described in previous part of this chapter. Most pronounced are dielectrophoresis, electrophoresis, electrorotation or traveling wave dielectrophoresis. Their contribution depends on many different parameters, such as frequency, size of particles, conductivity of electrolyte, distribution of the electric field and many others. Therefore, AC EPD is complex and complicated process and hence it is difficult to straightforward predict and analyze experimental observations.

First reports on using alternating field in electrophoretic deposition can be found in patents from 19th century for industrial applications, such as electro-coating of paint based polymers and copolymers. Typical example of symmetrical AC waveform is presented in Figure 1.4B.

It is generally known, that in symmetrical AC, distance that particle travel in first half of the cycle, equals exactly the distance travelled in another half. Thus, since particle

just oscillates around one fixed position, the net migration becomes zero. This can lead to the assumption, that symmetrical AC cannot be used for deposition process. However, in literature there are numerous examples of successful symmetrical AC EDP. This apparent contradiction arises from multiple contributions to AC EDP by different forces and interactions. Thus, unobvious phenomena occur and cause deposition of particles on different spots of electrode. Moreover, if particles adsorb due to chemical affinity on the surface in first half of the period, they may not be removed in second half of cycle. Thus, many cycles can result in effective deposition of the particles on the surface. Situation is even more complex if we consider unusual setup for deposition, such as non-planar and non-parallel electrodes. According to theoretical predictions, AC EDP should result in poor deposition yield. However, there are reports concerning thick layers obtained with this technique [71], [72]. Symmetrical AC EDP was exploited for deposition of Au and Ag [73], TiO₂ [74], ZnO [75], SnO₂ and WO₃ [60] nanoparticles or ceramic [76]. This method was also used in case of carbon nanotubes and even both eukaryotic and prokaryotic living cells [60]. Application of symmetrical AC EPD is further discussed in chapter 3 of this thesis.

Asymmetrical AC EPD with net DC

Alternating field can also be asymmetrical. Typical example of asymmetrical AC wave is shown in Figure 1.4C. In such case net DC component is created because voltage-time areas of positive and negative half cycles are not equal. Thus, there is a net drift and particles are dragged towards oppositely charged electrode. Main advantage of this approach over regular DC is higher quality of created coatings. It is due to a number of reasons, such as (1) better control of the process (to some extent); (2) particles are subjected to reversed field, which can resuspend them and hence they are more densely packed; (3) tuning the frequency could prevent formation of bubbles of gases created in electrolysis process.

The major drawback of this technique is similar to that of PDC method, i.e. lower deposition rate. This arises from the fact, that although in asymmetrical AC EPD there is the net drift of the particles, the effect is weaker than in regular DC, where drift is caused by constant voltage and the particles are dragged towards one electrode the whole time. Moreover, in asymmetrical AC EPD particles are subjected to a reverse field, that pull them back from the target electrode. That effect results in further decrease of number of particles deposited in a given time.

Nevertheless, due to many advantages over other electrophoretic deposition techniques, asymmetrical AC EPD was developed and used in number of applications, including deposition of hydroxyapatite particles [77], BaTiO₃ [78], TiO₂ [79] or SiC nanoparticles [80].

Asymmetrical AC EPD without net DC

Asymmetrical alternating field can also be designed in a special way that no net DC component is present. Exemplary waveform of asymmetrical AC EDP without net DC is shown in Figure 1.4D. It can be noticed, that although waveform is asymmetrical, surface

areas of the positive and negative half-cycles are equal. Thus, assuming that dependence between velocity of the particles v_{eph} and strength of the electric field E is linear, there should be no net DC component included. However, linear dependency is true only for low strength of the electric fields. If the applied voltage is high enough (around 100 V/cm) this dependency becomes non-linear and second term plays important role [81]:

$$v_{eph} = \mu_{eph}E + \mu_{eph}^{(3)}E^3 \quad (1.4)$$

where v_{eph} is electrophoretic velocity, μ_{eph} is field-independent electrophoretic mobility coefficient, $\mu_{eph}^{(3)}$ is non-linear electrophoretic mobility coefficient and E is strength of the electric field. This dependence means that during low voltage-pulse deposition net DC component is absent and becomes important in case of stronger fields. The theory of nonlinear electrophoresis was vastly developed and applied in creating layers of organic, organic-inorganic particles, enzymes and living cells [59].

1.3. Aim of the research and outline of this thesis

The potential of the electric field to improve detection and deposition methods have been clearly proven, as evidenced in above-described research summary. Main goal of research described in this thesis is to develop even further the application of the electric field and create solutions that will aid currently encountered issues. I focus here on creating the methods that improve sensing and biosensing techniques by applying electric and magnetic fields.

There is a shortage of methods for fast and efficient deposition of molecules, that can be applied in methods of analytical chemistry. Thus, method of deposition of analytes in the electric field on SERS substrates was developed (**chapter 3**). Second identified problem was inefficient performance of bacteria detection methods based on layers of bacteriophages. Problem of sterical hindrance of virions was solved by proper orientation of phages in the alternating electric field (**chapter 4**). Within the course of both of these projects it turned out, that deeper analysis of behavior of ions in the alternating electric field is needed. This resulted in basic research in which unusual phenomenon of strong repulsion between oppositely charged surfaces separated by the electrolyte was discovered (**chapter 2**). Finally, knowledge and experience, gained during project about improving bacteria detection by application of the electric field, inspired me to develop another method for bacteria detection, however in this case based on the magnetic field (**chapter 5**). Projects described in this work are ordered from basic research, through practical applications of the electric field, to the practical utilization of magnetic field.

In **chapter 2** analysis of behavior of ions upon application of the electric field is described. Unusual phenomena of strong, long-range repulsion between two oppositely charged surfaces upon application of AC voltage was discovered. Both electrodes were isolated from the solution by thin layer of dielectric and such created capacitor was filled with electrolyte having ions of unequal mobilities. Measured repulsion forces were two

orders of magnitude stronger than typical attraction of surfaces in water. Moreover, time scale of observed phenomena was in range of minutes. Thus, obtained values were over 8 orders of magnitude longer than typically predicted, i.e. in range of few μs .

Chapter 3 presents development of improvement of analytes deposition on conducting surfaces. Created method allowed for fast and efficient deposition of various analytes and was applied to improve surface-enhanced Raman spectroscopy (SERS). The challenge was to omit the problem of electrochemical reactions and at the same time to overcome the issue of suppression of the electric field by the electrical double layer. As a solution, the alternating electric field was applied. Frequency of utilized voltage was identified as crucial parameter for effective deposition and dependency between optimal frequency and electrophoretic mobility of deposited analyte was determined.

Another application of the electric field as improvement of detection method is shown in **chapter 4**. Proper geometrical orientation of bacteriophages obtained by alternating electric field resulted in improvement of sensitivity of phage layers for bacteria detection. Additional advancement was achieved by chemical modification of the surface. Obtained improvement in density of phages on the surface, combined with the proper orientation of phages in the electric field resulted in 50- to 64-fold increase in number of captured cells. Limit of detection was 100 CFU/ml and detection was possible in 15 min.

During research performed in chapter 4, I learned, that not only electric but also magnetic field has a great potential to improve sensing methods. Thus, in **chapter 5** project in which I developed another phage-based solution for bacteria detection is described. However, in this case it was based on magnetic field. I created bioconjugates composed of fluorescent-magnetic particles and bacteriophages. The main idea was to create solution easily adaptable, also in non-biological laboratories. Thus, all components were inexpensive and accessible. Additionally, developed bacteria detection protocol that exploit prepared bioconjugates as probes for flow cytometry was straightforward and at the same time efficient, specific and selective.

Chapter 6 summarizes all of the finding of this thesis and put them in perspective of future research and context of the field.

1.4. References

- [1] F. F. Reuss, “Sur un nouvel effet de l’électricité galvanique,” *Mem. Soc. Imp. Natur. Moscou*, vol. 2, pp. 327–337, 1809.
- [2] J. R. Brody and S. E. Kern, “History and principles of conductive media for standard DNA electrophoresis,” *Anal. Biochem.*, vol. 333, no. 1, pp. 1–13, 2004.
- [3] A. Revil, H. Schwaeger, L. M. Cathles, and P. D. Manhardt, “Streaming potential in porous media: 2. Theory and application to geothermal systems,” *J. Geophys. Res.*, vol. 104, no. B9, pp. 20033–20048, 1999.
- [4] T. Lindstrom, “Electrokinetics of the papermaking industry,” in *Paper chemistry*, J. C. Roberts, Ed. New York: Chapman & Hall, 1991.
- [5] L. Malaeb and G. M. Ayoub, “Reverse osmosis technology for water treatment: State of the art review,” *Desalination*, vol. 267, no. 1, pp. 1–8, 2011.
- [6] R. J. Hunter, *Zeta Potential in Colloid Science*. New York: Academic Press, 1981.
- [7] A. V. Delgado, F. González-Caballero, R. J. Hunter, L. K. Koopal, and J. Lyklema, “Measurement and interpretation of electrokinetic phenomena,” *J. Colloid Interface Sci.*, vol. 309, no. 2, pp. 194–224, 2007.
- [8] M. E. Suss, T. F. Baumann, W. L. Bourcier, C. M. Spadaccini, K. A. Rose, J. G. Santiago, and M. Stadermann, “Capacitive desalination with flow-through electrodes,” *Energy Environ. Sci.*, vol. 5, no. 11, p. 9511, 2012.
- [9] J. Voldman, “Electrical forces for microscale cell manipulation,” *Annu. Rev. Biomed. Eng.*, vol. 8, no. 1, pp. 425–454, 2006.
- [10] M. Mittal, P. P. Lele, E. W. Kaler, and E. M. Furst, “Polarization and interactions of colloidal particles in ac electric fields,” *J. Chem. Phys.*, vol. 129, no. 6, p. 064513, 2008.
- [11] T. M. Squires and S. R. Quake, “Microfluidics: Fluid physics at the nanoliter scale,” *Rev. Mod. Phys.*, vol. 77, no. 3, pp. 977–1026, 2005.
- [12] M. Z. Bazant, K. Thornton, and A. Ajdari, “Diffuse-charge dynamics in electrochemical systems,” *Phys. Rev. E*, vol. 70, no. 2, p. 021506, 2004.
- [13] T. M. Squires and M. Z. Bazant, “Induced-charge electro-osmosis,” *J. Fluid Mech.*, vol. 509, no. 509, pp. 217–252, 2004.
- [14] B. Balu and A. S. Khair, “Role of Stefan-Maxwell fluxes in the dynamics of concentrated electrolytes,” *Soft Matter*, vol. 14, no. 41, pp. 8267–8275, 2018.
- [15] C. Zhao and C. Yang, “Advances in electrokinetics and their applications in micro/nano fluidics,” *Microfluid. Nanofluidics*, vol. 13, no. 2, pp. 179–203, 2012.
- [16] J. H. Masliyah and S. Bhattacharjee, *Electrokinetic and colloid transport phenomena*. New Jersey: John Wiley & Sons, Inc., 2006.
- [17] B. J. Kirby, *Micro- and nanoscale fluid mechanics*. Cambridge University Press, 2010.
- [18] J. (Jayne) Wu, “AC electro-osmotic micropump by asymmetric electrode polarization,” *J. Appl. Phys.*, vol. 103, no. 2, p. 024907, 2008.
- [19] M. Lian and J. Wu, “Ultrafast micropumping by biased alternating current electrokinetics,” *Appl. Phys. Lett.*, vol. 94, no. 6, p. 064101, 2009.
- [20] A. Ramos, H. Morgan, N. G. Green, and A. Castellanos, “AC electric-field-induced fluid flow in microelectrodes,” *J. Colloid Interface Sci.*, vol. 217, no. 2, pp. 420–422, 1999.
- [21] N. Sasaki, “Recent applications of AC electrokinetics in biomolecular analysis on

- microfluidic devices,” *Anal. Sci.*, vol. 28, no. 1, p. 3, 2012.
- [22] N. G. Green, A. Ramos, A. González, H. Morgan, and A. Castellanos, “Fluid flow induced by nonuniform ac electric fields in electrolytes on microelectrodes. I. Experimental measurements,” *Phys. Rev. E*, vol. 61, no. 4, pp. 4011–4018, 2000.
- [23] M. Sigurdson, D. Wang, and C. D. Meinhart, “Electrothermal stirring for heterogeneous immunoassays,” *Lab Chip*, vol. 5, no. 12, pp. 1366–1373, 2005.
- [24] A. Salari, M. Navi, and C. Dalton, “A novel alternating current multiple array electrothermal micropump for lab-on-a-chip applications,” *Biomicrofluidics*, vol. 9, p. 014113, 2015.
- [25] S. J. Williams, “Enhanced electrothermal pumping with thin film resistive heaters,” *Electrophoresis*, vol. 34, pp. 1400–1406, 2013.
- [26] A. Salari and M. Thompson, “Recent advances in AC electrokinetic sample enrichment techniques for biosensor development,” *Sensors Actuators, B Chem.*, vol. 255, pp. 3601–3615, 2018.
- [27] Y. Lu, T. Liu, A. C. Lamanda, M. L. Y. Sin, V. Gau, J. C. Liao, and P. K. Wong, “AC electrokinetics of physiological fluids for biomedical applications,” *J. Lab. Autom.*, vol. 20, no. 6, pp. 611–620, 2015.
- [28] M. P. Hughes, “AC electrokinetics: applications for nanotechnology,” *Nanotechnology*, vol. 11, pp. 124–132, 2000.
- [29] O. D. Velev, S. Gangwal, and D. N. Petsev, “Particle-localized AC and DC manipulation and electrokinetics,” *Annu. Reports Sect. “C” Phys. Chem.*, vol. 105, pp. 213–246, 2009.
- [30] L. Besra and M. Liu, “A review on fundamentals and applications of electrophoretic deposition (EPD),” *Prog. Mater. Sci.*, vol. 52, no. 1, pp. 1–61, 2007.
- [31] M. Z. Bazant and T. M. Squires, “Induced-charge electrokinetic phenomena: theory and microfluidic applications,” *Phys. Rev. Lett.*, vol. 92, no. 6, pp. 1–4, 2004.
- [32] S. Li, H. Cui, Q. Yuan, J. Wu, A. Wadhwa, S. Eda, and H. Jiang, “AC electrokinetics-enhanced capacitive immunosensor for point-of-care serodiagnosis of infectious diseases,” *Biosens. Bioelectron.*, vol. 51, pp. 437–443, 2014.
- [33] I. F. Cheng, T. Y. Chen, and H. C. Chang, “Electrokinetics-based microfluidic technology for the rapid separation and concentration of bacteria/cells/biomolecules,” *Adv. Mater. Res.*, vol. 911, pp. 347–351, 2014.
- [34] A. Dev, J. Horak, A. Kaiser, X. Yuan, A. Perols, P. Björk, A. E. Karlström, P. Kleimann, and J. Linnros, “Electrokinetic effect for molecular recognition: A label-free approach for real-time biosensing,” *Biosens. Bioelectron.*, vol. 82, pp. 55–63, 2016.
- [35] R. Hart, R. Lec, and H. M. Noh, “Enhancement of heterogeneous immunoassays using AC electroosmosis,” *Sensors Actuators, B Chem.*, vol. 147, no. 1, pp. 366–375, 2010.
- [36] R. Hart, E. Ergezen, R. Lec, and H. M. Noh, “Improved protein detection on an AC electrokinetic quartz crystal microbalance (EKQCM),” *Biosens. Bioelectron.*, vol. 26, no. 8, pp. 3391–3397, 2011.
- [37] I. F. Cheng, H. L. Yang, C. C. Chung, and H. C. Chang, “A rapid electrochemical biosensor based on an AC electrokinetics enhanced immuno-reaction,” *Analyst*, vol. 138, no. 16, pp. 4656–4662, 2013.
- [38] H. Cui, S. Li, Q. Yuan, A. Wadhwa, S. Eda, M. Chambers, R. Ashford, H. Jiang, and J. Wu, “An AC electrokinetic impedance immunosensor for rapid detection of



- tuberculosis,” *Analyst*, vol. 138, no. 23, pp. 7188–7196, 2013.
- [39] C. C. Wu and D. J. Yang, “A label-free impedimetric DNA sensing chip integrated with AC electroosmotic stirring,” *Biosens. Bioelectron.*, vol. 43, no. 1, pp. 348–354, 2013.
- [40] D. Martins, R. Levicky, and Y. A. Song, “Enhancing the speed of morpholino-DNA biosensor by electrokinetic concentration of DNA in a microfluidic chip,” *Biosens. Bioelectron.*, vol. 72, pp. 87–94, 2015.
- [41] C. C. Wu, W. C. Huang, and C. C. Hu, “An ultrasensitive label-free electrochemical impedimetric DNA biosensing chip integrated with a DC-biased AC electroosmotic vortex,” *Sensors Actuators, B Chem.*, vol. 209, pp. 61–68, 2015.
- [42] D. S. Liao, J. Raveendran, S. Golchi, and A. Docoslis, “Fast and sensitive detection of bacteria from a water droplet by means of electric field effects and micro-Raman spectroscopy,” *Sens. Bio-Sensing Res.*, vol. 6, pp. 59–66, 2015.
- [43] K.-R. Huang and J.-S. Chang, “Three dimensional simulation on binding efficiency of immunoassay for a biosensor with applying electrothermal effect,” *Heat Mass Transf.*, vol. 49, no. 11, pp. 1647–1658, 2013.
- [44] M. Selmi, R. Khemiri, F. Echouchene, and H. Belmabrouk, “Enhancement of the analyte mass transport in a microfluidic biosensor by deformation of fluid flow and electrothermal force,” *J. Manuf. Sci. Eng.*, vol. 138, no. 8, p. 081011, 2016.
- [45] H. C. Feldman, M. Sigurdson, and C. D. Meinhart, “AC electrothermal enhancement of heterogeneous assays in microfluidics,” *Lab Chip*, vol. 7, no. 11, pp. 1553–1559, 2007.
- [46] X. Liu, K. Yang, A. Wadhwa, S. Eda, S. Li, and J. Wu, “Development of an AC electrokinetics-based immunoassay system for on-site serodiagnosis of infectious diseases,” *Sensors Actuators, A Phys.*, vol. 171, no. 2, pp. 406–413, 2011.
- [47] S. Li, Y. Ren, and H. Jiang, “Convection and mass transfer enhanced rapid capacitive serum immunoassay,” *RSC Adv.*, vol. 4, no. 18, pp. 9064–9071, 2014.
- [48] H. Cui, C. Cheng, X. Lin, J. Wu, J. Chen, S. Eda, and Q. Yuan, “Rapid and sensitive detection of small biomolecule by capacitive sensing and low field AC electrothermal effect,” *Sensors Actuators, B Chem.*, vol. 226, pp. 245–253, 2016.
- [49] T. Liu, M. L. Y. Sin, J. D. Pyne, V. Gau, J. C. Liao, and P. K. Wong, “Electrokinetic stringency control in self-assembled monolayer-based biosensors for multiplex urinary tract infection diagnosis,” *Nanomedicine Nanotechnology, Biol. Med.*, vol. 10, no. 1, pp. 159–166, 2014.
- [50] A. M. Rocha, Q. Yuan, D. M. Close, K. B. O’Dell, J. L. Fortney, J. Wu, and T. C. Hazen, “Rapid detection of microbial cell abundance in aquatic systems,” *Biosens. Bioelectron.*, vol. 85, pp. 915–923, 2016.
- [51] Y. Qiang, J. Liu, M. Mian, and E. Du, “Experimental electromechanics of red blood cells using dielectrophoresis-based microfluidic,” in *Mechanics of Biological Systems and Materials*, vol. 6, C. S. Korach, S. A. Tekalur, and P. Zavattieri, Eds. Springer, 2017, pp. 129–134.
- [52] H. Song, J. M. Rosano, Y. Wang, C. J. Garson, B. Prabhakarapandian, K. Pant, G. J. Klarmann, A. Perantoni, L. M. Alvarez, and E. Lai, “Continuous-flow sorting of stem cells and differentiation products based on dielectrophoresis,” *Lab Chip*, vol. 15, no. 5, pp. 1320–1328, 2015.
- [53] T. Zhou, S. F. Perry, Y. Ming, S. Petryna, V. Fluck, and S. Tatic-Lucic, “Separation and assisted patterning of hippocampal neurons from glial cells using positive

- dielectrophoresis,” *Biomed. Microdevices*, vol. 17, no. 3, 2015.
- [54] C. Páez-Avilés, E. Juanola-Feliu, J. Punter-Villagrasa, B. del Moral Zamora, A. Homs-Corbera, J. Colomer-Farrarons, P. Miribel-Català, and J. Samitier, “Combined dielectrophoresis and impedance systems for bacteria analysis in microfluidic on-chip platforms,” *Sensors*, vol. 16, no. 9, p. 1514, 2016.
- [55] J. Ding, R. M. Lawrence, P. V. Jones, B. G. Hogue, and M. A. Hayes, “Concentration of Sindbis virus with optimized gradient insulator-based dielectrophoresis,” *Analyst*, vol. 141, no. 6, pp. 1997–2008, 2016.
- [56] H. Maruyama and Y. Nakayama, “Trapping protein molecules at a carbon nanotube tip using dielectrophoresis,” *Appl. Phys. Express*, vol. 1, no. 12, pp. 1240011–1240013, 2008.
- [57] M. Javanmard, S. Emaminejad, C. Gupta, J. Provine, R. W. Davis, and R. T. Howe, “Depletion of cells and abundant proteins from biological samples by enhanced dielectrophoresis,” *Sensors Actuators, B Chem.*, vol. 193, pp. 918–924, 2014.
- [58] A. Henning, F. F. Bier, and R. Hölzel, “Dielectrophoresis of DNA: Quantification by impedance measurements,” *Biomicrofluidics*, vol. 4, no. 2, p. 022803, 2010.
- [59] M. Ammam, “Electrophoretic deposition under modulated electric fields: a review,” *RSC Adv.*, vol. 2, no. 20, pp. 7633–7646, 2012.
- [60] B. Neirinck, O. Van Der Biest, and J. Vleugels, “A current opinion on electrophoretic deposition in pulsed and alternating fields,” *J. Phys. Chem. B*, vol. 117, no. 6, pp. 1516–1526, 2013.
- [61] R. Riahifar, B. Raissi, E. Marzbanrad, and C. Zamani, “Effect of parameters on deposition pattern of ceramic nanoparticles in non-uniform AC electric field,” *J. Mater. Sci. Mater. Electron.*, vol. 22, no. 1, pp. 40–46, 2011.
- [62] A. R. Boccaccini, S. Keim, R. Ma, Y. Li, and I. Zhitomirsky, “Electrophoretic deposition of biomaterials,” *J. R. Soc. Interface*, vol. 7, no. 581–613, 2010.
- [63] A. R. Boccaccini and I. Zhitomirsky, “Application of electrophoretic and electrolytic deposition techniques in ceramics processing,” *Curr. Opin. Solid State Mater. Sci.*, vol. 6, pp. 251–260, 2002.
- [64] A. T. Poortinga, R. Bos, and H. J. Busscher, “Controlled electrophoretic deposition of bacteria to surfaces for the design of biofilms,” *Biotechnol. Bioeng.*, vol. 67, no. 1, pp. 117–120, 2000.
- [65] M. Ordnung, J. Lehmann, and G. Ziegler, “Fabrication of fibre reinforced green bodies by electrophoretic deposition of silicon powder from aqueous suspensions,” *J. Mater. Sci.*, vol. 39, no. 3, pp. 889–894, 2004.
- [66] J. Tabellion and R. Clasen, “Electrophoretic deposition from aqueous suspensions for near-shape manufacturing of advanced ceramics and glasses-applications,” *J. Mater. Sci.*, vol. 39, no. 3, pp. 803–811, 2004.
- [67] T. Uchikoshi, K. Ozawa, B. D. Hatton, and Y. Sakka, “Dense, bubble-free ceramic deposits from aqueous suspensions by electrophoretic deposition,” *J. Mater. Res.*, vol. 16, no. 2, pp. 321–324, 2001.
- [68] B. Neirinck, J. Fransær, O. Van der Biest, and J. Vleugels, “Aqueous electrophoretic deposition in asymmetric AC electric fields (AC-EPD),” *Electrochem. commun.*, vol. 11, no. 1, pp. 57–60, 2009.
- [69] M. Ammam and J. Fransær, “Two-enzyme lactose biosensor based on β -galactosidase and glucose oxidase deposited by AC-electrophoresis: Characteristics and performance for lactose determination in milk,” *Sensors Actuators, B Chem.*,

- vol. 148, no. 2, pp. 583–589, 2010.
- [70] M. Ammam and J. Fransaer, “Alternating current electrophoretic deposition of *Saccharomyces cerevisiae* cells and the viability of the deposited biofilm in ethanol production,” *Electrochim. Acta*, vol. 55, no. 9, pp. 3206–3212, 2010.
- [71] A. R. Gardeshzadeh, B. Raissi, and E. Marzbanrad, “Deposition of multiwall carbon nanotubes using low frequency alternating electrophoretic deposition,” *Key Eng. Mater.*, vol. 412, pp. 83–86, 2009.
- [72] E. K. Heidari, C. Zamani, E. Marzbanrad, B. Raissi, and S. Nazarpour, “WO₃-based NO₂ sensors fabricated through low frequency AC electrophoretic deposition,” *Sensors Actuators, B Chem.*, vol. 146, no. 1, pp. 165–170, 2010.
- [73] M. G. Song, K. J. M. Bishop, A. O. Pinchuk, B. Kowalczyk, and B. A. Grzybowski, “Formation of dense nanoparticle monolayers mediated by alternating current electric fields and electrohydrodynamic flows,” *J. Phys. Chem. C*, vol. 114, no. 19, pp. 8800–8805, 2010.
- [74] R. Riahifar, E. Marzbanrad, B. Raissi, and C. Zamani, “A new technique for micro-patterning of nanoparticles on non-conductive substrate by low frequency AC electrophoresis,” *J. Mater. Sci. Mater. Electron.*, vol. 22, no. 9, pp. 1218–1221, 2011.
- [75] S. Ghashghaie, E. Marzbanrad, and B. Raissi Dehkordi, “Low-frequency electrophoretic deposition of ZnO nanoparticles: Effect of organic medium on deposition pattern,” *J. Am. Ceram. Soc.*, vol. 94, no. 10, pp. 3431–3436, 2011.
- [76] R. Riahifar, B. Raissi, E. Marzbanrad, and C. Zamani, “AC electrophoresis, a new technique for deposition of ceramic nanoparticles; introduction, application and mechanism,” *Key Eng. Mater.*, vol. 507, pp. 41–45, 2012.
- [77] V. Ozhukil Kollath, Q. Chen, R. Closset, J. Luyten, K. Traina, S. Mullens, A. R. Boccaccini, and R. Cloots, “AC vs. DC electrophoretic deposition of hydroxyapatite on titanium,” *J. Eur. Ceram. Soc.*, vol. 33, no. 13–14, pp. 2715–2721, 2013.
- [78] K. Raju and D. H. Yoon, “Electrophoretic deposition of BaTiO₃ in an aqueous suspension using asymmetric alternating current,” *Mater. Lett.*, vol. 110, pp. 188–190, 2013.
- [79] A. Chávez-Valdez, M. Herrmann, and A. R. Boccaccini, “Alternating current electrophoretic deposition (EPD) of TiO₂ nanoparticles in aqueous suspensions,” *J. Colloid Interface Sci.*, vol. 375, no. 1, pp. 102–105, 2012.
- [80] K. Raju, H. W. Yu, and D. H. Yoon, “Aqueous electrophoretic deposition of SiC using asymmetric AC electric fields,” *Ceram. Int.*, vol. 40, no. 8 PART A, pp. 12609–12612, 2014.
- [81] S. Barany, F. Madai, and V. Shilov, “Study of nonlinear electrophoresis,” *Prog. Colloid Polym. Sci.*, vol. 128, pp. 14–20, 2004.

Chapter 2

Fluctuations of ions in the alternating electric field

2.1. Introduction

Electrostatic and electrodynamic phenomena have been extensively described over last two decades. First chapter of this thesis summarizes possible electrokinetic effects and shows their vast potential in practical applications. In numerous cases, detailed analysis of created electrodynamic forces acting on particles and surfaces is crucial for precise control over designed systems. In the most simple case of dielectric material, effective electric field is directly proportional to the applied voltage and inversely proportional to the thickness of the material. Thus, in any dielectric media two charged surfaces or objects attract or repel each other with force proportional to the voltage squared [1]. In case of oscillating electric field situation become much more complex and exerted forces depend on frequency of the applied voltage [2]. The effect changes even more if considered medium is composed of both polar and charged species. As described in the first chapter of this work, just upon application of the voltage, the electric field spreads through the medium. This causes movement of charged species, such as ions, according to gradient of the electrical potential. Eventually, created electrical double layer screens the potential completely, assuming lack of any redox reactions and Faradaic currents. At low applied voltages, the distribution of potential in EDL can be described by Poisson-Boltzmann equation:

$$\Psi = \Psi_d \exp(-\kappa x) \quad (2.1)$$

where Ψ is potential at distance x , Ψ_d is potential at Stern plane, κ is the Debye-Hückel parameter and x is distance from the electrode. Length of resulting exponential decay of the potential is characterized by the Debye length (λ_D or κ^{-1}), as described in previous chapter.

Behavior of charged surfaces in the ionic media have been broadly analyzed both theoretically and experimentally. Initially developed classical models, such as Poisson-Boltzmann equation, were further developed and expanded and number of non-ideal cases, such as finite sizes of ions, large voltage applied, or crowding effects were also described [3]. For instance, Borukhov et al. modified Poisson-Boltzmann equation and took into account finite sizes of ions [4]. Olesen et al. studied nonlinear dynamics at large AC voltage [5]. They showed two unobvious phenomena: significant salt depletion in the electrolyte near the electrodes and breakdown of quasi-equilibrium structure of EDLs. Similar problem was analyzed by Bazant et al. [6]. Authors described two effects arising from electroosmosis at large voltages: an increase of a viscosity upon ion crowding and a decrease of capacitance due to the crowding effect. Also dynamic response of the systems was highly investigated topic and, as discussed in previous chapter, many different time scales were reported, depending on parameters of the analyzed system [7]–[9].

Many non-linear phenomena, such as manipulation of colloids [10], AC electroosmosis [11], induce-charge electrophoresis [12], and AC pumping [13], have been analyzed theoretically and measured experimentally. At the beginning, majority of cases considered simplified conditions of weak applied potential, i.e. $V < k_B T/e \approx 25$ mV

at 25 °C. In such case Poisson-Boltzmann equation can be linearized and solved analytically [14], [15]:

$$\nabla^2 \Psi^{eq} = -\frac{e}{\varepsilon} \sum_i z_i n_{i\infty} \exp\left(-\frac{z_i e \Psi^{eq}}{k_B T}\right) \quad (2.2)$$

where Ψ^{eq} is electric potential for stationary system, z_i is valence of given ion, $n_{i\infty}$ is concentration of given ion in the bulk solution, e is elementary charge, k_B is Boltzmann constant, T is temperature, ε is permittivity of a solution. However, currently obtained numerical and analytical solutions for larger AC voltages differ substantially from previously calculated linearized results [16], [17]. When the applied alternating potential is high enough, nonlinear effects occur and behavior of the system changes drastically. Analytical analysis becomes even more complicated when real-life cases, including high ionic strength, multivalent ions, solvent-free ionic liquids or differences in mobilities of ions, are taken into account.

Influence of unequal ionic mobilities was recognized some time ago. García-Sánchez et al. showed that flow reversal in electroosmotic pumping (unwanted phenomenon that couldn't be predicted by theory), was explained by differences in mobilities between ionic species [18]. It was also proven that in case of concentrated solutions, asymmetry in the mobilities of ions caused presence of two distinct time scales of electrolyte dynamics [19], short one that dictates evolution of charge density, and longer which arises due to asymmetry of the mobilities of ions. Moreover, Wirth et al. showed that differences in electrophoretic mobilities of ions can strongly influence particle motion near the electrode under AC polarization [20].

In this chapter unusual phenomenon of strong, long-range repulsion between oppositely charged surfaces is described. Although repulsion between surfaces of opposite sign was reported in the literature before, all of these cases were strictly limited to narrow range of parameters. Parsegian and Gingell showed that such phenomenon is possible only if: 1) surface charge densities are not equal and 2) electrical double layers of surfaces overlap [21]. This effect was later demonstrated experimentally for positively charged vesicle and negatively charged particles [22]. Repulsion between oppositely charged objects was also proven to be caused by multivalent ions. Their presence caused charge inversion on the surfaces [23], [24].

Effect reported in this chapter cannot be simply described by any of developed theories and electrokinetic analyses. Distances of observed repulsion extend up to even 2.6 μm , which is two orders of magnitude longer than Debye length in studied system (~ 10 nm). Measured repulsion forces are in range of 300 μN and are two orders of magnitude stronger than typical attraction in water (less than 10 μN). Also time scales of observed effect are unusual. Observed development of repulsion over few minutes is in stark contrast to previously reported fractions of second.

2.1.1. Surface forces apparatus

All measurements were performed using device called surface forces apparatus (SFA) [25]. In SFA normal or lateral interaction forces are measured between two surfaces separated by air or a medium (e.g. electrolyte, confined film) (Figure 2.1). Most common setup consists of two backsilvered, molecularly smooth mica surfaces attached to silica half-cylindrical discs. Discs are mounted in crossed-cylinder geometry. Distance between surfaces is typically much smaller than radius of cylinders. Thus, this geometry is equivalent to sphere over flat plane [25]. One of the surfaces (bottom surface in Figure 2.1) is mounted on a spring of calibrated spring constant k . Forces normal to the surfaces cause movement of surface mounted on the spring. Change of distance between electrodes is then measured with subnanometer resolution (0.1 nm) by multiple beam interferometry (MBI). In MBI, white light passes along the system normally to the silver semitransparent surfaces. Between silver mirrors it undergoes multiple reflection and wavelengths that experience constructive interference are allowed to pass through the system. Then wavelengths are spectrally resolved as fringes of equal chromatic order (FECO). Finally, FECO fringes are used to calculate the distance between mica surfaces [26]. MBI enables not only real-time *in situ* monitoring of distance between surfaces but also of geometry of interacting surfaces at the contact region. SFA was proved to be useful for analysis of both surface interactions [27] and electrostatic forces [28]–[30].

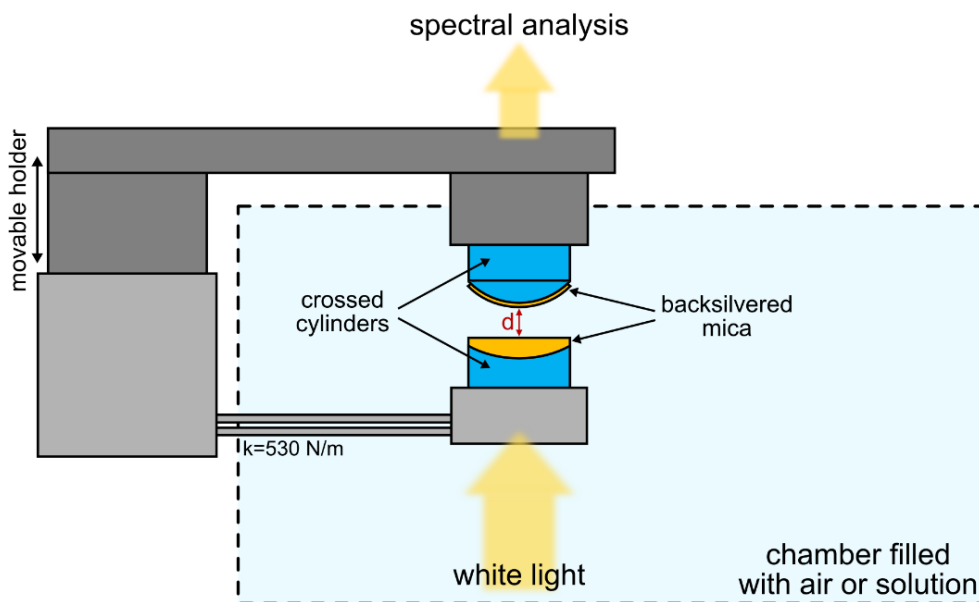


Figure 2.1 Surface forces apparatus. Two backsilvered mica surfaces are glued to silica discs aligned in crossed-cylinder geometry. SFA measurement can be performed in air or chamber can be filled with solution. Forces normal to the surfaces cause deflection of the spring of spring constant k and change the distance between surfaces d . White light passing through the system allows for real-time analysis of separation between surfaces.

2.2. Results and discussion

As in typical SFA, in case of studied system, two backsilvered mica pieces were attached to silica discs. Then discs were aligned in crossed-cylinder geometry. Both silver layers were also connected to a source of an external voltage. Such prepared capacitor consisted of two silver electrodes, each one isolated with layer of mica of thickness between 3.28 and 4.03 μm (Figure 2.2). Capacitor was filled with aqueous electrolytes. It is important to mention, that both mounted silica disks were completely immersed in the solution. Thus, the system was divided into the gap (the region around the point of the closest approach of mica surfaces) and the bulk (solution far away from the center of the capacitor). During the measurement AC square voltage was applied to silver electrodes. Changes in the distance between electrodes was measured by MBI and then recalculated to obtain forces between surfaces. Experiments were performed in electrolyte solution of 1 mM concentration upon application of 10 V of symmetrical applied AC voltage (voltage oscillated between -10 V and +10 V) of 100 kHz frequency, if not stated otherwise. Initial separation between mica surfaces was around 300 nm. Distance between mica surfaces was determined at the point of their closest approach, i.e. in the center of the utilized system.

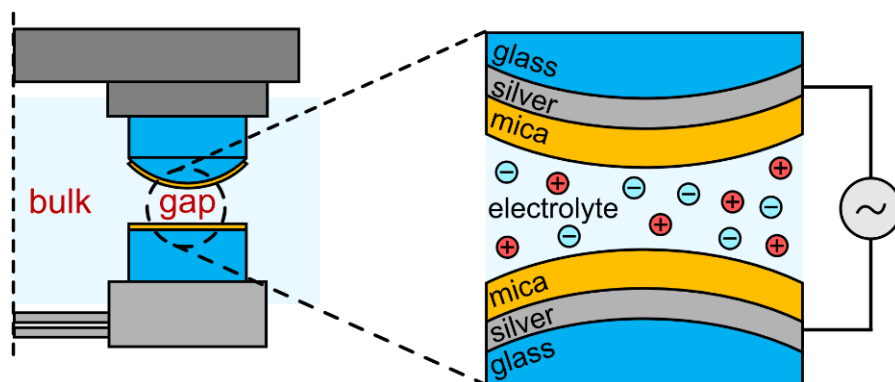


Figure 2.2 Utilized SFA system was capacitor filled with the electrolyte. Silver layers were connected to external source of voltage. Both silver electrodes were isolated with layers of mica.

2.2.1. Effect of repulsion between oppositely charged surfaces

In the first performed experiment, SFA was filled with 1 mM HNO_3 and voltage (10 V, 100 kHz) was applied. The whole measurement consisted of three stages: 3 minutes without voltage applied, 15 min with the electric field turned on and finally 15 minutes without the applied voltage. In case of such sudden application of the voltage between surfaces separated with the electrolyte, initial attraction was expected. Then, in the time scale of fractions of second, the attraction should decrease due to formation of the electrical double layers and after this moment no force should be observed. Instead, strong repulsion was measured (Figure 2.3). Immediately after application of the electric field, surfaces weakly attracted each other for 30 seconds. Then, the effect inverted and strong repulsion was observed. Time scale of observed phenomenon was in range of minutes. After the voltage

was turned off, the system relaxed with similar time scale and came back to the starting position.

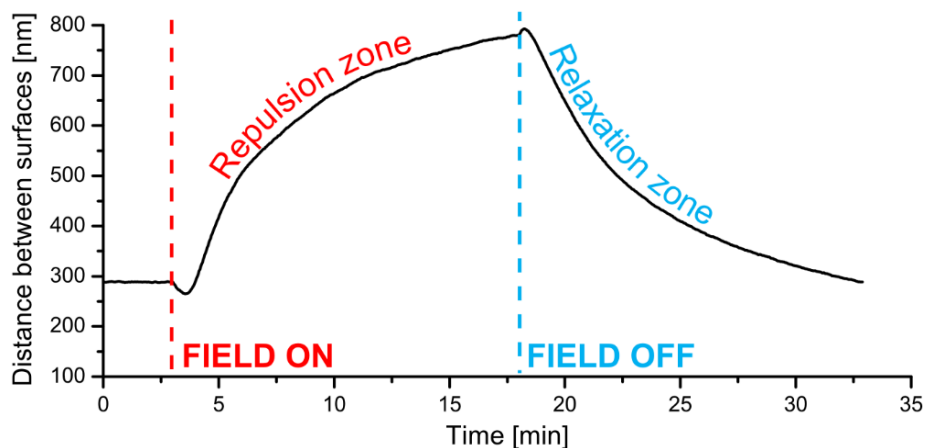
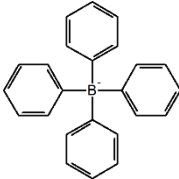


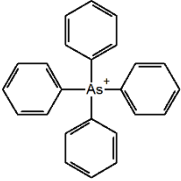
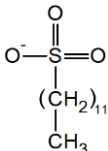
Figure 2.3 Observed phenomenon of repulsion between surfaces separated with electrolyte (1 mM HNO₃) upon application of the alternating voltage (10 V, 100 kHz). After application of the electric field repulsion force appeared with time scale of few minutes. When the field was turned off, there was the opposite effect of the relaxation of the system.

2.2.2. Selected compounds

To further analyze the observed effect, I chose 10 electrolytes that were composed of ions of wide range of electrophoretic mobilities. All utilized compounds and parameters of corresponding ions are summarized in the Table 2.1. All solutions were prepared using deionized water, except for two deuterated compounds (deuterated nitric acid – DNO₃ and deuterated sodium hydroxide – NaOD). These were made using pure deuterated water.

Table 2.1 Summary of all utilized compounds and electrophoretic mobilities of their corresponding ions. NaBPh₄, Ph₄AsCl, and LiDS are, respectively, sodium tetraphenylborate, tetraphenylarsonium chloride, and lithium dodecyl sulfate. DNO₃ and NaOD are, respectively, deuterated versions of nitric acid and sodium hydroxide.

Compound	Cation	Anion	Mobility of cation [10 ⁻⁸ m ² /sV]	Mobility of anion [10 ⁻⁸ m ² /sV]
HNO ₃	H ⁺	NO ₃ ⁻	36.2	7.4
NaOH	Na ⁺	OH ⁻	5.2	20.6
KOH	K ⁺	OH ⁻	7.6	20.6
NaBPh ₄	Na ⁺		5.2	2.1

Ph ₄ AsCl		Cl ⁻	2.4	7.9
NaNO ₃	Na ⁺	NO ₃ ⁻	5.2	7.4
Na ₂ SO ₄	Na ⁺	SO ₄ ²⁻	5.2	8.3
DNO ₃	D ⁺	NO ₃ ⁻	25.9	7.4
NaOD	Na ⁺	OD ⁻	5.2	12.4
LiDS	Li ⁺		4.0	2.5

2.2.3. Influence of applied voltage

One of the most crucial parameter in all electrokinetic phenomena is applied voltage. It defines the strength of the electric field and thus intensity of all electrostatic forces and electrodynamic process. I performed measurements in which various voltages were applied in the system filled with various analytes. Values of obtained repulsion forces were compared in Figure 2.4. Dashed lines in Figure 2.4 represent function fitted separately for each utilized compound:

$$F = AV^2 \quad (2.3)$$

where F is measured force, A is fitted parameter, and V is applied voltage.

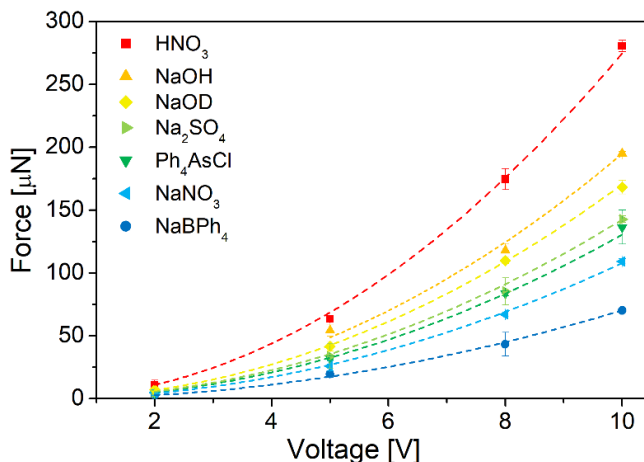


Figure 2.4 Repulsive force obtained for various applied voltages and different compounds. Dashed lines represent fit $F=AV^2$. In all cases R-squared was above 0.996.

I proved that observed effect depended on voltage squared, which is characteristic for many electrokinetic phenomena [31]. Moreover, for further analysis of this dependency, sinusoidal voltage waveform was studied. I measured forces in SFA filled with 1 mM KOH upon application of sinusoidal and square waveforms of alternating voltage (Figure 2.5). The rest of the parameters of measurement were kept the same (10 V and 100 kHz).

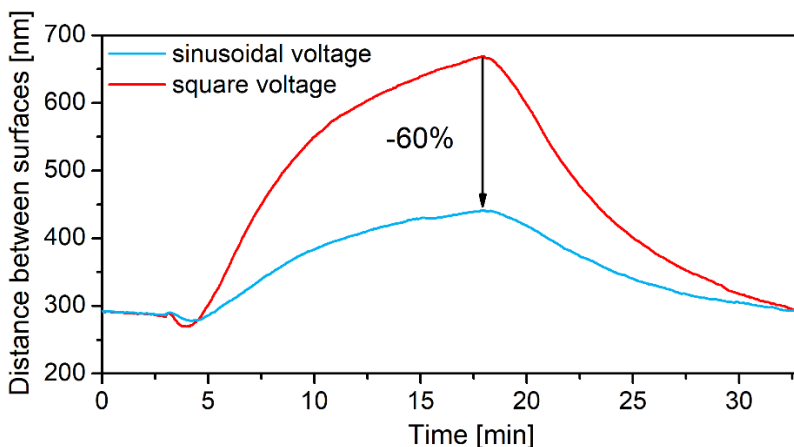


Figure 2.5 Measurement of the repulsion effect for sinusoidal or square voltage waveform. Application of sinusoidal shape resulted in 60% decrease of observed force in comparison to square waveform.

Obtained forces were 204.4 μN and 80.0 μN , for square and sinusoidal waveform, respectively. Observed 60% decrease was caused by different effective applied voltage. Although in both cases maximum voltage was 10 V, in case of sinusoidal shape effective voltage was reduced. For constant or symmetrical square waveforms, maximum value of voltage is applied constantly. Thus, the applied voltage is equal to the effective voltage. For sinusoidal waveform dependency between effective and maximum value (amplitude) is given by the equation:

$$V_{eff} = \frac{V_{app}}{\sqrt{2}} \quad (2.4)$$

where V_{eff} is effective voltage and V_{app} is applied voltage. It was proved that studied effect depended on voltage squared. Thus, in case of application of sinusoidal waveform, the measured force should decrease two times according to equation:

$$F \sim (V_{eff})^2 = \left(\frac{V_{app}}{\sqrt{2}}\right)^2 = \frac{(V_{app})^2}{2} \quad (2.5)$$

Obtained 60% of decrease of repulsive force was close to theoretical 50% and confirmed that the studied effect depended on applied voltage squared.

2.2.4. Influence of mobilities of ions

Many literature reports showed that unequal mobilities of ionic species give a raise to various unexpected phenomena and can vastly influence many electrokinetic

processes [18]–[20], [32]. Thus, I tested ten chosen analytes and compared obtained forces with differences in electrophoretic mobilities of ions. For this purpose I performed experiment similar to previously described in this chapter (for 5, 8 and 10 V). Obtained results are presented in Figure 2.6. For given value of the voltage results were fitted using equation

$F = A \cdot \ln(\mu_{diff}/\mu_0)$, where F was measured force, A was fitted parameter, μ_{diff} was difference in ionic mobilities, and μ_0 was unitary electrophoretic mobility of $1 \text{ m}^2/\text{sV}$.

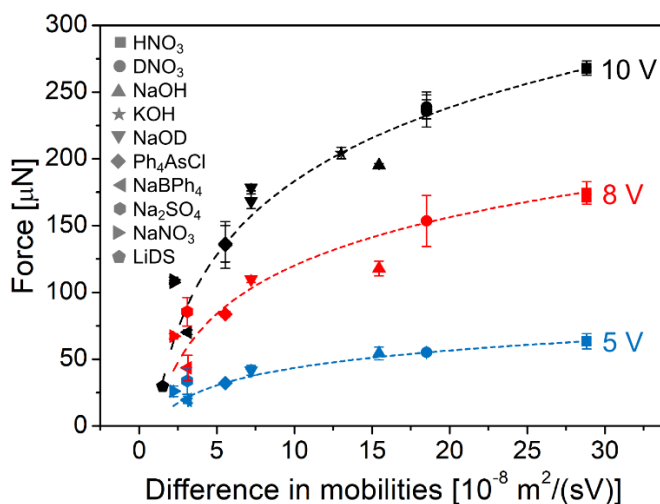


Figure 2.6 The effect of differences in mobilities of ions on measured force. Dashed lines represent fitted equation $F = A \cdot \ln(\mu_{diff}/\mu_0)$, where F is force, A is fitted parameter, μ_{diff} is difference in electrophoretic mobilities of ions, and μ_0 is unitary electrophoretic mobility of $1 \text{ m}^2/\text{sV}$. R-squared for 5, 8, and 10 V was 0.969, 0.832, and 0.942, respectively.

In case of each value of the applied voltage (5, 8 or 10 V), similar logarithmic dependency was observed. For almost equal mobilities, the measured effect decreased drastically. On the other hand, with increasing difference, the repulsion force increased and plateau characteristic for logarithmic dependencies was observed. Obtained results indicated that the origin of studied phenomena was unequal mobilities of ionic species. However, additional analysis was required for deeper understating of studied process.

2.2.5. Influence of concentration of ions

I already proved that types of ions fluctuating in gap between electrodes has crucial influence on the studied phenomenon. Next, influence of concentration of ions on described effect was analyzed. Series of measurements at various concentrations of NaNO_3 solution was performed (Figure 2.7). All other parameters were kept constant (10 V, 100 kHz of applied square voltage and 300 nm of initial separation between mica surfaces).

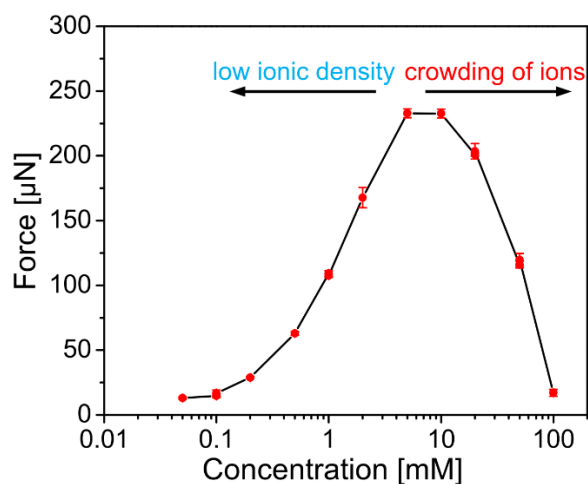


Figure 2.7 Effect of concentration of ions on measured force in case of NaNO_3 solution. Observed maximum force comes from two counterbalancing effects: not enough amount of ions to generate measurable force for low concentrations and crowding effect for higher concentrations [6].

Concentration of ions has great influence on the electrostatic screening due to formation of electrical double layers (Equation 1.1). Moreover, it was proven that electrostatic forces can vastly change and even reverse due to changes in concentrations of ions [23]. In majority of analyzed cases increase of concentration of ions caused only continuous increase or decrease of the effect [33]–[35]. However, in most of these reports narrow range of concentrations was analyzed (e.g. two orders of magnitude). Thus, only a part of overall dependency was investigated. In case of broader range of analyzed concentrations, maximum value of such dependency was observed [36]. This was similar to relationship observed in my experiments. For NaNO_3 solution and applied voltage of 10 V and 100 kHz, maximum repulsion force was present at concentration of ions of around 10 mM. This was caused by two counteracting effects. For small concentrations the amount of ions was too low to generate any effective forces. With increasing concentration, number of ions started to be sufficient to cause measurable forces. Finally, at high concentrations effect decreased, most likely due to crowding of ions, which is known and well characterized phenomenon [6]. Crowding of ions was reported especially for highly concentrated electrolytes and large applied voltages ($100 k_B T/e \approx 2.5$ V at 25 °C), which was the case in the studied system [36], [37].

Presence of ions is intrinsic property of all aqueous solution. Even ultrapure water of pH 7.0 has 10^{-7} M of hydronium ions and 10^{-7} M of hydroxide ions. Thus, analysis of studied system with aqueous solution without any ions was not feasible. However, to obtain the lowest possible amount of ions, I performed measurement with deionized water. In this case no repulsion was observed (Figure 2.8).

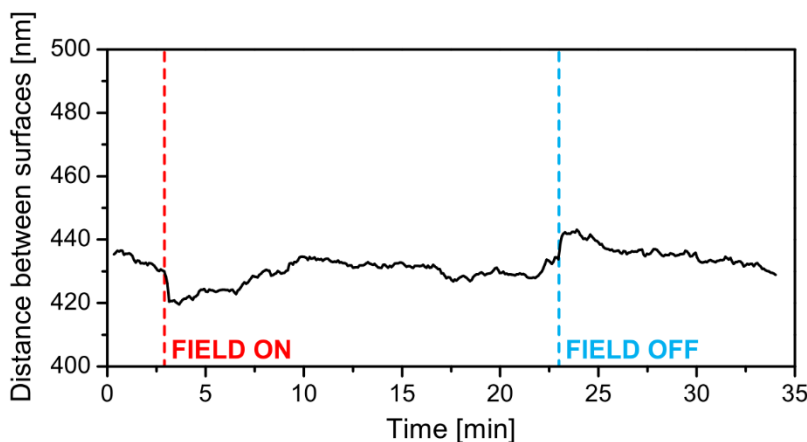


Figure 2.8 Application of AC voltage in system filled with deionized water. Measured change of distance between electrodes was in range of measurement error.

Upon application of the electric field, weak attraction was present, which was the expected result. Debye length of pure water is in range of 120 nm, which is roughly 5 times less than ideal 680 nm theoretically calculated for $2 \cdot 10^{-7}$ M of ions [38]. This is due to impurities and carbon dioxide which are adsorbed from air. Thus, in case of experiment showed in Figure 2.8, ends of diffusive parts of the electrical double layers overlapped and weak repulsion stable in time was observed. However, precise calculation of exerted force was not possible due to the fact, that change of distance between mica surfaces upon application of the electric field was in range of experimental error of constructed system. The only observation was that the attraction force was lower than 10 μ N. Nonetheless, performed experiment confirmed that presence of ions was crucial for analysis of strong repulsive effect and no repulsion was measured if amount of ions was too low.

2.2.6. Influence of distance between electrodes

Regardless of the complexity of the electrokinetic system, the effective electric field always depends on the applied voltage and the distance between electrodes. Thus, after previously described experiments, the next step was to analyze the influence of the distance separating the electrodes. In SFA experiments electrodes were covered with layers of mica, thus distance between silver electrodes and thickness of the solution were different. The crucial value was the distance between surfaces of mica (i.e. thickness of the electrolyte), as it was proven that observed phenomenon was caused by movement of ions inside the electrolyte. I performed the SFA experiments with various initial separations between mica surfaces. Forces were measured at final distance obtained after 15 min of application of the electric field. Thus, final separation was taken into account for comparison with measured forces (Figure 2.9). This test was performed for four different solutions. In each experiment the applied electric field was 10 V and 100 kHz (square waveform). Analyzed final distances ranged from 438 to 2684 nm. Smaller final separations could not be obtained due to strong

observed repulsion even in experiments with initial separation of 12 nm. On the other hand, larger distances were inaccessible due to limitations of MBI system.

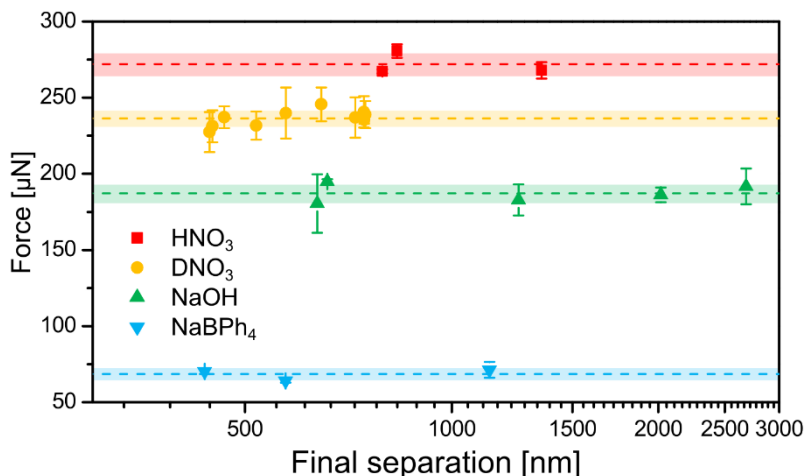


Figure 2.9 Comparison of final distances between mica surfaces and measured forces in case of four different ionic solutions. In case of every compound obtained force was independent from the separation between the surfaces. Dashed lines represent averaged forces and shaded areas show standard deviations.

Values of measured forces were independent from the final distance between surfaces. On first sight, this result was opposite to typical behavior of electrokinetic system. However, in case of the studied system, the effective electric field remained constant within the range of analyzed distances. In case of capacitor filled with mica and aqueous electrolyte, the effective electric field that gives a rise for movement of ions in the electrolyte is described by the equation:

$$E_i = \frac{V\varepsilon_c}{2c\varepsilon_i + s\varepsilon_c} \quad (2.6)$$

where E_i is the electric field inside electrolyte, V is applied voltage, ε_c is dielectric constant of mica, ε_i is dielectric constant of the electrolyte, c is thickness of mica, and s is distance between mica surfaces. Influence of change of the distance between mica surfaces on the effective electric field is presented in Figure 2.10. For mica of thickness of 3.5 μm and separations between 400 and 3000 nm the electric field changed by only 2.7%. Thus, this explained similar measured forces for different distances in the studied system.

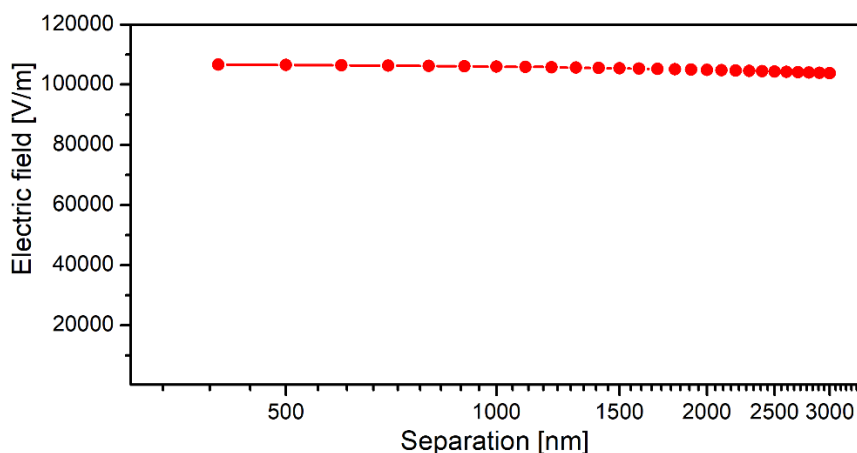


Figure 2.10 Influence of distance between mica surfaces on the effective electric field inside electrolyte in range of separations analyzed in the experiment showed in Figure 2.9.

2.2.7. Influence of frequency of applied alternating voltage

Frequency is second, besides amplitude, tunable parameter of the applied voltage. Thus, next stage of investigation of the studied effect was analysis of influence of frequency of the applied voltage on the measured force. Solutions of two compounds (NaNO_3 and Ph_4AsCl) of concentrations of 1 mM were used in these measurements. For each compound voltage of 10 V and various frequencies in range from 20 Hz to 500 kHz were applied. Obtained results are summarized in Figure 2.11. Repulsive forces observed in the system were very weakly dependent on the frequency of the applied voltage. In range of four orders of magnitude of frequency, observed forces decreased by only 30%. To better understand this dependency, detailed analysis of time constants of the studied effect had to be performed.

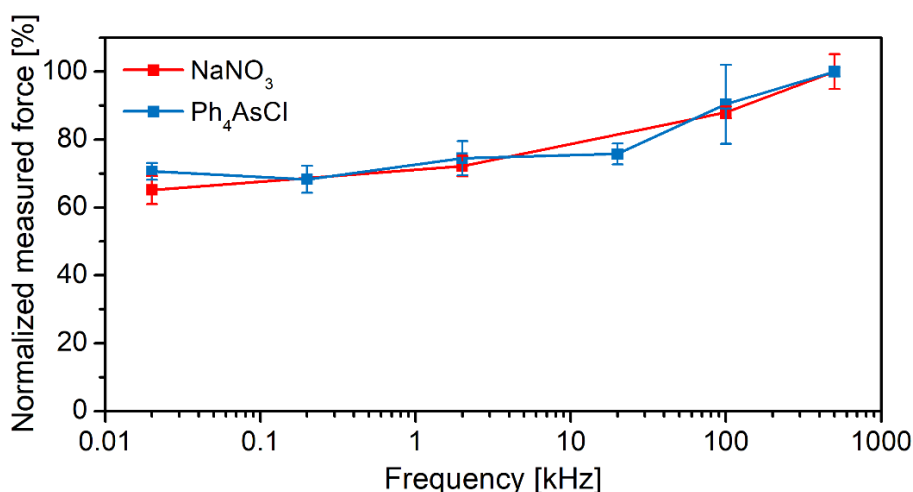


Figure 2.11 Dependency of measured repulsive forces from frequency of applied voltage. To enable comparison of results for both compounds, forces were normalized to value obtained for frequency 500 kHz.

2.2.8. Time scales of the observed effect

Next performed analysis was investigation of time scales of the observed phenomenon. For this purpose observed increase of distance upon application of the electric field was fitted using equation:

$$D = D_0 + D_1 \left(1 - \exp\left(\frac{t_0 - t}{\tau_D}\right) \right) \quad (2.7)$$

where D is distance between mica surfaces, D_0 is initial separation, D_1 is overall change of distance due to created force, t_0 is time of application of voltage, t is time in the experiment, and τ_D is time constant of the studied effect. Observed phenomena presented behavior similar to first-order linear time-invariant systems [39]. Thus, utilized equation was a solution of formula describing time-dependent behavior of such system. Representative example of such fitting in case of 1 mM solution of HNO_3 upon application of 10 V and 100 kHz voltage is presented in Figure 2.12. Fitted parameters were τ_D and D_1 . This comparison proved that selected equation properly described time development of analyzed repulsive effect.

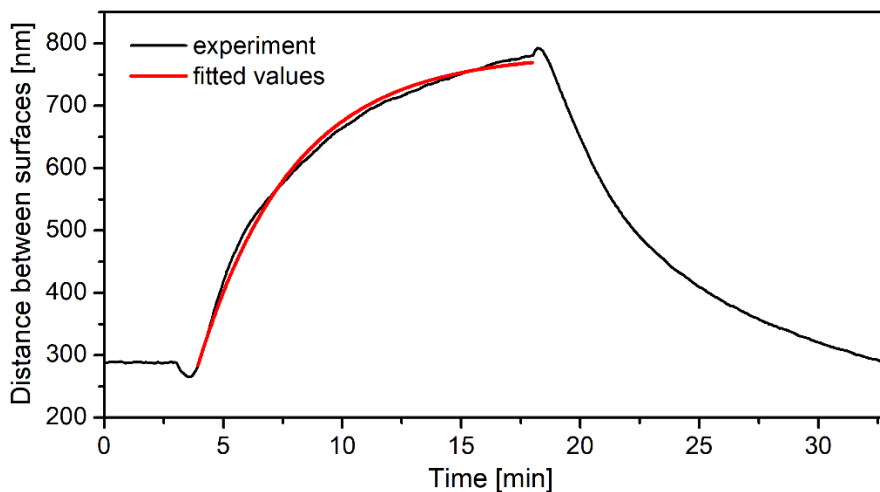


Figure 2.12 Comparison of experimental data and fitted line for measurement in 1 mM HNO_3 solution upon application of 10 V and 10 kHz alternating voltage. Fitted function was Equation 2.7. Obtained R-squared was 0.990.

Fitting procedure similar to presented in Figure 2.12 was performed for data obtained in various experiments. Different conditions of measurement were taken into account. In each case time constant of the effect was determined. Comparison of all time constants and parameters of the studied systems is provided in Figure 2.13. Obtained time scales were in range of few minutes and were independent from almost all characteristic parameters of the studied system, such as type of compound, concentration of ions, voltage, frequency, and separation between surfaces. Moreover, all calculated time scales were much longer than typically reported electrokinetic time scales (described in the first chapter of

this thesis). Even for the slowest ion and the largest distances typical time scales were in range of hundreds of microseconds. Detailed calculations are provided in section 2.4.4 of this chapter.

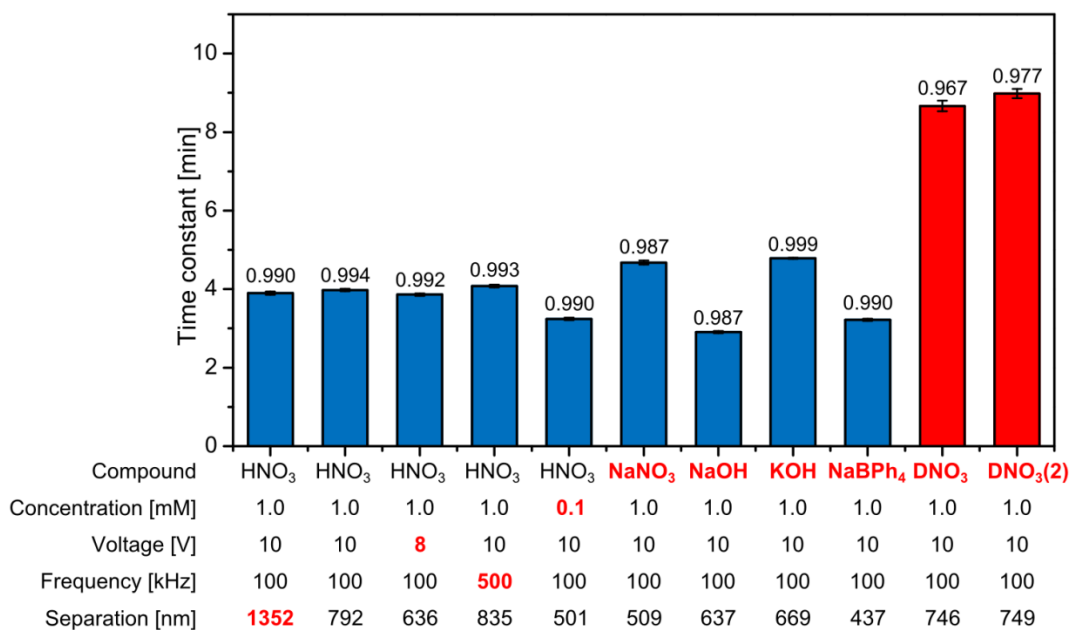


Figure 2.13 Summary of time constants calculated for various sets of parameters of observed phenomenon. Change of calculated time constant was caused only by the change of the solvent from regular to deuterated water. In case of DNO₃ two independent measurements were analyzed. R-squared of each fit is shown above respective column.

The only difference that was found in the calculated time constants was related to solvent of utilized solution. In case of deuterated water, time scale of the effect increased roughly two times. Diffusion coefficient of deuterated water is lower than regular one [40]. This indicated that the observed repulsive force was caused by the diffusion of water. This was in line with counterintuitively long time scales.

In case of studied system it was not trivial to determine its lateral size and thus the boundary between the gap and the bulk (Figure 2.2). However, it was reasonable to assume that this border occurred in place where distance between electrodes was 50 times longer than in the center of the system. In such case, according to Derjaguin approximation [1], in studied system (2 cm of radius of cylinders and 300 nm of distance between electrodes), water needed 4.26 min to diffuse from bulk to center of the gap [40]. This time was similar to the measured time constant. Thus, this additionally proved that effect which generates observed force was diffusion of water from bulk to the gap of the capacitor.

2.2.9. Long-time measurements

As a last part of the analysis of the studied phenomenon, I performed long-time measurement. For this purpose 1 mM HNO₃ solution was used. The experiment again was

composed of three stages: for the first 5 minutes distance was measured without the external electric field, then voltage (10 V, 100 kHz) was applied for 90 minutes, and finally the electric field was turned off and measurement was performed for next 90 minutes (Figure 2.14). Obtained results confirmed presence of plateau of observed effect. This plateau was located at the distance, where repulsive force equaled force exerted by the deflected spring, on which lower silica disc were mounted. Minor changes of distance visible between 60 and 90 minute and between 140 and 190 minute was caused by thermal fluctuations which were unavoidable in such long measurement.

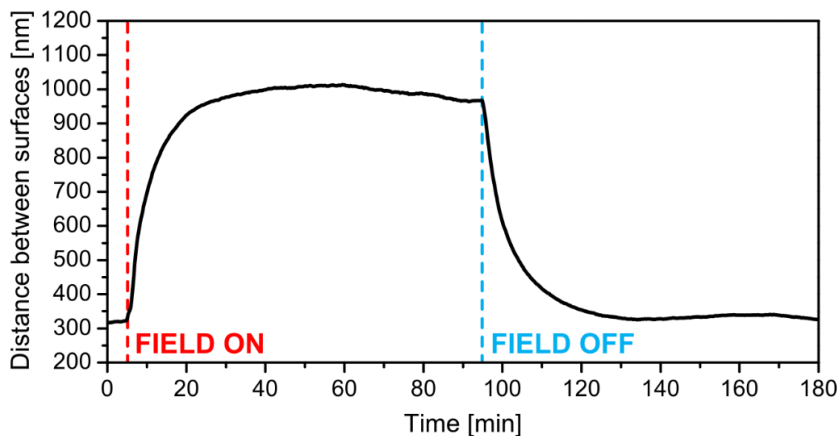


Figure 2.14 Long-time measurement performed in the studied system. The analysis confirmed presence of plateau of the effect.

2.2.10. Proposed explanation of the observed phenomenon

Electrokinetic phenomena can include very complicated non-linear effects. Thus, for their description many non-trivial aspects often have to be taken into account, such as unusual geometries, large AC voltages, unequal mobilities of ions, finite sizes of ions, and more. Observed unusual phenomenon of strong long-range repulsion between oppositely charged surfaces was a complex effect. Therefore, its precise and analytical explanation was obscured. However, due to wide range of analyzed parameters and determined dependencies, proposed explanation of measured data can be provided.

The observed effect is caused by the fluctuation of ions upon application of the alternating electric field. Unequal mobilities of ions create a situation in which faster ions accumulate in the vicinity of both electrodes. This effect is possible in wide range of frequencies of applied voltage. It was proven in literature, that such fluctuations of ions of different mobilities can even create long-range steady electric fields, which also could be a case in the studied system [32]. Such accumulation of ions increase osmotic pressure, which has to be compensated by the influx of water from the bulk towards center of the system. This generate repulsive force due to the fact, that water is incompressible. Studied electrokinetic effect scale with voltage squared, which is in line with the literature [31]. Moreover, differences in mobilities of ions are crucial for presence of the repulsive force,

which also corroborates discussed explanation. Proposed mechanisms explain also apparent mismatch between typically reported and measured time scales. In the observed phenomenon two distinct time scales are observed. First is related to the fluctuations of ions and building up of the osmotic pressure. It most likely happen within a second or even less. Due to time resolution of the surface forces apparatus, it is impossible to measure this effect. Second time scale is related to the diffusion of water towards the gap and, as was proven in this chapter, time scale of this effect is in line with measured time constants of the studied effect.

2.3. Conclusions

Despite being developed for over two centuries, electrokinetics is still considered to be enigmatic and full of unresolved issues. This specific field of science is a subtle mixture of fluid dynamics, mass transport and electrostatics and even nowadays it is considered to be area in which important and interesting findings are revealed every day.

Main goal of this chapter was to present and characterize unusual electrokinetic phenomenon of long-range repulsion between oppositely charged surfaces. Surfaces were separated with the electrolyte and isolated from the solution by mica layers. Strength, range and time scale of the studied effect were exceeding the values described in previous works. Effect was observed in separation ranging from 438 to 2684 nm. Time scale of few minutes was much longer than typical time development of electrokinetic processes. Moreover, the only parameter that strongly influenced time constant of studied system was type of utilized solvent. Repulsion was present in wide range of applied frequencies, but very pronounced dependency between concentration and differences of mobilities of utilized ions was developed.

Proposed explanation was based on performed measurements complemented with analysis of previously reported phenomena. Combination of the alternating electric field and unbalanced mobilities of ions resulted in a rise of the osmotic pressure, which was then compensated by the influx of water towards the center of the capacitor. Although provided description was in line with obtained data, detailed theoretical analysis would be very beneficial for further insight into reported phenomenon.

2.4. Materials and methods

2.4.1. Materials

All chemicals were purchased from Carl Roth (Germany) and were used without further purification. Aqueous solutions were prepared with MiliQ water of resistivity of 18.2 M Ω ·cm at 25 °C. Solutions of two compounds: DNO₃ and NaOD were prepared with deuterated water.

2.4.2. Surface forces apparatus

To prepare the SFA system, two freshly cleaved molecularly smooth pieces of mica of thickness ranging from 3.28 to 4.03 μm were utilized. First, 40 nm layers of silver were thermally evaporated on mica pieces. Next, pieces were glued with thermosetting Epikote 1004 on a silica cylindrical discs of normal radius of curvature 2 cm. To provide electrical contact, thin stainless electrodes were placed between epoxy resin and silver layer. Then, prepared pair of discs was mounted in crossed-cylinder geometry in surface forces apparatus setup. The bottom disc was placed on a spring of calibrated spring constant. The top one was mounted in piezoelectric holder that enable controlled movement of the disc. Then, chamber in which both discs were placed was filled with 50 ml of water or electrolyte, so that both discs were fully immersed. Temperature was set at constant value of 25 $^{\circ}\text{C}$. Next, mica surfaces were brought together at the controlled distance and capacitor between electrodes was created.

In described system silver layers served as both semi-transparent silver mirror and electrodes for generation of the external electric field. For precise sub-nanometric measurement of distance between electrodes the multiple beam interferometry (MBI) was used. In TRIAX Imaging Spectrograph (Jobin Yvon), wavelengths, which experienced constructive interference between mirrors, were spectrally resolved as fringes of equal chromatic order (FECO). Finally, FECO fringes were used to calculate the distance between mica surfaces [26].

Second application of silver layers was electrodes of the capacitor. Silver layers were connected through stainless steel electrodes and thin isolated wires to the power supply (Elektro-Automatik) and alternating electric voltage was applied. It was checked before measurement that attached wires do not influence movement of both discs and the spring.

2.4.3. Calculation of the force

To calculate the forces created in the SFA system, changes of distance between the mica surfaces were analyzed. After every measurement difference between initial distance and maximum value of the separation was determined (Figure 2.15). Then, based on spring constant, which in studied case was 530 N/m, difference in distances was used to calculate the force according to the equation:

$$F = k \cdot \Delta d \tag{2.8}$$

where F is calculated force, k is spring constant, and Δd is difference between initial and maximum separation.

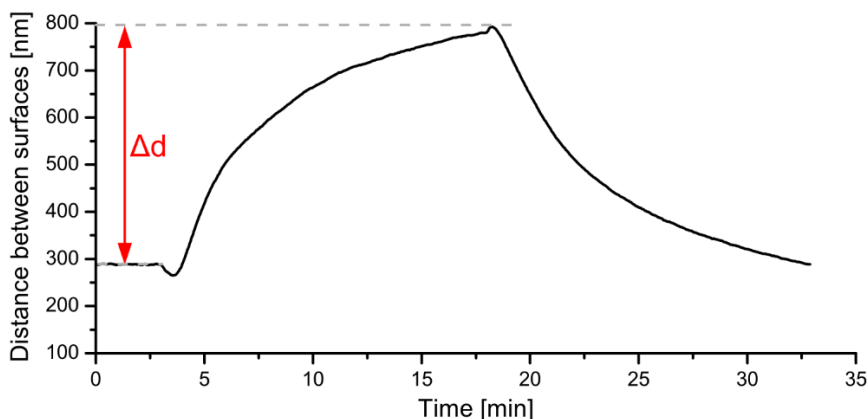


Figure 2.15 Representative performed measurement. Difference between initial and maximum separation was taken into account to calculate effective force exerted in the system.

2.4.4. Calculation of typically reported time scales

Most commonly reported time scales were calculated for experiments described in Figure 2.13. Mobilities of slower ions were taken into account to analyze longer values of time scales. Parameters of performed measurements as well as obtained time constants are summarized in Table 2.2. Calculated time scales were orders of magnitude smaller than values observed in the experiments.

Table 2.2 Summary of typically reported time scales calculated for parameters utilized in studies system. If not stated otherwise, all experiments were performed in 1 mM solutions upon application of 10 V and 100 kHz. In case of DNO_3 two independent measurements were analyzed.

Compound	Diffusion coefficient of slower ion (D) [10^{-9} m ² /s]	Separation (d) [nm]	Debye length (λ_D) [nm]	Time scales		
				λ_D^2/D [ns]	$(\lambda_D \cdot d)/D$ [μ s]	d^2/D [μ s]
HNO_3	1.90	1352	9.61	48.64	6.84	963
HNO_3	1.90	792	9.61	48.64	4.01	331
HNO_3	1.90	636	9.61	48.64	3.22	213
HNO_3	1.90	835	9.61	48.64	4.23	367
HNO_3 (0.1 mM)	1.90	500	30.40	486.40	8.02	132
NaNO_3	1.34	509	9.61	68.97	3.65	194
NaOH	1.34	637	9.61	68.97	4.57	303
KOH	1.95	669	9.61	47.39	3.30	230

NaBPh ₄	0.54	437	9.61	171.14	7.78	353
DNO ₃	1.90	746	9.61	48.64	3.78	293
DNO ₃ (2)	1.90	749	9.61	48.64	3.79	295

2.4.5. Calculation of diffusion of water in the studied system

Surface forces apparatus setup had a geometry of crossed cylinders. According to Derjaguin approximation [1], if radius of cylinders is much bigger than distance between them, such geometry can be represented as sphere over a plane, as presented in Figure 2.16. Distance between surfaces in any given point can be correlated with equation:

$$s = \sqrt{a^2 - (a - H + h)^2} \quad (2.9)$$

where s is lateral distance between point of the closest approach and point of interest, a is radius of the cylinder, h is distance between surfaces in the point of the closest approach, and H is distance between surfaces in a point of interest, as presented in Figure 2.16.

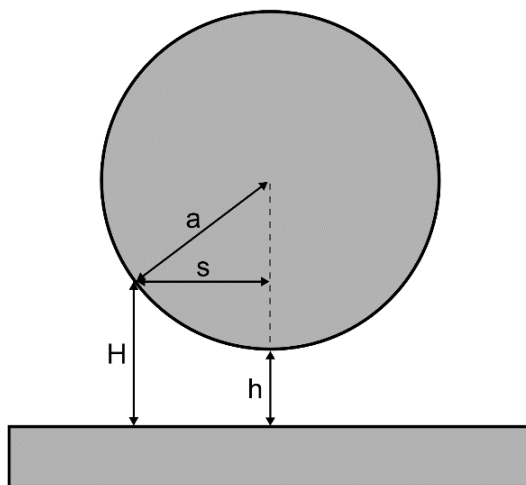


Figure 2.16 Schematic representation of geometry of sphere over a plane.

It was reasonable to assume that boundary between gap and the bulk in studied SFA setup was in the place where distance between surfaces was 50 times larger than distance at the point of the closest approach. Then, lateral distance of the gap s can be calculated:

$$a = 2 \text{ cm} = 2 \cdot 10^4 \mu\text{m}$$

$$h = 300 \text{ nm} = 0.3 \mu\text{m}$$

$$H = 50 \cdot h = 15 \mu\text{m}$$

$$s = 766.7 \mu\text{m}$$

Diffusion coefficient of water equals $2.29 \cdot 10^{-9}$ m²/s, thus time of diffusion through such distance equals:

$$\tau_{H_2O} = \frac{s^2}{D_{H_2O}} \quad (2.10)$$

$$\tau_{H_2O} = 4.26 \text{ min}$$

2.5. References

- [1] J. H. Masliyah and S. Bhattacharjee, *Electrokinetic and colloid transport phenomena*. New Jersey: John Wiley & Sons, Inc., 2006.
- [2] F. Kremer and A. Schonhals, *Broadband Dielectric Spectroscopy*, 1st editio. Berlin: Springer Berlin Heidelberg, 2003.
- [3] M. S. Kilic, M. Z. Bazant, and A. Ajdari, “Steric effects in the dynamics of electrolytes at large applied voltages. I. Double-layer charging,” *Phys. Rev. E*, vol. 75, no. 2, pp. 1–16, 2007.
- [4] I. Borukhov, D. Andelman, and H. Orland, “Steric effects in electrolytes : a modified Poisson-Boltzmann equation,” *Phys. Rev. Lett.*, vol. 79, no. 3, pp. 435–438, 1997.
- [5] L. Højgaard Olesen, M. Z. Bazant, and H. Bruus, “Strongly nonlinear dynamics of electrolytes in large ac voltages,” *Phys. Rev. E*, vol. 82, no. 1, p. 011501, 2010.
- [6] M. Z. Bazant, M. Sabri Kilic, B. D. Storey, and A. Ajdari, “Nonlinear electrokinetics at large voltages,” *New J. Phys.*, vol. 11, no. 7, p. 075016, 2009.
- [7] M. Mittal, P. P. Lele, E. W. Kaler, and E. M. Furst, “Polarization and interactions of colloidal particles in ac electric fields,” *J. Chem. Phys.*, vol. 129, no. 6, p. 064513, 2008.
- [8] M. Z. Bazant, K. Thornton, and A. Ajdari, “Diffuse-charge dynamics in electrochemical systems,” *Phys. Rev. E*, vol. 70, no. 2, p. 021506, 2004.
- [9] T. M. Squires and M. Z. Bazant, “Induced-charge electro-osmosis,” *J. Fluid Mech.*, vol. 509, no. 509, pp. 217–252, 2004.
- [10] T. J. Woehl, B. J. Chen, K. L. Heatley, N. H. Talken, S. C. Bukosky, C. S. Dutcher, and W. D. Ristenpart, “Bifurcation in the steady-state height of colloidal particles near an electrode in oscillatory electric fields: Evidence for a tertiary potential minimum,” *Phys. Rev. X*, vol. 5, no. 1, pp. 1–11, 2015.
- [11] A. Ramos, H. Morgan, N. G. Green, and A. Castellanos, “AC electric-field-induced fluid flow in microelectrodes,” *J. Colloid Interface Sci.*, vol. 217, no. 2, pp. 420–422, 1999.
- [12] M. Z. Bazant and T. M. Squires, “Induced-charge electrokinetic phenomena: theory and microfluidic applications,” *Phys. Rev. Lett.*, vol. 92, no. 6, pp. 1–4, 2004.
- [13] A. Ajdari, “Pumping liquids using asymmetric electrode arrays,” *Phys. Rev. E*, vol. 61, no. 1, pp. 45–48, 2000.
- [14] C. S. Mangelsdorf and L. R. White, “Dielectric response of a dilute suspension of spherical colloidal particles to an oscillating electric,” *J. Chem. Soc. Faraday Trans.*, vol. 93, no. 17, pp. 3145–3154, 1997.
- [15] J. E. Hinch, J. D. Sherwood, W. C. Chew, and P. N. Sen, “Dielectric response of a dilute suspension of spheres with thin double layers in an asymmetric electrolyte,” *J. Chem. Soc. Faraday Trans. 2 Mol. Chem. Phys.*, vol. 80, pp. 535–551, 1984.
- [16] O. Schnitzer and E. Yariv, “Nonlinear oscillations in an electrolyte solution under ac voltage,” *Phys. Rev. E - Stat. Nonlinear, Soft Matter Phys.*, vol. 89, no. 3, pp. 7–10, 2014.
- [17] R. F. Stout and A. S. Khair, “Moderately nonlinear diffuse-charge dynamics under an ac voltage,” *Phys. Rev. E*, vol. 92, no. 3, p. 032305, 2015.
- [18] P. Garcia-Sanchez and A. Ramos, “Flow reversal in traveling-wave electrokinetics: an analysis of forces due to ionic concentration gradients,” *Langmuir*, vol. 25, no. 9, pp. 4988–4997, 2009.

- [19] B. Balu and A. S. Khair, "Role of Stefan-Maxwell fluxes in the dynamics of concentrated electrolytes," *Soft Matter*, vol. 14, no. 41, pp. 8267–8275, 2018.
- [20] C. L. Wirth, P. J. Sides, and D. C. Prieve, "Electrolyte dependence of particle motion near an electrode during ac polarization," *Phys. Rev. E*, vol. 87, no. 3, p. 032302, Mar. 2013.
- [21] V. A. Parsegian and D. Gingell, "On the electrostatic interaction across a salt solution between two bodies bearing unequal charges," *Biophys. J.*, vol. 12, no. 9, pp. 1192–1204, 1972.
- [22] H. Aranda-Espinoza, Y. Chen, N. Dan, T. C. Lubensky, P. Nelson, L. Ramos, and D. A. Weitz, "Electrostatic repulsion of positively charged vesicles and negatively charged objects," *Science (80-.)*, vol. 285, pp. 394–397, 1999.
- [23] K. Besteman, M. A. G. Zevenbergen, H. A. Heering, and S. G. Lemay, "Direct observation of charge inversion by multivalent ions as a universal electrostatic phenomenon," *Phys. Rev. Lett.*, vol. 93, no. 17, p. 170802, 2004.
- [24] M. Trulsson, B. Jönsson, T. Åkesson, J. Forsman, and C. Labbez, "Repulsion between oppositely charged surfaces in multivalent electrolytes," *Phys. Rev. Lett.*, vol. 97, no. 6, p. 068302, 2006.
- [25] C. Drummond and M. Ruths, "Surface forces apparatus," in *Encyclopedia of Nanotechnology*, Bhushan B., Ed. Dordrecht: Springer, 2012, pp. 2574–2582.
- [26] M. Heuberger, "The extended surface forces apparatus. Part I. Fast spectral correlation interferometry," *Rev. Sci. Instrum.*, vol. 72, no. 3, pp. 1700–1707, 2001.
- [27] J. Israelachvili, Y. Min, M. Akbulut, A. Alig, G. Carver, W. Greene, K. Kristiansen, E. Meyer, N. Pesika, K. Rosenberg, and H. Zeng, "Recent advances in the surface forces apparatus (SFA) technique," *Reports Prog. Phys.*, vol. 73, p. 036601, 2010.
- [28] C. Drummond, "Electric-field-induced friction reduction and control," *Phys. Rev. Lett.*, vol. 109, p. 154302, 2012.
- [29] K. Kristiansen, H. Zeng, B. Zappone, and J. N. Israelachvili, "Simultaneous measurements of molecular forces and electro-optical properties of a confined 5CB liquid crystal film using a surface forces apparatus," *Langmuir*, vol. 31, no. 13, pp. 3965–3972, 2015.
- [30] R. Tivony, D. Ben Yaakov, G. Silbert, and J. Klein, "Direct observation of confinement-induced charge inversion at a metal surface," *Langmuir*, vol. 31, no. 47, pp. 12845–12849, 2015.
- [31] B. J. Kirby, *Micro- and nanoscale fluid mechanics*. Cambridge University Press, 2010.
- [32] S. M. H. M. H. Hashemi Amrei, S. C. Bukosky, S. P. Rader, W. D. Ristenpart, and G. H. Miller, "Oscillating electric fields in liquids create a long-range steady field," *Phys. Rev. Lett.*, vol. 121, no. 18, p. 185504, 2018.
- [33] M. Trulsson, B. Jönsson, T. Åkesson, J. Forsman, and C. Labbez, "Repulsion between oppositely charged macromolecules or particles," *Langmuir*, vol. 23, no. 23, pp. 11562–11569, 2007.
- [34] B. D. Storey and M. Z. Bazant, "Effects of electrostatic correlations on electrokinetic phenomena," *Phys. Rev. E - Stat. Nonlinear, Soft Matter Phys.*, vol. 86, no. 5, pp. 1–11, 2012.
- [35] V. Studer, A. Pépin, Y. Chen, and A. Ajdari, "An integrated AC electrokinetic pump in a microfluidic loop for fast and tunable flow control," *Analyst*, vol. 129, no. 10, pp. 944–949, 2004.

- [36] M. Z. Bazant, M. S. Kilic, B. D. Storey, and A. Ajdari, "Towards an understanding of induced-charge electrokinetics at large applied voltages in concentrated solutions," *Adv. Colloid Interface Sci.*, vol. 152, no. 1–2, pp. 48–88, 2009.
- [37] M. Z. Bazant, B. D. Storey, and A. A. Kornyshev, "Double Layer in Ionic Liquids: Overscreening versus crowding," *Phys. Rev. Lett.*, vol. 106, no. 4, p. 046102, 2011.
- [38] U. Raviv, P. Laurat, and J. Klein, "Fluidity of water confined to subnanometre films," *Nature*, vol. 413, no. 6851, pp. 51–54, 2001.
- [39] "Analytical solutions for first-order LTI systems." [Online]. Available: <http://www.dartmouth.edu/~sullivan/22files/1storder.pdf>. [Accessed: 23-Apr-2019].
- [40] R. Mills, "Self-diffusion in normal and heavy water in the range 1-45.deg.," *J. Phys. Chem.*, vol. 77, no. 5, pp. 685–688, 1973.

Chapter 3

Deposition of the analytes in the electric field for SERS technique

Parts of this chapter are published as:

Ł. Richter, J. Paczesny, M. Książopolska-Gocalska, R. Hołyst, „Method for deposition of analyte from solution onto the substrate for surface-enhanced spectroscopy in the electric field” (no **P.412548**, submitted **02.06.2015**)

3.1. Introduction

The ultimate goal of all techniques of sensing and biosensing is to detect single molecule or object selectively from complex matrix in the most rapid, easy, repeatable and inexpensive way. Very common structure of sensor consists of the sensing layer combined with the transducer. Examples include quartz crystal microbalance [1], optical fibers [2], electrochemistry [3], surface enhanced luminescence [4] or fluorescence [5], surface plasmon resonance [6], localized surface plasmon resonance [7] and surface enhanced Raman scattering [8]. All above-mentioned methods are similar in one important aspect: they require proximity of the detected analyte and sensing surface. Thus, to obtain useful analytical method it is required not only to have efficient sensing layer combined with sensitive transducer that can generate signal even from single molecules but also to ensure presence of analyte on such surface. Therefore, precise and well-controlled deposition of an analyte on the sensing surface is one of the most important aspects of the whole detection process. It is crucial especially in case of very low concentrations of the analyte. Surprisingly, development of new methods of proper, fast and efficient deposition of analyte is often omitted by community and thus still poorly addressed. In this chapter I presented versatile method of deposition of analytes in the electric field, which was applied to improve surface enhanced Raman spectroscopy (SERS).

3.1.1. Surface-enhanced Raman spectroscopy

Raman scattering was first reported by Raman and Krishnan in 1928 [9]. Raman spectroscopy is a method providing information about structure of the molecule. When light interacts with a molecule, the latter is promoted to virtual energy state. The largest part of incident light is scattered without changing its energy (and thus also frequency and wavelength are constant). This is because the initial and final vibrational energy states are the same. This is Rayleigh (elastic) scattering. Very rarely (approximately one in a million events) the molecule ends up in different (comparing to initial) vibrational state upon relaxation from virtual energy state. Therefore, scattered photons have different energy than incident beam. Such phenomena is called Raman scattering. Difference between energies of incident and Raman scattered light is characteristic for given functional group, as it is related to vibrational energy states [10]. Therefore it can be used for identification of molecules in samples. On the other hand the intensity of the signal might be of importance for quantitative or semi quantitative analysis.

Although Raman scattering can be potentially used as technique for detection and identifications of many compounds, unfortunately number of photons scattered in inelastic way (Raman scattering) is very small. Therefore, large concentrations of analyzed compound need to be used to obtain reliable data. In 1974, many years after the first discovery of Raman scattering, Fleischmann et al. described very strong Raman scattering from pyridine adsorbed on silver electrodes [11]. After two years it was proved independently by Jeanmaire and Van Duyne [12], as well as by Albrecht and Creighton [13].

This phenomenon is called surface-enhanced Raman scattering, and technique based on it – surface enhanced Raman spectroscopy (SERS).

Theoretical explanation of such enhancement of a signal coming from molecule adsorbed on the metal surface was proposed by Moskovits in 1979 [14]. Currently it is believed that high enhancement of the signal in SERS technique is caused by surface plasmon resonance at the surface of the substrate. Plasmons are collective oscillations of free electron gas density, which could be excited by the incident light (Figure 3.1). The interactions between electromagnetic field, plasmons and molecules of interest cause the enhancement of Raman signal. The exact mechanism is still discussed. Spots on a surface of SERS substrate with especially high signal enhancement are called *hot spots*. Hot spots occur within interstitial crevices in metal structures [15]. In such places enhancement might be extraordinary, even up to 15 orders of magnitude [16]. Therefore, the higher number of hot spots present on the surface, the better SERS substrate performs.

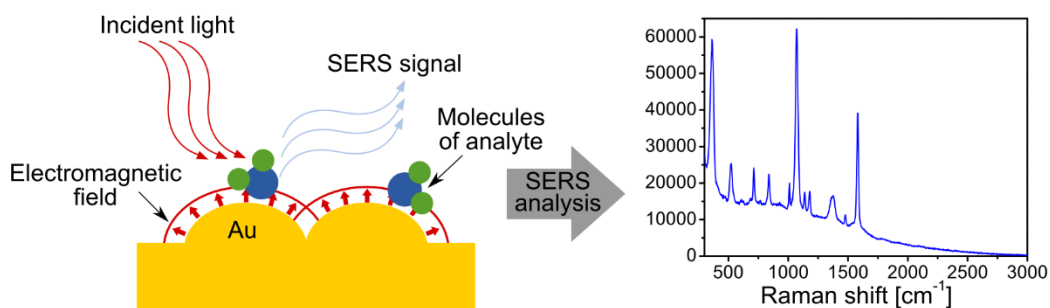


Figure 3.1 Schematic representation of surface enhanced Raman spectroscopy. The interaction between incident light, plasmons of metal structures and deposited molecules results in enhancement of Raman scattering and can be detected in SERS technique.

Currently SERS is considered a highly promising technique, which allows for simultaneous detection of many non-labeled molecules. SERS enables enhancement of the signal in a range of orders of magnitude (10^2 - 10^6 , in some cases even 10^8 - 10^{15}) and it provides possibility of detection of single molecules [17]. Enhancement factor is defined as

$$EF = \frac{I_{SERS}/N_{Surf}}{I_{RS}/N_{Vol}} \quad (3.1)$$

where I_{SERS} is a SERS signal; N_{Surf} is the average number of adsorbed molecules in the scattering volume for the SERS experiments; I_{RS} is Raman signal under non-SERS conditions and N_{Vol} is the average number of molecules in the scattering volume for the Raman (non-SERS) measurement [18].

At the beginning most SERS surfaces gave unrepeatable results. Therefore, till the end of twentieth century, SERS technique was mostly a curiosity, without almost any practical application. Moreover, to this day there is still no unified model that properly describes SERS phenomena [19]. But even despite these drawbacks, recent rapid progress in nanotechnology enables manufacturing of new, specialized SERS surfaces. Many

applications of SERS was described in literature, ranging from archeology [20], analysis of works of art [21], forensic science [22], detection of bioterrorist threats [23], diagnosis of diseases [24], detection of bacteria [25] and viruses [26] and more.

There are two main ways for preparation of efficient SERS substrates:

- 1) “Top-down” methods are chemical and physical processes that in general require macroscopic equipment to create nano-scale devices. One of the most straightforward examples is high energy milling for preparation of nanoparticles. Another example of “top-down” approach is patterning on large scale while reducing the lateral dimensions to the nanoscale (lithographical techniques) [27]. They provide high reproducibility and allow good control over the geometrical parameters. However such methods are time-consuming. Moreover, the cost of miniaturization associated with lithography equipment can create financial barrier, especially in a large scale approach.
- 2) To overcome the limitations of “top-down” methods, there is a great interest in development of “bottom-up” approach. In such methods, single atoms, molecules or nanoparticles assemble into more complex nanostructures due to precisely controlled chemical reactions or self-assembly driven by specific interactions and properties of properly designed building blocks (small portions of matter). One example is exploitation of wet chemistry to create plasmonic metal nanoparticles [28]–[30]. Due to specific way of preparation of SERS substrates, these methods are inexpensive, however provide less control over the preparation process comparing to “top-down” methods.

Despite great number of scientific reports published on SERS, there are still barely any real-life applications of SERS. All of these efforts to create sensitive SERS surfaces are necessary, yet insufficient to obtain good, reliable and reproducible SERS analysis. Despite having ideal, homogeneous, good-enhancing substrate, molecules of analyzed compound could still concentrate in one area, instead of being homogeneously deposited or could be so rarely distributed, omitting majority of hotspots, that obtained signal is too weak to be recorded. Thus, even the best substrate with the best enhancement factor will be ineffective, if we do not properly apply the analyte on its surface. Efforts to create best SERS substrates have to be accompanied by development of efficient methods of application of the analyte on such surfaces. However, very little attention has been paid to this problem. Typical characteristics of a procedure of SERS-based analysis are: 1) large volumes of analyzed samples; 2) long time of deposition of an analyte on the surface (commonly dozens of hours; it is the longest part of the whole analysis procedure); 3) high concentration of an analyte in the sample. Last two issues are connected to the fact, that deposition of molecules is usually based only on the diffusion and there is a need for the system to equilibrate. Although in the whole sample a sufficient number of molecules to cover the whole surface is present, the process is restricted and not enough molecules are deposited on the surface of the substrate. Usually higher concentrations of analyte or longer times are needed to

enhance the deposition process, what is in stark contrast with need for fast ultrasensitive analysis.

One of the possibility to improve deposition of analyte on SERS substrates is utilization of the electric field. As plenty of molecules and objects are charged, especially in aqueous solutions (except narrow cases of isoelectric point, etc.), the electric field seems to be promising solution. The idea of combining the electric field and SERS technique was partially exploited [31]. However, the electric field was initially used mostly to enhance and modulate the signal coming from the molecules already present on the SERS surface. In this approach, called electric field induced SERS, the application of static or oscillating electric field can change the Raman spectrum in two different ways [32], [33]. First, the electric field can give rise to an electro-optical interaction and as a result mix stationary states of the molecules. Secondly, molecules with dipole moment can interact with the electric field and give an anisotropic distribution of orientations in the solution. This can result in changes of intensities of Raman shifts. Few practical applications of electric field induced SERS can be found in literature. For instance Walia et al. showed that depending on frequency of applied electric field thiophenol can be selectively detected from mixture of other molecules [34]. The same group performed also detailed analysis of influence of low frequency oscillating electric fields on the SERS spectra of thiophenol [35]. Moreover, very recently Almohammed et al. proved that this approach can improve performance of peptide nanotube-graphene oxide SERS substrates in detection of various biomolecules [36].

Although electric field induced SERS is interesting approach, I wanted to use the application of voltage in a different way. The electric field can be applied as a driving force to draw analyte onto the surface. One of example of such approach was proposed around 10 years ago by Lacharmoise et al. [37]. The Authors applied constant electric field between parallel electrodes, which allowed for “guiding” the dyes of a given charge towards the SERS-active surface. As a result selective enhancement of different types of dyes according to their charge was possible. Very similar approach was proposed a few months later by Cho et al. [38]. Their system was composed of two electrodes: wire and SERS substrate. In such system electrophoresis of adenine towards SERS-active surface in constant electric field allowed for increase of signal 51 times after 25 min. Electrokinetic preconcentration was also proved to be useful in detection of such molecules as serotonin, Congo red dye or Rhodamine 6G. For this purpose the nanogap-rich silver nanoislands on glass nanopillar arrays were used [39].

Combination of SERS and the electric field was also used in lab-on-a-chip devices. For instance device composed of chip with microwells enabled detection of viral DNA. Properly designed electrodes allowed for local attraction or repulsion of different viral species from solution, increasing the selectivity [40]. Other lab-on-a-chip system was shown by Liu et al. [41]. They showed an photonic-plasmonic hybrid type Raman nanosensor integrated with electrokinetic manipulation. The applied electric field not only assembled the plasmonic nanocapsules on the photonic crystal slabs, but also focused analyte

molecules to the hot spots. Besides direct electrophoresis, also other electrokinetic mechanisms were used to selectively concentrate analyte on SERS surfaces. For example in work of Cheng et al. AC electric field induced electrokinetic forces (ACEK) were used to separate and concentrate bacteria from blood for on-chip SERS analysis.

All of these electric field-based methods share a number of drawbacks that hinders broad practical implementation. First, in all cases deposition in the electric field and SERS measurements were combined and performed simultaneously in the solution and in the same device. Such approach, although useful in initial development of the method and detailed analysis of influence of the electric field on SERS signal, is difficult to implement in everyday use. Typically used equipment for SERS is not designed for this type of measurement. Secondly, in all of the above-described cases both electrodes were not isolated and were in direct contact with the solution. This can cause electrochemical reactions to occur. They can be beneficial in some cases [18], but in general they can change the SERS surface and possibly cause its deactivation. Moreover, redox reactions can modify or even destroy the analyzed molecules. Such situation forces utilization of low potentials and even then it is not certain that no redox reactions are present. Finally, every developed approach is focused on only one or just few similar analytes. To date, there is no comprehensive analysis that examines and confirms robustness and versatility of deposition of many different compounds in the electric field. In this chapter I will present the method to deposit the analyte on the SERS surface that omits these problems. Developed solution allows for deposition of numerous analytes during short process performed separately and before SERS analysis. Moreover, one of the electrode is isolated, thus no Faradaic currents flow through the system.

3.2. Results and discussion

In typically performed SERS analysis deposition of the analyte usually takes several hours and even then obtained results can be heterogeneous within single sample and across the samples. Main goal of this chapter was to create a method for fast deposition of the molecules on SERS surfaces to obtain reliable and homogenous readout. Important issue was to deposit the analyte in single step in separate device to easily combine it with final SERS analysis.

3.2.1. Process of deposition of analytes in the electric field

The deposition process was performed separately from SERS analysis in the specially designed cell, which was made from polytetrafluoroethylene (PTFE) and was basically a cube with properly shaped pocket. Cell was designed to be robust and simple and to allow for convenient exchange of SERS surface, counter electrode and solution of analyte. Counter electrode was glass substrate covered with indium tin oxide (ITO). To avoid flow of faradaic currents, it was isolated with PTFE separator of thickness of 200 μm . Both electrodes were connected via copper tape to the function generator that allowed application

of proper voltage waveform. If not stated otherwise, in typical procedure analyte was deposited from 50 μl of solution upon application of square voltage of 10 V and given frequency (the only variable beside polarity of the potential) for 5 minutes. Distance between electrodes was 1 mm. After deposition step, SERS substrate was removed from the cell, dried in the open air and standard SERS analysis was performed. Obtained spectra that are presented on the plots in this chapter are shifted in Y axis for clarity of the presentation. Thus, only intensities of the peaks with respect to their base line should be used for comparison with other data.

In my experiments I used aqueous solutions of variety of analytes and additional components, such as small amounts of organic solvents or buffers. Therefore, studied system was in fact a capacitor filled with the electrolyte. Immediately after application of voltage to the electrodes, the electric field appeared in the solution. Then, the charged species present in the solution (hydrogen and hydroxide ions, analytes, buffering ions, etc.) moved according to the electric field and created the electrical double layers (EDLs). As a results, the effective electric field in solution decreased in time and eventually became screened by the charged species. After that, no electric field was present in the bulk and thus no additional drag of the analyte occurred.

To solve this problem, I applied alternating electric field that oscillated between zero and maximum designed potential. I used square waveform of the applied voltage. Due to isolation utilized to avoid Faradaic currents, behavior of the system was very similar to the symmetrical alternating current electrophoretical deposition (symmetrical AC EPD), described in first chapter of this thesis. At the beginning of each pulse the effective electric field appeared in the solution and molecules were dragged to the surfaces via electrophoresis. Next, decrease of the potential at the end of every pulse also created the electric field but oppositely directed. Molecules were repelled from the surface, however, some of them stayed adsorbed and did not detach from the silver SERS-active surfaces. It is known that many chemical groups, such as thiols, amines or carboxyl groups can adsorb on the silver surfaces and create monolayers [42]. Therefore, the molecules were in fact scavenged from the vicinity of such SERS substrate. This was regenerated as abundance of molecules, even for low initial molar concentrations (for example 10^{-6} M is $6 \cdot 10^{17}$ molecules/l), was available in bulk, from where analyte diffused towards the depletion zone (due to differences in chemical potentials) and new equilibrium was established. In the next pulse these new molecules could be again deposited onto the SERS surface. Many cycles of such step-by-step deposition allowed for efficient deposition of target molecules on the SERS substrates.

Key aspect of the deposition process was polarization of SERS substrate. Two ranges of applied potential were used: oscillations between 0 V and +10 V or between -10 V and 0 V. To effectively drag desired molecules towards SERS substrate, potential applied to the SERS surface had to be opposite to charge of the molecule. For every deposited analyte, structure of the molecule was analyzed and polarization of applied voltage was

chosen according to present chemical groups. pH of all utilized solutions was in range between 6.0 and 7.5, thus most common groups that provided charge were amines, phosphate and carboxyl groups. Thus if groups such as amines were in majority, negative potential was applied. In case of majority of carboxyl and phosphate groups – positive potentials were used. This simple division was later confirmed by comparison of positive and negative applied potentials (section 3.2.8) and by analysis of electrophoretic mobility described in section 3.2.7.

Number of various analytes was deposited in the electric field. For each experiment, two types of control measurements were used. To check the actual effect of the applied electric field and not confinement or other factors related to deposition in specially designed cell, a control deposition of the analyte according to developed approach but without application of the electric field was performed. Secondly, also standard SERS protocol was used, i.e. SERS substrate was immersed in solution of the analyte for 20 hours and then SERS signal was collected. My goal was to obtain similar or even better result in several minutes.

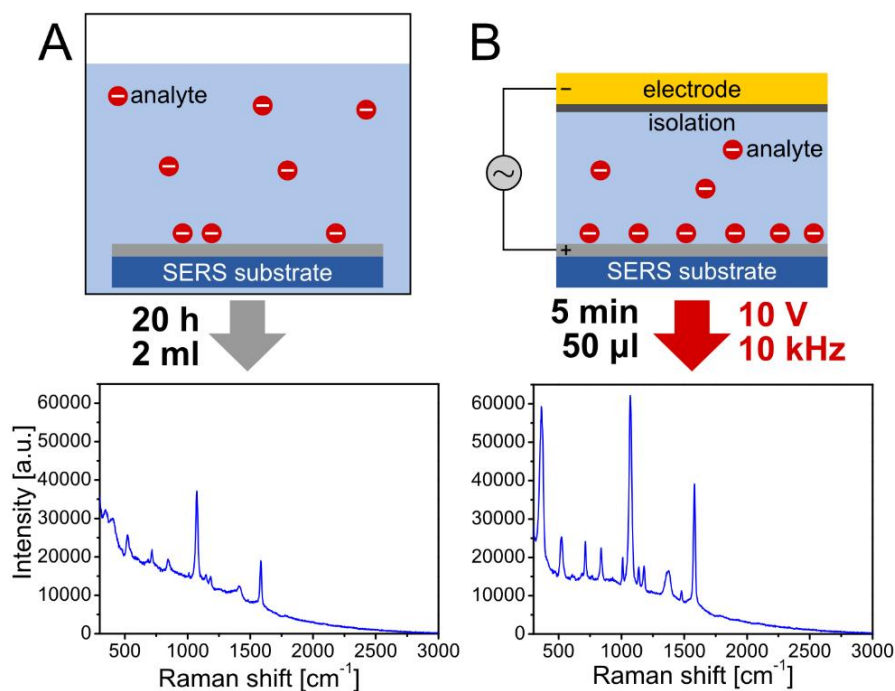


Figure 3.2 Comparison of standard and improved SERS protocol. Spectra obtained for para-mercaptobenzoic acid (PMBA, 10^{-6} M) with (A) typical method and (B) newly designed approach. Prepared method was based on electrophoretic deposition of analyte in alternating electric field. It was possible to decrease both time and volume of sample and nonetheless to obtain two times higher analytical signal.

As a benchmark para-mercaptobenzoic acid (PMBA) was used. PMBA is model molecule in SERS technique due to its well defined peaks in Raman spectra [43]–[45] and presence of thiol group that provides attachment to metal SERS-active surfaces [46]. PMBA

was also useful from the point of view of deposition in the electric field, as it has a carboxyl group that provides charge in pH above 4.8 [47]. Thus in used solution of pH 6.0, PMBA was negatively charged. It was proved that deposition of PMBA in prepared cell upon application of square voltage (+10 V, 10 kHz) allowed for decrease of time from 20 h to 5 min, reduction of volume from 2 ml to 50 μ l and nonetheless obtained SERS spectra had two times higher intensities of peaks.

3.2.2. Time of the deposition

One of the most crucial aspects of SERS technique is time of the deposition of the analyte. Longer times should be more favorable, as more analyte can be accumulated on the surface. On the other hand, after long enough period of time surface can saturate with analyte or amount of molecules remained in the solution will be too small to make any additional contribution in layer adsorbed on SERS substrate. To analyze this parameter, I deposited PMBA molecules without application of the electric field for 1, 5, 15 and 30 minutes and compared them with results obtained for 20 hours. Increase of time of deposition resulted in increase of SERS signal (Figure 3.3). However, after 5 min of deposition improvement was not very significant. Therefore, 5 minutes were chosen as time of deposition for most experiments. This time is good balance between obtaining sufficient signal and keeping the time of the process as short as possible.

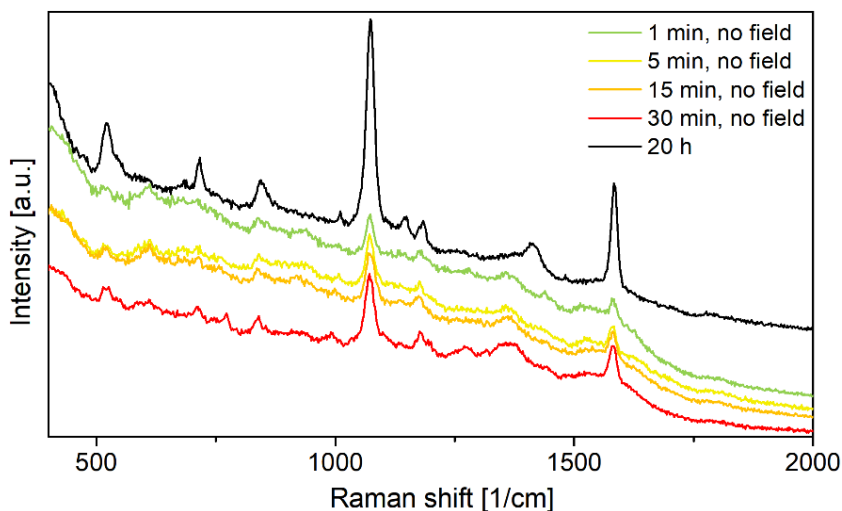


Figure 3.3 Comparison of different times of deposition of PMBA (10^{-6} M) without the electric field. As control measurement, standard procedure with 20-hour deposition was performed.

3.2.3. Influence of applied voltage

Second analyzed parameter was applied voltage. In the simplest case, the electric field depends linearly on applied voltage as $E = V/d$, where V is applied voltage and d is distance between electrodes. In case the studied system, the situation was more complex due to PTFE isolation and ions that screened the electric field over time by creating the electrical double layer. However, maximum value of the electric field that was present at the beginning of

every pulse should also be dependent on applied voltage. To check that, I deposited PMBA from solution of 10^{-6} M upon application of different voltages of 10 kHz frequency. Results are presented in Figure 3.4. As expected, the increased values of applied voltage improved deposition procedure. Higher potentials resulted in higher electric fields and faster electrophoresis of molecules of PMBA. As a consequence more molecules were deposited on the SERS surface and obtained signal was more intense. Inset of Figure 3.4 presents analysis of intensities of peaks for 1072 cm^{-1} . This confirms increasing effect of deposition with increase of the applied voltage. Based on obtained results (Figure 3.4), 10 V was chosen for further experiments as it allowed to obtain reliable data and at the same time did not have drawbacks that characterize utilization of higher voltages, i.e. more complicated and expensive equipment and dangerous conditions of work.

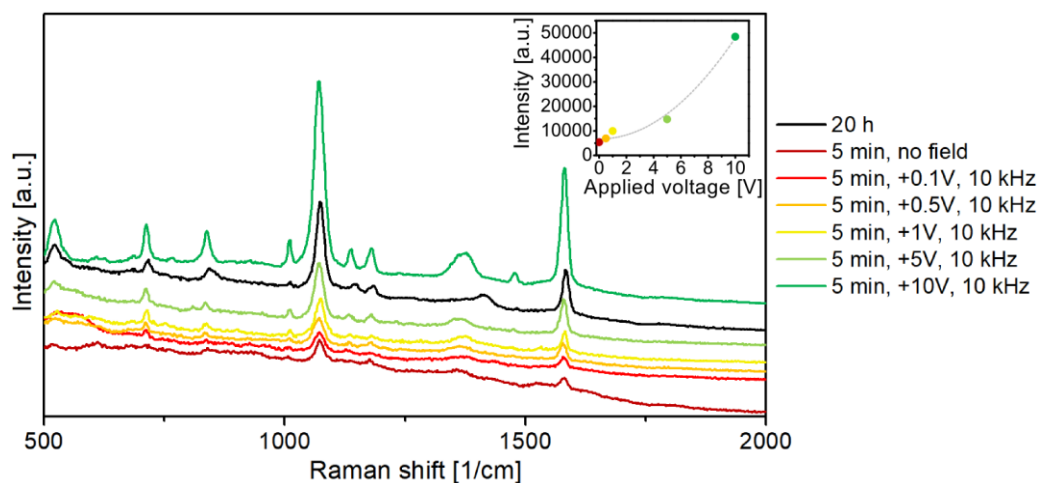


Figure 3.4 Dependency of obtained SERS signal after deposition of PMBA (10^{-6} M) upon application of different voltages. Obtained results confirmed that increase of applied voltage improved deposition process. Inset presents analyzed intensities of peaks for 1072 cm^{-1} . Grey line indicates fitted equation $I = AV^2 + C$, where I is intensity, V is applied voltage, whereas A and C are fitted parameters. R-squared was 0.984.

3.2.4. Influence of the electric field on homogeneity of results

Until this point I proved that application of the electric field can improve intensity of obtained signal and significantly shorten the time of deposition. However, developed method could also influence homogeneity of obtained signal. In my approach the electric field actively dragged molecules down to the SERS surfaces. In contrast, in typical procedure molecules get to the SERS substrate through Brownian motion and adsorb on the surface reaching the equilibrium. Upon application of voltage the highest electric field occurred in spots with high density of sharp edges, i.e. *hot spots* of SERS surface. Thus, utilization of the electric field should provide better coverage of hot spots of SERS substrates. This should manifest not only in higher measured intensities of peaks, which was already proved in previous sections of this chapter, but also in higher homogeneity of collected spectra. In order to verify this, I deposited PMBA (10^{-6} M) with and without the

electric field and each time number of spectra were collected. Obtained results presented in Figure 3.5 are not shifted in order to present how homogenous data were obtained. I proved that application of the electric field increased homogeneity of obtained spectra, as it provided higher occupation of hot spots by analyte. In randomly chosen spot for measurement, it was much more likely to record the signal from area comprising high and similar number of hot spots.

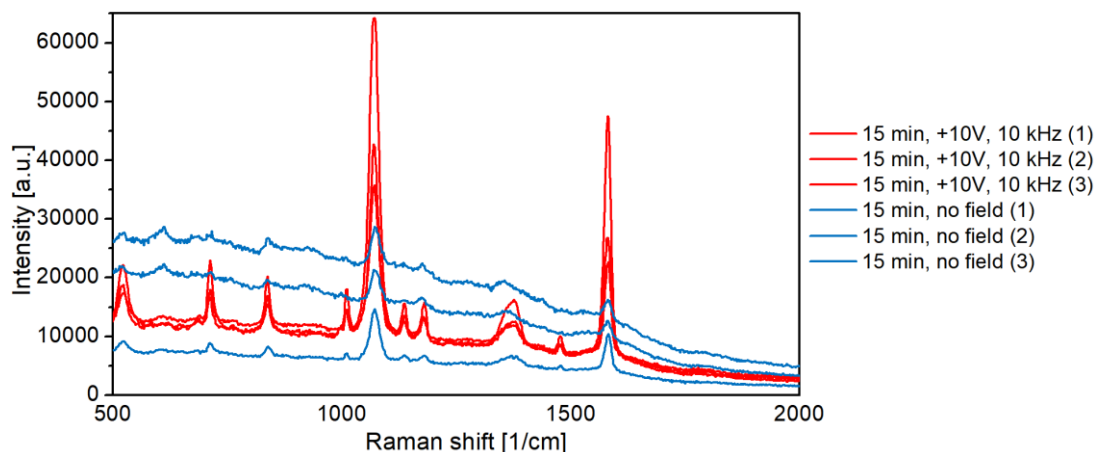


Figure 3.5 Analysis of influence of applied electric field on homogeneity of obtained results. PMBA was deposited from 10^{-6} M solution. It was proved that deposition upon voltage application resulted in more homogenous results. It was due to higher coverage of hot spots with analyte and thus increased chances of finding occupied hot spot during measurement in randomly chosen place on the SERS substrate. The results are not shifted in any axis.

3.2.5. Influence of the frequency of applied voltage

Another important parameter of designed procedure was frequency of applied voltage. As it was mentioned, application of square voltage waveform allowed to overcome the problem of suppression of the electric field in the solution by the electrical double layers. Thus, applied frequency should be adjusted according to the time scale of charging of EDLs. In literature there are many reported time scales of development of EDLs, as it was discussed in first chapter of this thesis. Time constant depends on wide range of parameters such as Debye length, present ions, strength of the electric field, geometry of the system, properties of the solvent, electrochemical reactions and more. Thus, analytical analysis of this effect was difficult in the studied case. Due to low concentrations of all compounds in utilized solutions, even small amounts of absorbed impurities from air could both influence the pH and introduce uncontrolled amounts of other ions, which changed parameters of solution. To prepare all solutions I used deionized water of pH around 7.0. However, due to absorption of carbon dioxide and other species from air, pH of final solutions changed to 6.0. Therefore, in this specific case I decided to apply a range of different frequencies and to determine experimentally most optimal values. I deposited the PMBA (10^{-6} M) in the electric field of 10 V and varying frequencies (Figure 3.6).

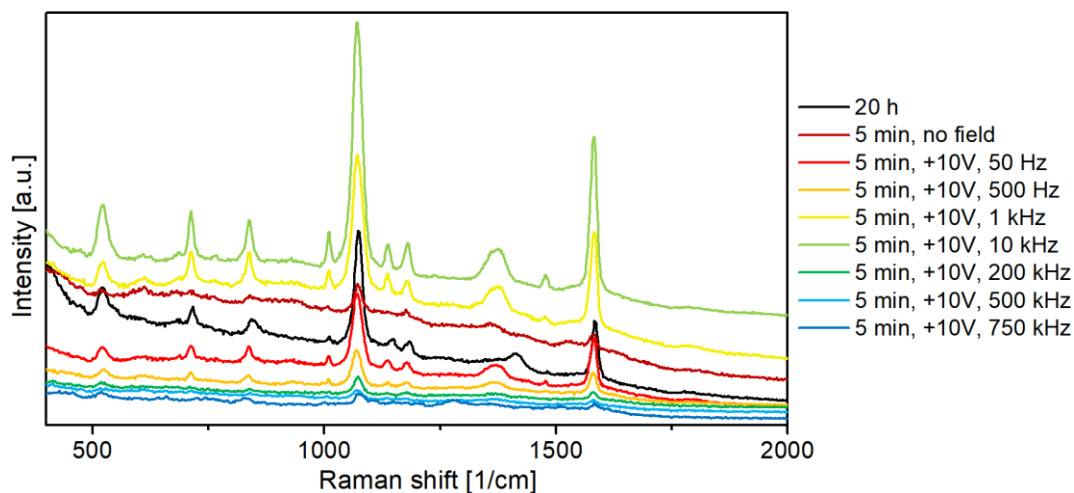


Figure 3.6 Analysis of influence of frequency on efficiency of deposition of PMBA (10^{-6} M) on SERS substrates. 10 kHz was the most optimal frequency that resulted in the highest measured signal.

In contrast to previously analyzed parameters (voltage and time of deposition) there was an optimal value of frequency that ensured efficient deposition. In case of PMBA it was 10 kHz. Both higher and lower frequencies resulted in decrease of the signal. Thus, in order to provide effective deposition in the electric field, frequency seems to be crucial parameter that have to be properly adjusted. Although dependence between most optimal frequency and properties of deposited molecules were already shortly discussed in this chapter, deeper understanding of this dependency requires additional analysis utilizing broader range of deposited analytes.

3.2.6. Deposition of various analytes

One of the goals of the research on deposition in the electric field was to create robust and versatile method applicable for broad range of analytes. Thus, designed approach should be applicable not only to model molecules, such as PMBA, that are known to be easily detected and produce strong signal with well-defined peaks in SERS measurements. Therefore, I have chosen eight other analytes, which detection with SERS technique is of importance and will be beneficial in different branches of industry and science. Structures of all studied compounds and biomolecules is shown in Figure 3.7.

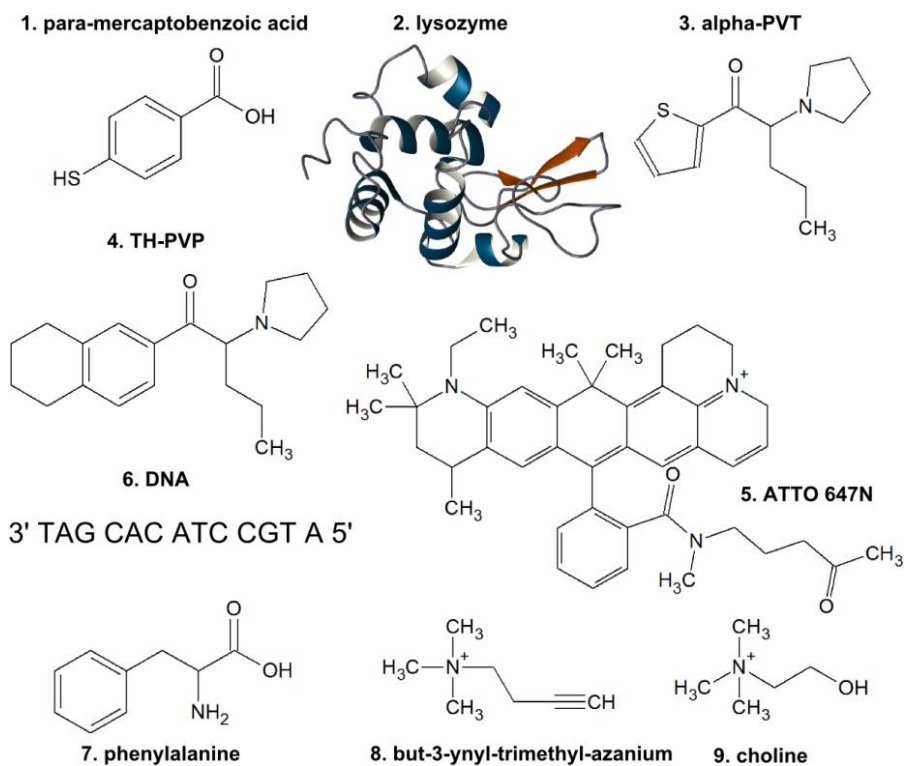


Figure 3.7 Summary of all analytes deposited in the electric field for SERS analysis (image of lysozyme adapted from www.bmrb.wisc.edu).

First group of compounds, which deposition is relevant in number of cases (including biomedical) are proteins. Proteins are backbone of the machinery of every cell. They are responsible for vast majority of biological catalytic processes (enzymes), act as antigens and antibodies and also as building blocks of cells (structural proteins) [48]. Thus studies on proteins are crucial in vast number of possible applications. Proteins can be detected as biomarkers of many diseases. They can also act as sensing or catalytic layers. Size of proteins makes it challenging to obtain reliable SERS results. As test protein I have chosen lysozyme. It has positive charge in wide pH [49] and exhibit catalytic properties.

DNA is another compound which wide importance is growing constantly since discovery of its structure by Watson, Crick, Franklin and Wilkins in 1953 [50]. Although detection of DNA is interesting and beneficial in itself [51], deposited layers of DNA can also be used as sensing layers [52], [53]. Thus applying the developed method for fast and effective deposition of DNA can open new possibilities for further studies.

To prove versatility of designed method, beside big biomolecules, also smaller compounds were studied. Amino acids are perfect for this purpose. They play key role in numerous biological processes. Deposition of amino acids is beneficial not only for detection of these compounds as biomarkers of diseases [54] but also renders new method of surface modification [55]. Amino acids have advantageous physicochemical characteristics (charge, functional groups, polarity, etc.), what make them suitable for

undertaken studies. Phenylalanine was chosen as it not only possess aromatic ring (which gives strong signal in SERS [43]), but also is practical as a marker of the genetic disorder called phenylketonuria [56].

Another chosen small biomolecule was choline, which is known to be essential nutrient for humans [57]. Studies show that choline is important for brain development in plenty of body mechanisms [58]. Moreover, it participates in synthesis of acetylcholine – messenger involved in neurotransmission. Choline molecule is rather simple, which usually makes it challenging to obtain reliable SERS signal.

Since the deposition method should extend beyond biological applications, another type of chosen analyte was substrate for click chemistry. Click chemistry reactions is a recent and rapidly developing field with a great potential for chemists, comprising bond-forming reactions that can be used to connect molecular building blocks via heteroatoms [59], [60]. Deposition of alkynes, which are one of the substrates for click reactions, gives possibilities for further surface modification via click chemistry. For this purpose I have chosen but-3-ynyl-trimethyl-azanium.

I also studied two types of designer drugs, in Poland known as “dopalacze”. This family of synthetic drugs continue to be significant challenge both for the criminal justice system and for analytical laboratories. It is especially difficult to detect and identify constantly growing number of different compounds, which are being manufactured, distributed and consumed [61]. Studied method of deposition can improve currently used methods of detection [62]. I have chosen two synthetic drugs: 3',4'-tetramethylene- α -pyrrolidinovalerophenone (denoted as TH-PVP) and α -pyrrolidinopentiothiophenone (known as α -PVT).

Last chosen analyte was ATTO-647N dye, which is rather big organic molecule (size of 1.75 nm). This fluorescent molecule allowed for utilization of confocal microscopy as second method to determine efficiency of developed technology. Moreover fast deposition of dyes can in future open new possibilities in labeling of biological samples.

“Proof of concept” experiments showed that the most important parameter determining efficient deposition process is frequency. Therefore, in case of listed compounds frequency of applied square potential was optimized. Similarly to previous experiments, I deposited analytes for 5 min in the electric field of 10 V and different frequencies. Then, standard SERS analysis was performed and obtained spectra were compared (Figure 3.8). For each deposited compound utilization of the electric field allowed for obtaining results similar to standard 20-hour procedure. Moreover, for most compounds, such as DNA, but-3-ynyl-trimethyl-azanium, ATTO-647N dye, α -PVT and TH-PVP, signal obtained after 5 min deposition in the electric field with proper frequency was more intensive than after standard 20-hour protocol. This confirmed that developed method is versatile, as it allows for deposition of variety of compounds, differing in sizes, charges and structures. In addition, it allowed for deposition of molecules both from water, as well as from buffer solution (DNA was deposited from TE buffer).

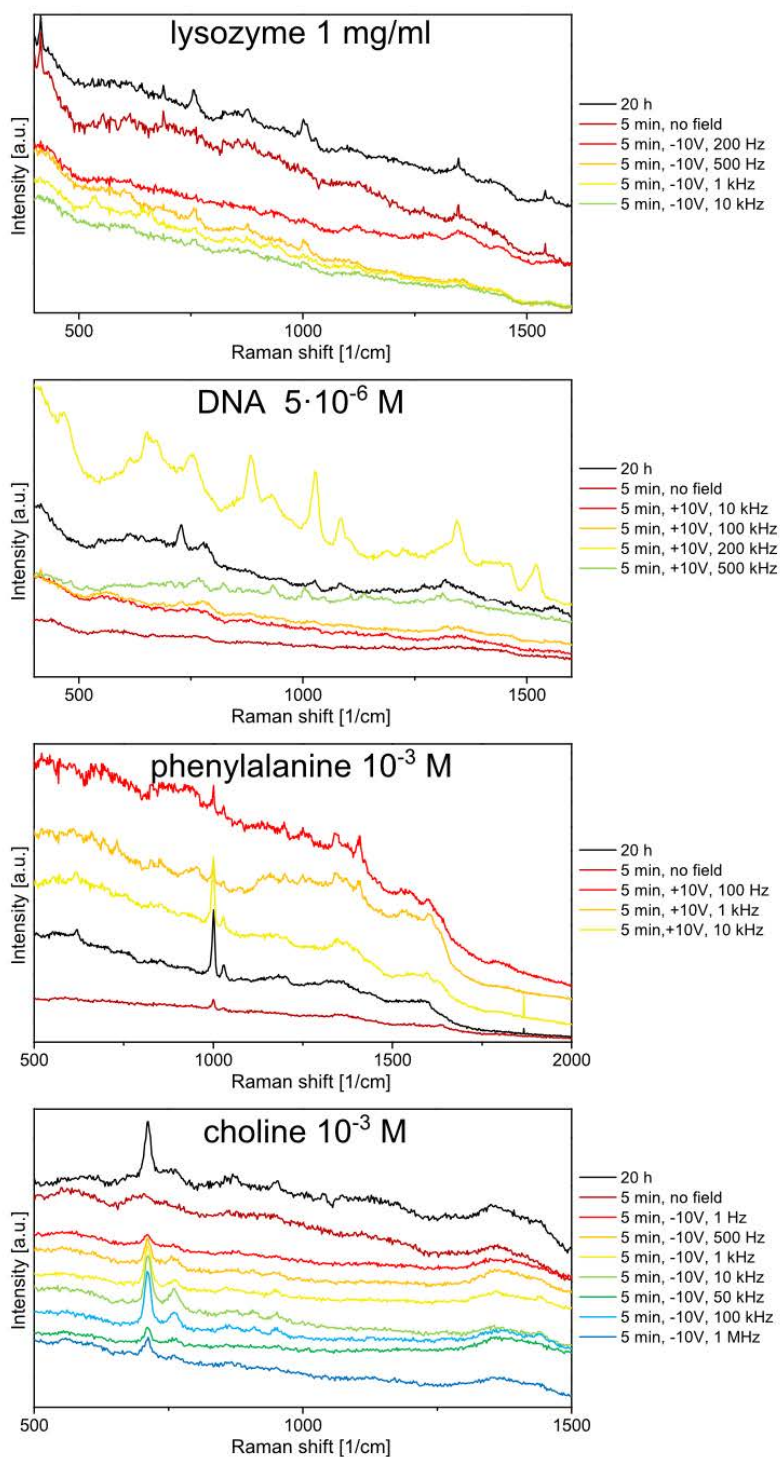


Figure 3.8 (part 1) Deposition of different analytes in the electric field on SERS surfaces. For every compound different frequencies were applied. Obtained results confirmed that frequency is crucial parameter and the most optimal value can vary between different compounds.

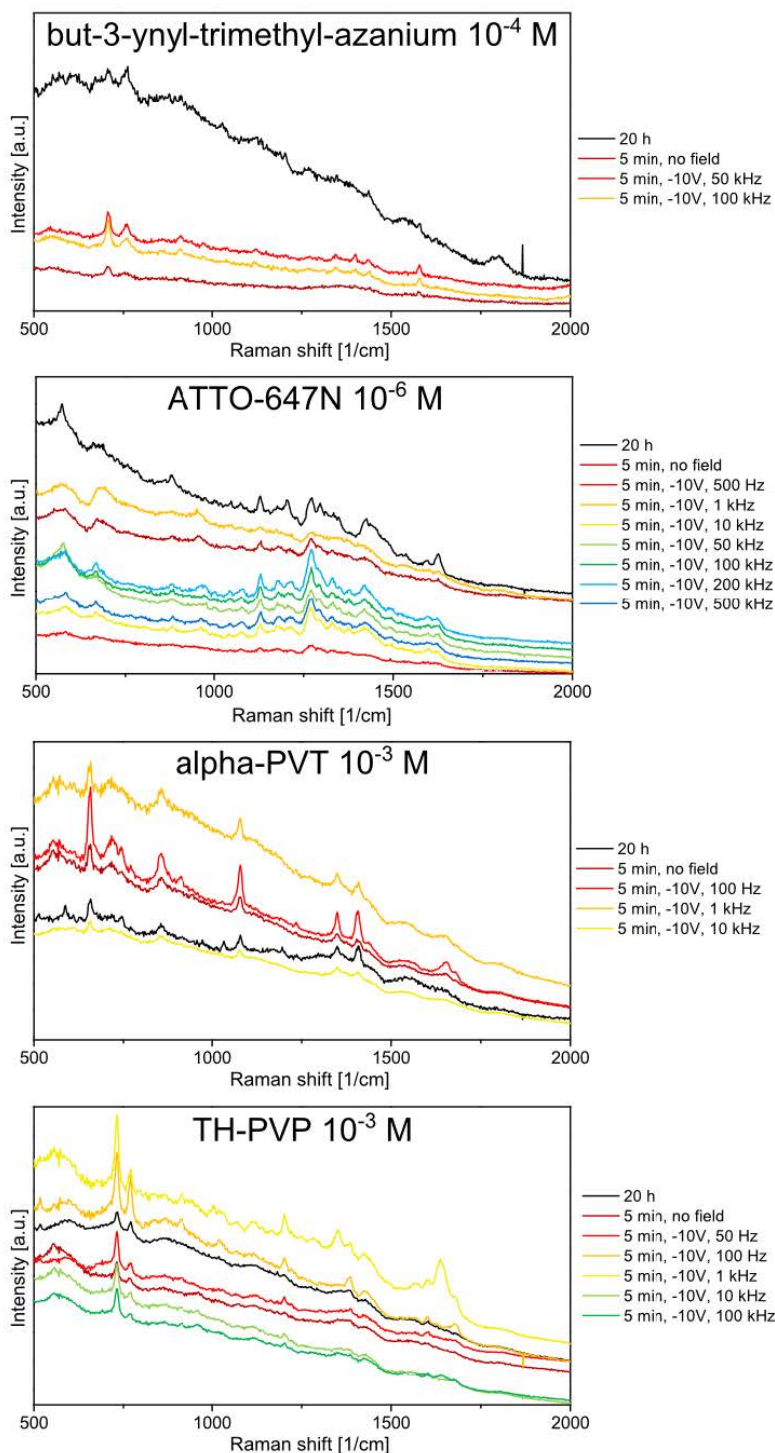


Figure 3.8 (part 2) Deposition of different analytes in the electric field on SERS surfaces. For every compound different frequencies were applied. Obtained results confirmed that frequency is crucial parameter and the most optimal value can vary between different compounds.

Obtained results confirmed that for every compound specific frequency had to be applied to ensure efficient deposition process. Optimal value of frequency ranged from 100 Hz for synthetic drugs up to 200 kHz for DNA and ATTO dye. Parameters of applied voltage that were effective for each compound are summarized in Table 3.1. For each analyte utilized polarization of applied potential was based on the analysis of chemical structure of molecule, as described in section 3.2.1 of this chapter. Successful deposition confirmed effectiveness of such approach.

Table 3.1 Summary of all deposited analytes and corresponding parameters of applied voltage which provided efficient deposition.

Compound	Type of molecule	Charge	Applied potential	Optimal frequency
para-mercaptobenzoic acid	model SERS molecule	negative	positive	10 kHz
lysozyme	protein	positive	negative	500 Hz
α -PVT	drug	positive	negative	100 Hz
TH-PVP	drug	positive	negative	100 Hz
ATTO-647N	dye	positive	negative	200 kHz
DNA	nucleic acid	negative	positive	200 kHz
phenylalanine	amino acid	negative	positive	10 kHz
but-3-ynyl-trimethyl-azanium	click chemistry compound	positive	negative	100 kHz
choline	nutrient and signaling molecule	positive	negative	100 kHz

3.2.7. Electrophoretic mobility of deposited compounds

Frequency of applied potential determined the length of applied pulses and in consequence the time for movement of molecules in the solution. Thus, there should be a dependency between frequency and electrophoretic mobility of analyte, as it is discussed in first chapter of this thesis. To check whether in case of the studied system these two values were correlated, I used capillary electrophoresis to measure electrophoretic mobility of compounds used in my research. All measurements were performed in the same pH as in case of deposition on SERS substrates to maintain properties (e.g. charge) of the analyte. The absolute values of obtained electrophoretic mobilities were compared with optimal frequencies (Figure 3.9). Some compounds (e.g. ATTO-647N, choline) could not be

measured (due to technical limitations, such as weak absorbance of molecules in UV spectra) and were not included in the comparison.

Obtained results showed logarithmic dependence between electrophoretic mobilities and optimal deposition frequencies. As expected, compounds with higher mobilities require less time to move in the external electric field and thus higher frequencies should be applied. Although such comparison did not provide detailed insight in the phenomena, it was nonetheless important from point of view of practical usage. In case of other analytes, this dependency allows for estimation of range of frequencies that enable successful deposition. Therefore, it is an important addition to the whole developed technique.

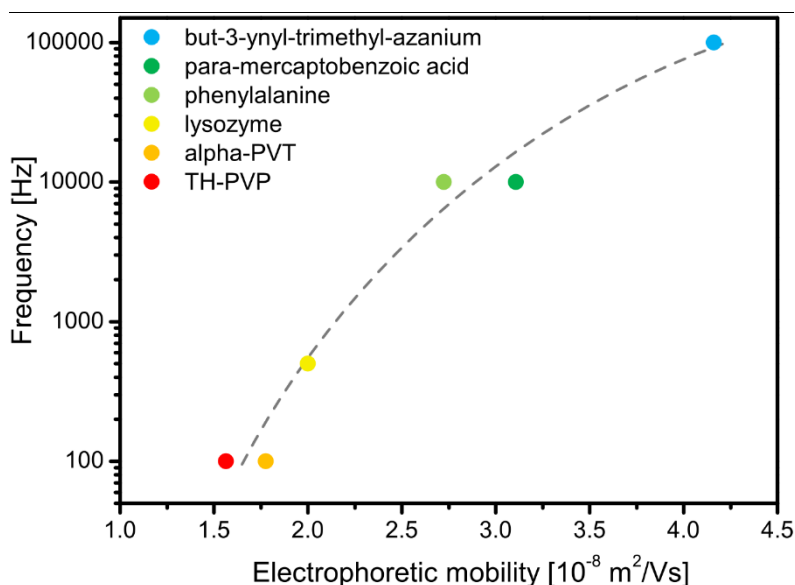


Figure 3.9 Analysis of dependency between optimal frequency of voltage applied during deposition and electrophoretic mobility of deposited compounds.

3.2.8. Influence of polarization of the applied voltage

It was mentioned already that proper polarization of applied voltage is of great importance. In case of application of wrong sign of charge, particles are repelled, instead of attracted to the surface. To ensure effective deposition, proper polarization was estimated based on structure and chemical groups of deposited molecules. However, to additionally check and prove that only proper polarization guarantee efficient deposition, I deposited both designer drugs (TH-PVP and α -PVT) in the same parameters of the electric field except the polarization (Figure 3.10). In both cases only proper polarization (negative) enabled successful deposition. Thus, it confirmed that correctly adjusted polarization was important for deposition process.

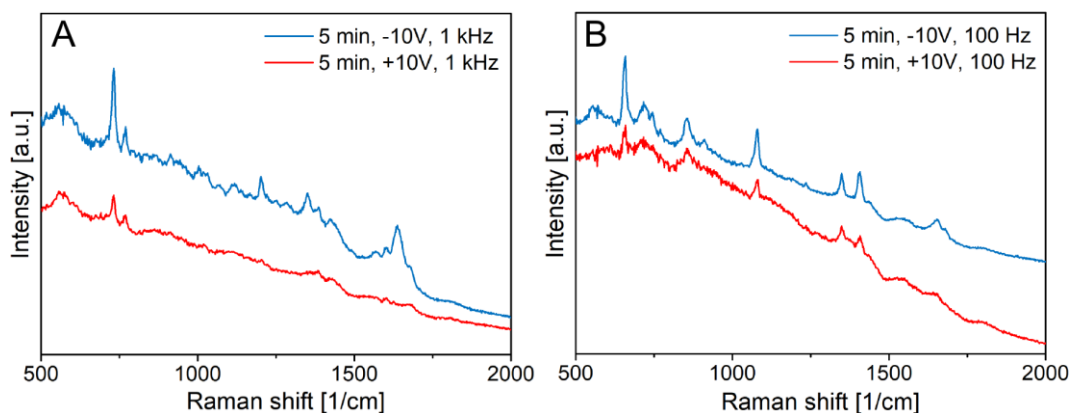


Figure 3.10 Deposition of (A) TH-PVP and (B) α -PVT on SERS substrate in the electric field with the same parameters (time, voltage, frequency) but opposite polarization.

3.2.9. Confocal microscopy analysis of deposited ATTO-647N

All results presented so far confirmed that designed process of deposition was successful and promising for practical applications. However, only SERS was used. In order to confirm effectiveness of my method with another analytical technique, I utilized dye ATTO-647N (excitation 646 nm, emission 664 nm). After deposition of this compound with and without the electric field, both SERS substrates were analyzed under confocal fluorescence microscope and red fluorescence of a dye was compared (during the same experimental session and using the same parameters of the microscope). As control, fluorescence from pure substrate was recorded. As presented in Figure 3.11, in case of deposition in the electric field obtained image was brighter, as more dye molecules were deposited on the surface. Thus, confocal imaging confirmed that application of the electric field is effective method for deposition of the analyte.

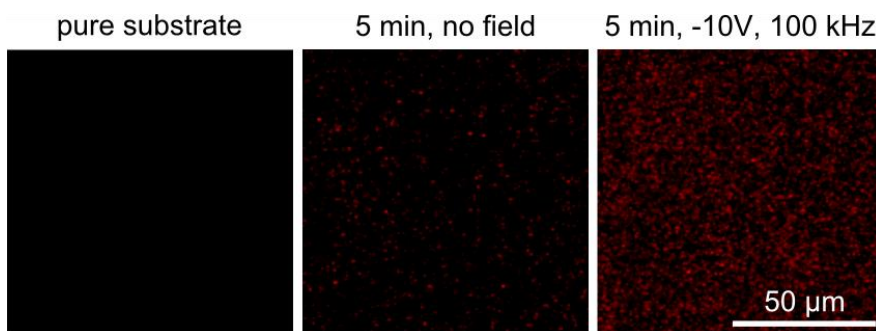


Figure 3.11 Comparison of confocal fluorescence microscopy images of samples with dye ATTO-647N deposited with and without the electric field. Analysis confirmed that application of alternating voltage resulted in effective deposition of the molecules.

3.3. Conclusions

Cutting-edge methods of analytical chemistry are constantly developed and improved. However, it is often ignored that successful detection is usually composed of two distinct

processes: analyte reaching sensing surface and generation of signal. The second issue is broadly addressed, as many new sensing layers and transducers are created regularly. This effort have to be complemented with development of methods that enable effective deposition of analyte on the sensing surface, even in unfavorable conditions of low concentration of analyte or short times of deposition. Only such connection of efficient method of deposition with sensitive and selective sensor guarantee successful detection.

In this chapter method that fill this gap was developed. Presented technology allowed for deposition of broad variety of analytes on SERS substrates in just 5 minutes. Created solution enabled obtaining results similar or, in many cases even better, than typical 20-hour analysis. Deposition was utilized to improve SERS technique, but independent from utilized analytical method, the deposition process is universal. The only requirement is that surface, on which analyte is deposited should be conductive.

I proved that the application of the electric field resulted in dragging of the molecules towards desired surface. I overcame the problem of creation of electrical double layer by application of properly designed alternating voltage. I determined the influence of many parameters of the process, such as voltage, time, polarity of applied potential. Finally, I proved that for every deposited analyte there is the most optimal frequency and I provided dependency that allow for determining its value for new compounds without additional optimization.

In this chapter process of electrophoresis was utilized. However translational movement of objects in the electric field is not the only possibility to maneuvering of matter and not the only way to improve sensing techniques. In the next chapter the electric field will be applied to rotate particles (viruses), which will allow for creation of ordered layers that detect bacteria in fast and sensitive way.

3.4. Materials and methods

3.4.1. Materials

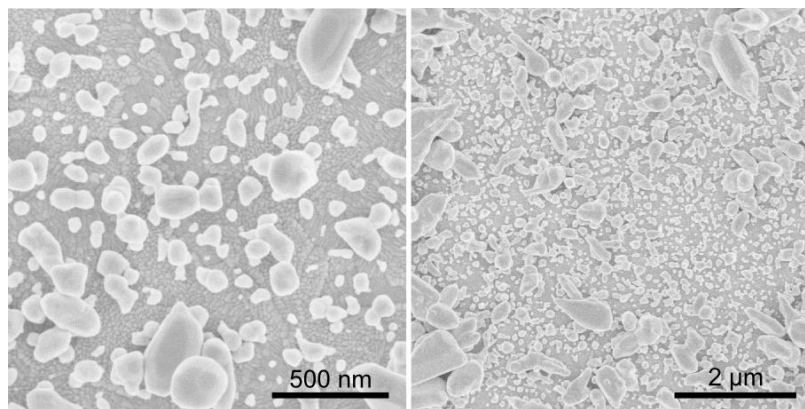
Chemicals were purchased from Sigma Aldrich (USA) and were used without further purification. DNA was purchased from IBA GmbH (Germany). Designer drugs were obtained in form of solution from Research Institute of Central Forensic Laboratory of the Police (Warsaw, Poland). Compound but-3-ynyl-trimethyl-azanium was synthesized and purified in the Institute of Physical Chemistry of the Polish Academy of Sciences (Warsaw, Poland).

Concentrations of deposited analytes, compositions of solutions and parameters of SERS analysis are summarized in Table 3.2. As PMBA, α -PVT and TH-PVP are poorly soluble in water, addition of ethanol or methanol allowed for preparation of desired concentrations. DNA was deposited from TE buffer of pH 7.0 composed of 10 mM TRIS (tris(hydroxymethyl)aminomethane) and 1mM EDTA (ethylenediaminetetraacetic acid).

Table 3.2 Summary of deposited molecules and their solvents.

Compound	Concentration	Solution	Parameters of SERS analysis
para-mercaptobenzoic acid	10^{-6} M	water with 1% of ethanol	6 s, 19.5 mW
lysozyme	1 mg/ml	water	15 s, 19.5 mW
α -PVT	10^{-3} M	water with 10% of methanol	9 s, 19.5 mW
TH-PVP	10^{-3} M	water with 10% of methanol	9 s, 19.5 mW
ATTO-647N	10^{-6} M	water	4 s, 19.5 mW
DNA	$5 \cdot 10^{-6}$ M	buffer TE	4 s, 19.5 mW
phenylalanine	10^{-3} M	water	9 s, 30.5 mW
but-3-ynyl-trimethyl-azanium	10^{-4} M	water	6 s, 19.5 mW
choline	10^{-3} M	water	9 s, 30.5 mW

SERS substrates were provided by *SERSitive* (Warsaw, Poland). In short, SERS-active silver nanoparticles were deposited electrochemically from aqueous solution on glass substrate covered with indium tin oxide. Process was performed according to patent application no P-408785 [63]. Scanning electron microscope (SEM) images of utilized SERS substrates are provided in Figure 3.12.

**Figure 3.12** Scanning electron microscope images of utilized SERS substrates.

3.4.2. Deposition of analytes in the electric field

Deposition process consisted of few steps. First, both electrodes were connected to power source via copper tape and placed in the deposition cell. If needed, SERS substrate was pre-wetted by immersing for few seconds in 1:4 mixture of ethanol and water. Next, 50 μl of solution of deposited analyte was placed in the cell between electrodes and voltage of desired parameters was applied. If not stated otherwise, square waveform of voltage of 10 V and different frequencies was applied for 5 min. After deposition, SERS substrate was removed from deposition call, dried in open air and standard SERS analysis was performed.

The deposition cell was connected to the function generator (DG1022, Rigol, China) that provided desired voltage waveform. Parallel connected oscilloscope (DS1052E, Rigol, China) allowed for precise control of output voltage.

Standard deposition process was performed by immersion of SERS substrate for 20 hours in 2 ml of solution of analyte. The following part of the procedure remained the same.

3.4.3. SERS measurement

In order to perform SERS measurement, i-Raman BWS415 (B&W Tek, USA) system equipped with diode laser with wavelength of 785 nm was used. The laser light was focused on a sample mounted on an X–Y–Z translation stage with a 50x microscope objective. The microscope was equipped with BAC100 Raman trigger probe that allowed for 4.5 cm^{-1} spectral resolution and measurement in range of 175–3200 cm^{-1} . The experiments were performed under ambient conditions using laser power from 19.5 to 30.5 mW at the sample.

The SERS spectra were collected immediately after the SERS substrate was removed from the solution and dried. The SERS signal was measured in at least 5 different randomly chosen spots. The spectra were processed with the BWSpec software provided by B&W Tek company.

3.4.4. Measurement of electrophoretic mobility

To ensure proper measurement of electrophoretic mobility by capillary electrophoresis, excitation wavelength had to be determined for each compound. For this purpose NanoDrop spectrometer (Thermo Fisher Scientific, USA) was used to collect absorbance spectra of all deposited analytes. Spectra of analytes with clear absorbance peaks, that allowed for successful capillary electrophoresis, are presented in Figure 3.13.

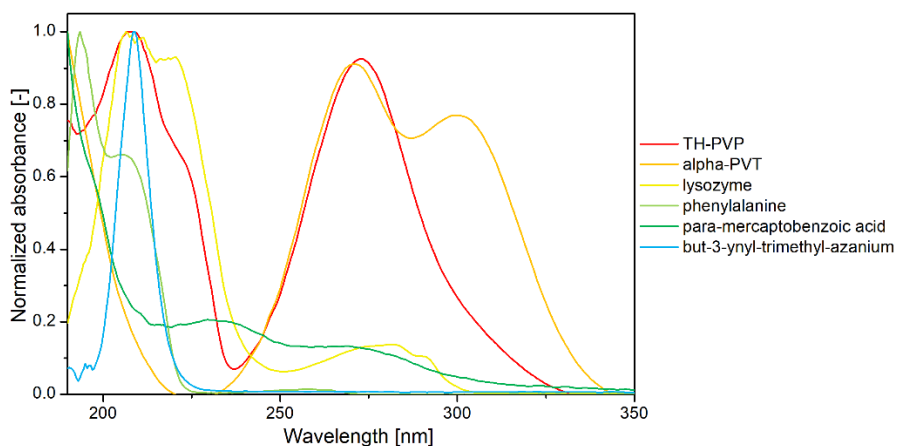


Figure 3.13 Absorption spectra of deposited analytes. Information about absorption bands was necessary to perform capillary electrophoresis.

To perform capillary electrophoresis Beckman P/ACE MDQ with diode detector UV-VIS was used. System was equipped with filters that allowed for excitation with 200, 214, 254 and 280 nm. For every analyte excitation wavelength was chosen separately, based on obtained absorbance spectrum. Utilized capillary had 75 μm in diameter and 60 cm in length. Distance from one end of capillary (sample loading) to detector window was 50 cm. To induce the electric field in capillary, 20 kV voltage was applied. Sample was loaded into capillary with 0.5 psi pressure.

Before measurements, the capillary was prepared by washing many times with different solutions: 15 min of methanol, 5 min of water, 15 min of 1M HCl, 5 min of water, 15 min of 1M NaOH and 5 min of water. Before first measurement, capillary was additionally washed for 15 min with phosphate buffer. After each sample, washing with phosphate buffer for 5 min was also performed. To provide sufficient conductivity during measurements, capillary was filled with 20 mM phosphate buffer pH 7.0. To determine electroosmotic flow (EOF) in the system, mobility of dimethyl sulfoxide (DMSO) was measured. DMSO is neutral molecule, thus its mobility in capillary electrophoresis is equal to electroosmotic flow.

In capillary electrophoresis measurement, for every analyzed molecule migration time was determined. This was time between sample injection and signal detection in detector window. Based on this value and other measurement parameters, apparent mobility μ_a was calculated:

$$\mu_a = \frac{lL}{tV} \quad (3.2)$$

where l is effective capillary length (to the detector), L is total capillary length, t is migration time, and V is applied voltage.

Apparent mobility depends on the effective mobility of molecule μ_e and electroosmotic flow μ_{EOF} . Knowing the value of the electroosmotic flow (determined in measurement of DMSO), effective mobility was calculated as:

$$\mu_e = \mu_a - \mu_{EOF} \quad (3.3)$$

3.4.5. Additional instrumentation

Nikon Ti Eclipse with confocal system A1R was used for analysis of deposition of ATTO-647N dye. The system included diode laser emitting light of wavelength of 635 nm, objective CFI Plan Fluor 40x and NIS-Elements AR 4.13 software.

Scanning electron microscopy images were made with use of a NovaSEM (FEI, USA) scanning electron microscope.

3.5. References

- [1] M. A. Cooper and V. T. Singleton, "A survey of the 2001 to 2005 quartz crystal microbalance biosensor literature: applications of acoustic physics to the analysis of biomolecular interactions," *J. Mol. Recognit.*, vol. 20, pp. 154–184, 2007.
- [2] M. El-Sherif, L. Bansal, and J. Yuan, "Fiber optic sensors for detection of toxic and biological threats," *Sensors*, vol. 7, no. 12, pp. 3100–3118, 2007.
- [3] C. C. Wu, W. C. Huang, and C. C. Hu, "An ultrasensitive label-free electrochemical impedimetric DNA biosensing chip integrated with a DC-biased AC electroosmotic vortex," *Sensors Actuators, B Chem.*, vol. 209, pp. 61–68, 2015.
- [4] A. Wokaun, H. P. Lutz, A. P. King, U. P. Wild, and R. R. Ernst, "Energy transfer in surface enhanced luminescence," *J. Chem. Phys.*, vol. 79, no. 1, pp. 509–514, 1983.
- [5] E. Fort and S. Grésillon, "Surface enhanced fluorescence," *J. Phys. D. Appl. Phys.*, vol. 41, no. 1, p. 013001, 2008.
- [6] J. Homola, S. S. Yee, and G. Gauglitz, "Surface plasmon resonance sensors: review," *Sensors Actuators B Chem.*, vol. 54, no. 1–2, pp. 3–15, 1999.
- [7] K. M. Mayer and J. H. Hafner, "Localized Surface Plasmon Resonance Sensors," *Chem. Rev.*, vol. 111, no. 6, pp. 3828–3857, 2011.
- [8] A. Campion and P. Kambhampati, "Surface-enhanced Raman scattering," *Chem. Soc. Rev.*, vol. 27, pp. 241–250, 1998.
- [9] C. V. Raman and K. S. Krishnan, "A new type of secondary radiation," *Nature*, vol. 121, pp. 501–502, 1928.
- [10] C. L. Haynes, A. D. McFarland, and R. P. Van Duyne, "Surface-enhanced Raman spectroscopy," *Anal. Chem.*, vol. 77, no. 17, p. 338 A-346 A, 2005.
- [11] M. Fleischmann, P. J. Hendra, and A. J. McQuillan, "Raman spectra of pyridine adsorbed at a silver electrode," *Chem. Phys. Lett.*, vol. 26, no. 2, pp. 163–166, 1974.
- [12] D. L. Jeanmaire and R. P. Van Duyne, "Surface raman spectroelectrochemistry: Part I. Heterocyclic, aromatic, and aliphatic amines adsorbed on the anodized silver electrode," *J. Electroanal. Chem. Interfacial Electrochem.*, vol. 84, no. 1, pp. 1–20, 1977.
- [13] M. G. Albrecht and J. A. Creighton, "Anomalously intense Raman spectra of pyridine at a silver electrode," *J. Am. Chem. Soc.*, vol. 99, no. 15, pp. 5215–5217, 1977.
- [14] M. Moskovits, "Enhanced Raman scattering by molecules adsorbed on electrodes--a theoretical model," *Solid State Commun.*, vol. 32, no. 1, pp. 59–62, 1979.
- [15] A. Shiohara, Y. Wang, and L. M. Liz-Marzán, "Recent approaches toward creation of hot spots for SERS detection," *J. Photochem. Photobiol. C Photochem. Rev.*, vol. 21, pp. 2–25, 2014.
- [16] R. C. Maher, "SERS Hot Spots," in *Raman Spectroscopy for Nanomaterials Characterization*, Berlin, Heidelberg: Springer Berlin Heidelberg, 2012, pp. 215–260.
- [17] S. Nie and S. R. Emory, "Probing single molecules and single nanoparticles by surface-enhanced Raman scattering," *Science (80-.)*, vol. 275, pp. 1102–1106, 1997.
- [18] A. Sivanesan, W. Adamkiewicz, G. Kalaivani, A. Kamińska, J. Waluk, R. Hołyst, and E. L. Izake, "Electrochemical pathway for the quantification of SERS enhancement factor," *Electrochem. commun.*, vol. 49, pp. 103–106, 2014.

- [19] K. Kneipp, H. Kneipp, I. Itzkan, R. R. Dasari, and M. S. Feld, "Surface-enhanced Raman scattering and biophysics," *J. Phys. Condens. Matter*, vol. 14, pp. 597–624, 2002.
- [20] S. Bruni, V. Guglielmi, and F. Pozzi, "Surface-enhanced raman spectroscopy (SERS) on silver colloids for the identification of ancient textile dyes: Tyrian purple and madder," *J. Raman Spectrosc.*, vol. 41, no. 2, pp. 175–180, 2010.
- [21] S. A. Centeno and J. Shamir, "Surface enhanced Raman scattering (SERS) and FTIR characterization of the sepia melanin pigment used in works of art," *J. Mol. Struct.*, vol. 873, no. 1–3, pp. 149–159, 2008.
- [22] C. Muehlethaler, M. Leona, and J. R. Lombardi, "Review of Surface Enhanced Raman Scattering Applications in Forensic Science," *Anal. Chem.*, vol. 88, no. 1, pp. 152–169, 2016.
- [23] A. Hakonen, P. O. Andersson, M. Stenbæk Schmidt, T. Rindzevicius, and M. Käll, "Explosive and chemical threat detection by surface-enhanced Raman scattering: A review," *Anal. Chim. Acta*, vol. 893, pp. 1–13, 2015.
- [24] R. A. Alvarez-Puebla and L. M. Liz-Marzán, "SERS-based diagnosis and biodetection," *Small*, vol. 6, no. 5, pp. 604–610, 2010.
- [25] R. M. Jarvis and R. Goodacre, "Characterisation and identification of bacteria using SERS," *Chem. Soc. Rev.*, vol. 37, no. 5, pp. 931–936, 2008.
- [26] S. Shanmukh, L. Jones, J. Driskell, Y. Zhao, R. Dluhy, and R. A. Tripp, "Rapid and sensitive detection of respiratory virus molecular signatures using a silver nanorod array SERS substrate," *Nano Lett.*, vol. 6, no. 11, pp. 2630–2636, 2006.
- [27] M. Fan, G. F. S. Andrade, and A. G. Brolo, "A review on the fabrication of substrates for surface enhanced Raman spectroscopy and their applications in analytical chemistry," *Anal. Chim. Acta*, vol. 693, no. 1–2, pp. 7–25, 2011.
- [28] L. Polavarapu and Q. H. Xu, "Water-soluble conjugated polymer-induced self-assembly of gold nanoparticles and its application to SERS," *Langmuir*, vol. 24, no. 19, pp. 10608–10611, 2008.
- [29] Y. Wang, L. Polavarapu, and L. M. Liz-Marzán, "Reduced graphene oxide-supported gold nanostars for improved SERS sensing and drug delivery," *ACS Appl. Mater. Interfaces*, vol. 6, no. 24, pp. 21798–21805, 2014.
- [30] L. Guerrini and D. Graham, "Molecularly-mediated assemblies of plasmonic nanoparticles for Surface-Enhanced Raman Spectroscopy applications," *Chem. Soc. Rev.*, vol. 41, no. 21, pp. 7085–7107, 2012.
- [31] F. Aussenegg, M. Lippitsch, R. Möller, and J. Wagner, "Depolarization ratio measurement of Rayleigh scattering in high field electric strength," *Phys. Lett. A*, vol. 55, no. 3, pp. 199–200, 1975.
- [32] D. L. Andrews and N. P. Blake, "Electric-field-induced Raman spectroscopy," *J. Chem. Phys.*, vol. 88, pp. 6039–6048, 1988.
- [33] D. L. Andrews, N. P. Blake, and K. P. Hopkins, "Theory of electro-optical effects in two-photon spectroscopy," *J. Chem. Phys.*, vol. 88, no. 10, pp. 6022–6029, 1988.
- [34] S. Walia, A. K. Shah, P. R. Stoddart, M. Bhaskaran, and S. Sriram, "Electric field induced surface-enhanced Raman spectroscopy for multianalyte detection," *Phys. Chem. Chem. Phys.*, vol. 17, no. 11, pp. 7095–7099, 2015.
- [35] S. Sriram, M. Bhaskaran, S. Chen, S. Jayawardhana, P. R. Stoddart, J. Z. Liu, N. V. Medhekar, K. Kalantar-Zadeh, and A. Mitchell, "Influence of electric field on SERS: Frequency effects, intensity changes, and susceptible bonds," *J. Am. Chem. Soc.*,

- vol. 134, no. 10, pp. 4646–4653, 2012.
- [36] S. Almohammed, F. Zhang, B. J. Rodriguez, and J. H. Rice, “Electric field-induced chemical surface-enhanced Raman spectroscopy enhancement from aligned peptide nanotube–graphene oxide templates for universal trace detection of biomolecules,” *J. Phys. Chem. Lett.*, vol. 10, pp. 1878–1887, 2019.
- [37] P. D. Lacharmoise, E. C. Le Ru, and P. G. Etchegoin, “Guiding molecules with electrostatic forces in surface enhanced raman spectroscopy,” *ACS Nano*, vol. 3, no. 1, pp. 66–72, 2009.
- [38] H. Cho, B. Lee, G. L. Liu, A. Agarwal, and L. P. Lee, “Label-free and highly sensitive biomolecular detection using SERS and electrokinetic preconcentration,” *Lab Chip*, vol. 9, no. 23, pp. 3360–3363, 2009.
- [39] M. Park, Y. J. Oh, S. G. Park, S. B. Yang, and K. H. Jeong, “Electrokinetic preconcentration of small molecules within volumetric electromagnetic hotspots in surface enhanced Raman scattering,” *Small*, vol. 11, no. 21, pp. 2487–2492, 2015.
- [40] Y. S. Huh, A. J. Chung, B. Cordovez, and D. Erickson, “Enhanced on-chip SERS based biomolecular detection using electrokinetically active microwells,” *Lab Chip*, vol. 9, no. 3, pp. 433–439, 2009.
- [41] C. Liu, Z. Wang, E. Li, Z. Liang, S. Chakravarty, X. Xu, A. X. Wang, R. T. Chen, and D. Fan, “Electrokinetic manipulation integrated plasmonic-photonic hybrid Raman nanosensors with dually enhanced sensitivity,” *ACS Sensors*, vol. 2, no. 3, pp. 346–353, 2017.
- [42] S. A. Jadhav, “Self-assembled monolayers (SAMs) of carboxylic acids: An overview,” *Cent. Eur. J. Chem.*, vol. 9, no. 3, pp. 369–378, 2011.
- [43] A. Michota and J. Bukowska, “Surface-enhanced Raman scattering (SERS) of 4-mercaptobenzoic acid on silver and gold substrates,” *J. Raman Spectrosc.*, vol. 34, no. 1, pp. 21–25, 2003.
- [44] A. Kamińska, I. Dzięcielewski, J. L. Weyher, J. Waluk, S. Gawinkowski, V. Sashuk, M. Fiałkowski, M. Sawicka, T. Suski, S. Porowski, and R. Hołyst, “Highly reproducible, stable and multiply regenerated surface-enhanced Raman scattering substrate for biomedical applications,” *J. Mater. Chem.*, vol. 21, no. 24, pp. 8662–8669, 2011.
- [45] K. Winkler, A. Kaminska, T. Wojciechowski, R. Hołyst, and M. Fialkowski, “Gold micro-flowers: one-step fabrication of efficient, highly reproducible surface-enhanced Raman spectroscopy platform,” *Plasmonics*, vol. 6, no. 4, pp. 697–704, 2011.
- [46] P. E. Laibinis, G. M. Whitesides, D. L. Allara, Y. T. Tao, A. N. Parikh, and R. G. Nuzzo, “Comparison of the structures and wetting properties of self-assembled monolayers of n-alkanethiols on the coinage metal surfaces, copper, silver, and gold,” *J. Am. Chem. Soc.*, vol. 113, no. 19, pp. 7152–7167, 1991.
- [47] H. Hiramatsu and F. E. Osterloh, “pH-controlled assembly and disassembly of electrostatically linked CdSe-SiO₂ and Au-SiO₂ nanoparticle clusters,” *Langmuir*, no. 19, pp. 7003–7011, 2003.
- [48] W. H. Freeman, “Chapter 3, Protein Structure and Function,” in *Biochemistry. 5th edition*, J. M. Berg, J. L. Tymoczko, and L. Stryer, Eds. New York, 2002.
- [49] W. S. Price, F. Tsuchiya, and Y. Arata, “Lysozyme aggregation and solution properties studied using PGSE NMR diffusion measurements,” *J. Am. Chem. Soc.*, vol. 121, pp. 11503–11512, 1999.

- [50] J. D. Watson and F. H. C. Crick, "Molecular structure of nucleic acids: a structure for deoxyribose nucleic acid," *Nature*, vol. 171, pp. 737–738, 1953.
- [51] A. Barhoumi, D. Zhang, F. Tam, and N. J. Halas, "Surface-enhanced Raman spectroscopy of DNA," *J. Am. Chem. Soc.*, vol. 130, no. 16, pp. 5523–5529, 2008.
- [52] M. R. Saidur, A. R. A. Aziz, and W. J. Basirun, "Recent advances in DNA-based electrochemical biosensors for heavy metal ion detection: A review," *Biosens. Bioelectron.*, vol. 90, pp. 125–139, 2017.
- [53] V. C. Diculescu, A.-M. Chiorcea-Paquim, and A. M. Oliveira-Brett, "Applications of a DNA-electrochemical biosensor," *TrAC Trends Anal. Chem.*, vol. 79, pp. 23–36, 2016.
- [54] F. Manig, K. Kuhne, C. von Neubeck, U. Schwarzenbolz, Z. Yu, B. M. Kessler, J. Pietzsch, and L. A. Kunz-Schughart, "The why and how of amino acid analytics in cancer diagnostics and therapy," *J. Biotechnol.*, vol. 242, pp. 30–54, 2017.
- [55] A. Pinazo, M. A. Manresa, A. M. Marques, M. Bustelo, M. J. Espuny, and L. Pérez, "Amino acid-based surfactants: New antimicrobial agents," *Adv. Colloid Interface Sci.*, vol. 228, pp. 17–39, 2016.
- [56] G. Schlegel, R. Scholz, K. Ullrich, R. Santer, and G. M. Rune, "Phenylketonuria: Direct and indirect effects of phenylalanine," *Exp. Neurol.*, vol. 281, pp. 28–36, 2016.
- [57] S. H. Zeisel, "Choline: an essential nutrient for humans," *Nutrition*, vol. 16, pp. 669–671, 2000.
- [58] S. H. Zeisel, "Nutritional importance of choline for brain development," *J. Am. Coll. Nutr.*, vol. 23, p. 621S–626S, 2004.
- [59] L. Liang and D. Astruc, "The copper(I)-catalyzed alkyne-azide cycloaddition (CuAAC) 'click' reaction and its applications. An overview," *Coord. Chem. Rev.*, vol. 255, no. 23–24, pp. 2933–2945, 2011.
- [60] A. Tăbăcaru, B. Furdui, I. O. Ghinea, G. Cârâc, and R. M. Dinică, "Recent advances in click chemistry reactions mediated by transition metal based systems," *Inorganica Chim. Acta*, vol. 455, pp. 329–349, 2017.
- [61] L. Karila, B. Megarbane, O. Cottencin, and M. Lejoyeux, "Synthetic cathinones: A new public health problem," *Curr. Neuropharmacol.*, vol. 13, pp. 12–20, 2015.
- [62] V. Halouzka, B. Halouzкова, D. Jirovsky, D. Hemzal, P. Ondra, E. Siranidi, A. G. Kontos, P. Falaras, and J. Hrbac, "Copper nanowire coated carbon fibers as efficient substrates for detecting designer drugs using SERS," *Talanta*, vol. 165, pp. 384–390, 2017.
- [63] M. Książkowska-Gocalska, W. Michałowicz, M. Siek, J. Niedziółka-Jönsson, M. Opałło, and R. Hołyst, "Sposób osadzania nanocząstek metalu na powierzchni w procesie elektrochemicznym, powierzchnia otrzymana tym sposobem i jej zastosowanie," P-408785, 2014.

Chapter 4

Layers of phages ordered in the electric field for bacteria detection

Parts of this chapter are published as:

Ł. Richter, K. Bielec, A. Leśniewski, M. Łoś, J. Paczesny, R. Hołyst, “Dense layer of bacteriophages ordered in alternating electric field and immobilized by surface chemical modification as sensing element for bacteria detection”, *ACS Applied Materials & Interfaces* **2017**, 9, 19622-19629

Ł. Richter*, K. Matuła*, A. Leśniewski, K. Kwaśnicka, J. Łoś, M. Łoś, J. Paczesny, R. Hołyst, “Ordering of bacteriophages in the electric field: application for bacteria detection”, *Sensors and Actuators B: Chemical* **2016**, 224, 233-240; doi:10.1016/j.snb.2015.09.042

Ł. Richter*, M. Janczuk-Richter*, J. Niedziółka-Jönsson, J. Paczesny, R. Hołyst, „Recent advances in bacteriophage-based methods for bacteria detection”, *Drug Discovery Today* **2018**, 23, 448-455; doi:10.1016/j.drudis.2017.11.007

J. Paczesny, M. Łoś, Ł. Richter, M. Fiałkowski, R. Hołyst, „Method of preparation of biosensor containing organized layers of bacteriophages as sensing element and biosensor itself” (no **PL.227746**, patent granted **01.08.2017**)

*equal contribution

Reproduced in part with permission from Ł. Richter et al., ACS Applied Materials & Interfaces 2017, 9, 19622-19629. Copyright 2019 American Chemical Society.

4.1. Introduction

As unobvious as it sounds, the most ubiquitous organisms on Earth are not bacteria, but special type of viruses, called bacteriophages. Bacteriophages, or in short: *phages*, are viruses that host organisms are bacteria. Total number of all phages on the Earth is estimated to be 10^{30} - 10^{32} (more than all other organisms combined together). These arguably the oldest (3 billion years old, by some estimates) organisms on our planet play key role in maintaining microbial balance in all ecosystems [1]. Despite having such tremendous impact on life in general, they were discovered relatively recently, independently by Frederick Twort and Felix d'Herelle in the early years of 20th century [2].

Typical sizes of phages ranges from 50 to 200 nm, however the largest can be even more than 400 nm in length [3]. Although phages have many different shapes and structures (Figure 4.1), vast majority of them (over 95%) belong to the *Caudovirales* order and share a common structure, i.e. icosahedral head which contains genetic information (double stranded DNA) with spike-tail having fibers attached [4]. Stiffness and length of the tail of head-tail type phages depends on the family; *Myoviridae* have long and contractile (e.g. T4), *Siphoviridae* – long and noncontractile (e.g. λ), *Podoviridae* have short tail (e.g. T7). Head-tail structure have a substantial negative charge and fibers are strongly positively charged. Such asymmetry results in high electric dipole moment, that can be even 20 000 D, i.e. 10 000 times stronger than in molecule of water [5]–[8]. Much less common structures in comparison to *Caudovirales* order are filamentous (e.g. M13 from *Inoviridae* family) and spherical (e.g. MS2 from *Leviviridae* family) that can store genetic information in form of RNA or single stranded DNA.

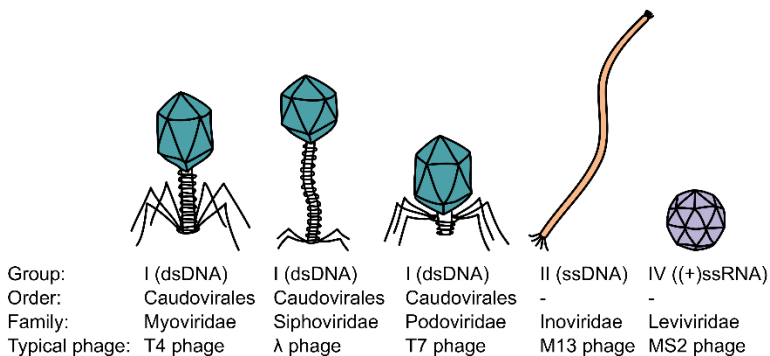


Figure 4.1 Typical structures of bacteriophages. Classification of phages is mostly based on their structure and type of genetic material.

Bacteriophages are obligate intracellular parasites. They can only replicate inside living cells. Phages, like any living organisms, undergo evolution, thus they are typically highly selective for one strain or even species of bacteria. However, there are usually many types of phages that share the same host bacteria. For every species of bacteria it is possible to find many different yet selective bacteriophages. Only recognition of proper host ensures multiplication of genetic material, thus crucial step for phage life cycle is ‘identification’ of

bacteria. First stage of identification process is typically driven by electrostatics – positively charged fibers of bacteriophages are attracted to the negatively charged surface of the bacteria. Second stage is much more selective – receptor binding proteins located at the end of the fibers recognize receptors present on the bacteria surface. The nature and location of the host cell receptors are significantly different depending on the type of phage and bacteria. Receptors can vary from polysaccharide moieties, through peptide sequences, to proteins [9].

When attached to proper host, phages introduce genetic material inside bacterial cells and utilize their intercellular machinery to reproduce (Figure 4.2). Within tens of minutes up to several hundreds of new virions (viral particles) are created, folded and released from a single bacterium. This path is called lytic cycle. Some phages can enter lysogenic cycle, in which genetic material of phage is integrated into nucleic acid of bacteria. In this form (called prophage) bacteriophage genetic information can be transferred upon cell division to the daughter bacterium. In this condition bacteria continues to live and reproduce normally. At the later event (e.g. DNA damage due to UV irradiation) prophage can activate and switch to lytic cycle, causing proliferation of progeny phages and eventually death of the host cell. Phages undergoing only lytic cycle are called virulent and those that can enter both cycles are called temperate [10]. There are also some phages that causes continuous secretion of progeny phages from infected cells without lysis of bacterial cell (e.g. filamentous M13 phage). These are called chronic phages.

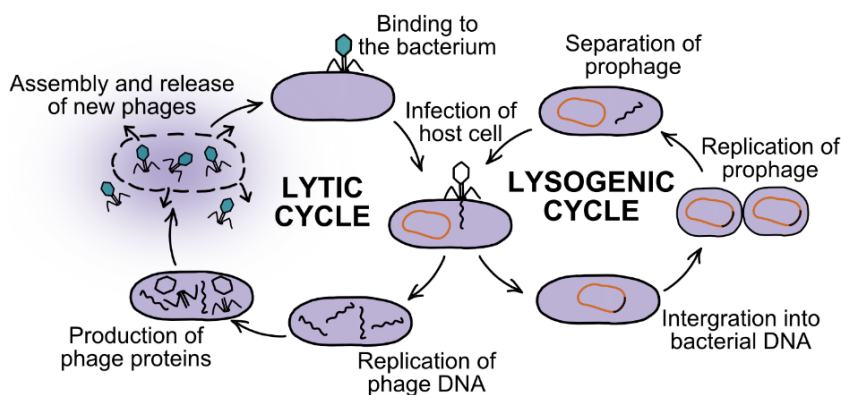


Figure 4.2 Two alternative life cycles of bacteriophage. In lytic cycle phage infects host cell, utilizes intercellular machinery to produce its own copies and finally causes lysis of the bacterium and release of progeny phages. In lysogenic cycle, after infection, phage integrates its genome into bacterial nucleic acid. This hidden form is called prophage. In given conditions phage can switch from one type of cycle to another (e.g. breakage of bacterial DNA).

There are numerous applications of phages in medicine, industry, agriculture and many more. Immediately after their discovery in the early 1900s, they were used as a medical agents against some bacterial infections [2]. Curing bacterial diseases with phages is called phage therapy. Despite early successes, phage therapies were largely abandoned when antibiotic came along [11]. Due to unrepeatability of early results, initial lack of

knowledge in molecular biology and genetics, and stunning success of antibiotics, until recently, phages were used as medical aid only in few countries, such as Georgia, Russia and Poland [12]. However, spread of drug-resistant superbugs and lack of new antibiotics cause renaissance of phage therapies [13]. They became a new, and often last, hope for millions of patients suffering from bacterial diseases, which do not respond to classical antibiotics therapies. Phage therapies are commonly used as experimental treatment and recently they even reached first attempts of clinical trials [14].

Another application of phages is phage display – a technique that allows for expression of exogenous (poly)peptide or protein fused with a bacteriophage coat protein and display on the surface of the virion [15]. It was first described by George P. Smith in 1985 [16] and further developed in groups of Greg Winter and John McCafferty. Core concept of this technique is to screen a wide diversity of peptides or proteins to find those that are the most selective for a given target. Phages are easy to amplify in bacteria in big quantities, thus by application of phage display it is possible to produce big amounts of different proteins, that can be further use for screening. The most common phage used as a vector to create such libraries is filamentous phage M13 [17]. Over the years, developed innovations and modifications turned phage display into powerful technique. Phage display was used in such applications as selection of inhibitors for the active and allosteric sites of the enzymes, receptor agonists and antagonists, and G-protein binding modulatory peptides. The specific ligands selected in this technique were used in drug delivery, drugs design, vaccine development, and validations of therapeutic target [18]. Its importance was recently underlined by Nobel Prize in chemistry that Greg and Winter obtained in 2018 for their contribution to development of the technique of phage display [19].

Phages can be also used to improve food safety. Such approach is called “phage biocontrol”. It can be used in three main types of applications: protection of domesticated livestock from bacterial infections, decontamination of surfaces in food-processing factories, and post-harvest treatment of food (e.g. direct application of phages on food). Phage biocontrol is increasingly accepted as green and natural technology for targeting specific pathogens in food chains [20]. Among over 50 biggest bacteriophage-based companies all over the world, 15 of them are focused on phage biocontrol [21]. There are currently more than 10 products approved for food safety applications, distributed in among others, Switzerland, USA, Canada and Israel [22]. In the context of food safety, bacteriophages address many of the concerns reported by consumers and producers, providing safe, selective, environmentally-friendly and noncorrosive methods of bacteria eradication from food [23]. For example, diseases such as fire blight in apples or bacterial spot of tomato and peaches can be reduced by species-specific phages against *Erwinia amylovora* and *Xanthomonas campestris* [24], [25], respectively. Phage biocontrol was also proved to be useful in control of food related animals diseases, such as salmonellosis in chickens, *E. coli* O157:H7 shedding by beef cattle, and enteropathogenic *E. coli* infections in calves, piglets, and lambs [26], [27]. Moreover, phages can also be applied in processed

foods such as poultry, dairy products, red meats, and fruits to reduce growth of such bacteria as *Listeria monocytogenes*, *Salmonella*, and *Campylobacter jejuni* [23].

Yet another application of phages is broad field of phage-based biosensors for bacteria detection. The idea of utilization of phages for sensing is gaining increasing interest among scientists [28]–[34] and can be realized in several ways (Figure 4.3). Phages can be used to infect target bacteria. This event can be a signal trigger for further detection. In a case of phage lysis, number of released progeny phages can be detected and correlated with initial bacterial concentration [35], [36]. Alternatively, released cell content can be detected. This can be performed by analysis of activity of intracellular enzymes, such as β -galactosidase released upon phage-mediated lysis [37], [38] or measurement of resulting changes of conductivity [39]. Another approach for bacteria detection is to treat whole phages as a part of bioconjugates in a variety of assays. In this approach, virions are attached to different micro- or nano-spheres and such prepared bioconjugates are used for targeting the bacteria, separation of bacteria from complex samples and/or as a direct tool for bacteria detection [40], [41]. This method will be further discussed in chapter 5.

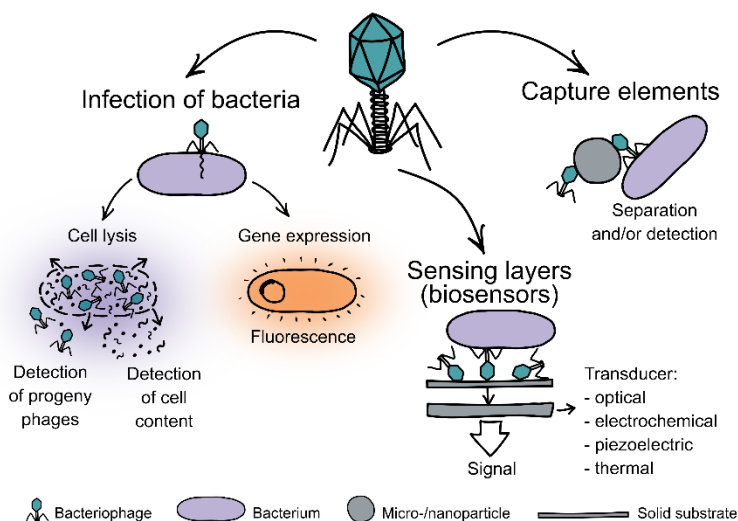


Figure 4.3 Bacteriophage-based methods for detection of bacteria.

Another approach for phage-based bacteria detection is immobilization of virions at a solid substrate. Such prepared phages can be treated as a sensing layer and further combined with transducer to obtain classical sensor. Until now, improvements of the phage-based biosensors were introduced mainly due to increase in number of phages within the sensing elements. First, physisorbed layers of phages were used. For example Olsen et al. showed the possibility of detection of *Salmonella typhimurium* with limit of detection of around 100 cells/ml [42]. However, authors utilized filamentous phages isolated from phage library, which is very difficult, expensive and time-consuming procedure. Another approach replaced physisorption with more sophisticated chemical binding of phages on chemically modified surfaces. Comparing to bare gold Singh et al. increased a number of deposited T4

phages by factor of 5 to 7 using dextrose- and sucrose-covered surfaces, and 37-times due to modification of the surface with cysteamine and glutaraldehyde [43]. However, this manifested in only 4- and 12-fold increase of the sensitivity of detection of *Escherichia coli* bacteria, respectively. These results indicated significant deviation from the linearity in improvement of the sensitivity of phage-based sensors with increase of phage surface coverage. This was caused by random orientation of virions at the surface. As receptor binding proteins (RBPs) are present only at the end of the tail spike of T4 phage, such random orientation of phages resulted in majority of RBPs being unavailable due to steric hindrance [44]. Moreover, the horizontal alignment of the virions is favored by entropy. To overcome this limit, virions should be positioned in tail-up orientation, i.e. arrangement in which majority of receptor binding proteins is involved in detection process.

The problem of proper orientation of phages was recognized, yet not addressed. For instance, Tawil et al. suggested that smaller phages are more likely to attach to a surface by its head [45]. No evidence for that was given in the literature. Tolba et al. showed the biosensors based on genetically modified T4 phages [46]. Biotin carboxyl carrier protein gene was fused with small outer capsid protein gene. Therefore, the heads were tagged with ligand, which formed stable complex with streptavidin-coated magnetic beads. This forced the orientation of phage with receptors exposed towards the analyte. Anyhow, such method required preparation of recombinant phages, which is laborious process that can inactivate the phages. Orientation of phages was used also to control the growth of the bacteria in ready-to-eat and raw meat. Anany et al. immobilized phages on cellulose membranes, which surface was modified to possess a positive surface charge [47]. As a result the negatively charged heads of the virions were in proximity of the surface, whereas the positively charged tails were pointing upwards. Similar approach was utilized to increase the number of phages deposited on the nanostructured interface [48]. This was achieved by electrophoretic capture upon application of positive potential to indium thin oxide electrode. However, there is no direct comparison of results for ordered and unordered phages in the literature and how it improves the characteristics of biosensors for bacteria detection.

In this chapter I describe layer of phages properly oriented in the electric field for bacteria detection (Figure 4.4). Here I provide the evidence that bacteriophages might be oriented in the electric field due to non-zero permanent dipole moment of virions. Combined effect of increased phage surface coverage and proper orientation of virions in alternating external electric field is presented.

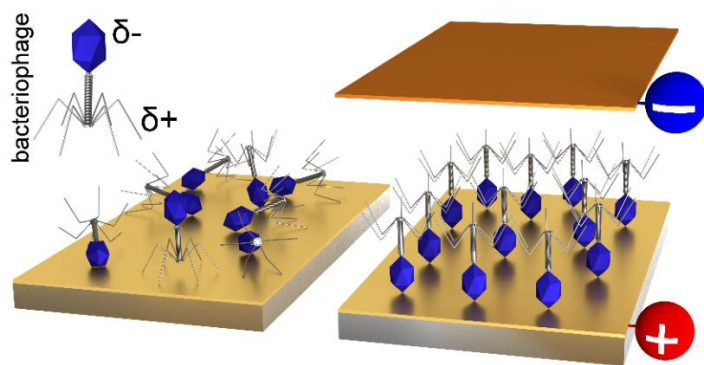


Figure 4.4 Layers of phages properly oriented in the electric field for bacteria detection. Both constant and alternating electric field was exploited. Additionally, in case of alternating electric field, to increase phage surface coverage, chemical modification of the surface was applied.

4.2. Results and discussion

Main goal was to develop a method, which could be easily adaptable for creating sensors based on bacteriophages for detection of any desired strain of bacteria. Therefore, I studied T4 bacteriophage together with its host bacteria *Escherichia coli* as a model system. T4 phage belongs to *Caudovirales* order, which contains vast majority of all known bacteriophages. Virion of bacteriophage T4 is composed of 110×80 nm icosahedral head (capsid) and 98 nm contractile tail ended with fibers. dsDNA of length of 168.9 kbp is stored in the capsid [49]–[51]. Depending on the conformation of the fibers the measured values of permanent dipole moment of T4 bacteriophages varies from 20 000 to 200 000 D [5]–[8]. Baran and Bloomfield showed that tail fibers are highly positively charged and the head-tail structure is negatively charged [52]. Such distribution of charges was developed in the process of evolution as an improvement facilitating the infection of the host bacteria. Positively charged fibers are electrostatically attracted to the bacteria, that have negatively charged surface [52]. As a result of such distribution of charges along the virion, phages are susceptible to electric field, which allows then to be orientated in the electric field.

I aimed to develop a method for preparation of chemisorbed ordered layers of bacteriophages. The procedure consists of two steps: 1) chemical modification of surface in one of two different ways and 2) deposition of phages in alternating electric field. Chemical immobilization of bacteriophages allowed obtaining densely packed layers. Simultaneously, properly designed alternating electric field enabled effective orientation of phages.

4.2.1. Preparation of the deposition cell

I used experimental set, which I previously created to obtain results with constant applied electric potential. The main concern was to assure repeatability of the obtained results. This work was described within my Master thesis. Setup was designed to be robust, easy-to-use and to enable convenient exchange of both gold surface and solution of phages. The specially designed cell allowed for simple and rapid deposition of phages at the solid

substrate. The deposition cell was in fact a capacitor (which plates were gold surface at which phages were deposited and copper electrode) filled with solution of bacteriophages (Figure 4.5). To minimize negative effects of applied potential on activity of deposited phages and morphology of gold surface, copper electrode was isolated with PTFE separator of thickness of 200 μm . Such design provided lack of any net Faradaic currents flowing through the system and redox reactions during deposition process. Direct current deactivates both bacteria and viruses. Drees et al. proved that the effect of the direct current up to 350 mA is much more pronounced in case of bacteria compared to bacteriophages [53].

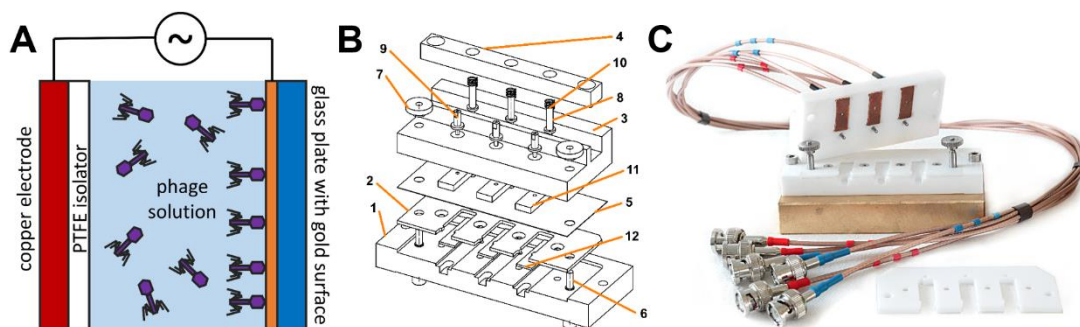


Figure 4.5 (A) Schematic representation of the deposition cell. The cell is a capacitor filled with solution of bacteriophages. Plates of capacitor are gold layer and copper electrode; (B) Blueprint of developed cell (taken from the Master thesis of the author); (C) Photograph of ready-to use cell with three parallel channels for simultaneous deposition of phages on three substrates. In the picture PTFE separator was removed, to reveal copper electrodes.

I analyzed the possibility of occurrence of electrochemically forced redox reactions in microenvironment. In such a case separated spots at the gold surface could play a role of microelectrodes. This should manifest as changes of morphology of the gold surface after the application of the electric potential. Bare gold plate was inserted into the deposition cell, the cell was filled with TM buffer and constant voltage of 50 V was applied for 60 min. No changes in morphology were observed between tested and reference gold surface. Representative scanning electron microscopy pictures are shown in Figure 4.6.

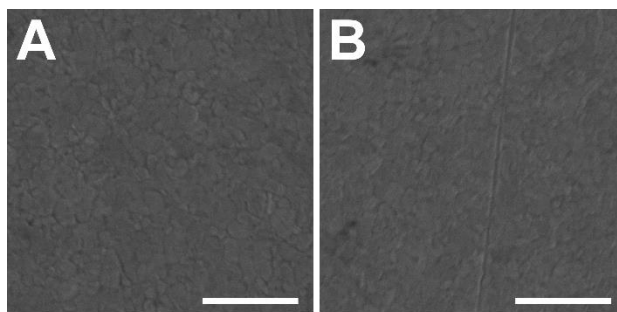


Figure 4.6 SEM images present morphology of gold surfaces of plates. No changes in morphology of gold surface were observed between (A) control plate and (B) plate after the experiment in which deposition cell was filled with TM buffer and constant voltage of 50 V was applied for 60 min. Scale bars correspond to 500 nm.

4.2.2. Deposition of phages in the constant electric field

During research for my Master thesis, it was proven that phage-based sensing layers created upon application of constant voltage show four times higher sensitivity in detection of *E. coli* bacteria in comparison to layers of randomly oriented phages (Figure 4.7). In short, phages were deposited on gold surface in the described above deposition cell upon application of constant voltage of 10 V. Then substrates with phages were placed in the solution of casein. Casein covered gold surface between phages and prevented unspecific binding of the bacteria to the uncovered gold. To test such prepared samples, they were immersed in the solution of bacteria *E. coli* BL21(DE3) for a given amount of time (15 minutes). Used bacteria produced green fluorescence protein (GFP). Finally, surface of the sensing layers were observed using confocal microscopy and number of caught bacteria per 1 mm² was calculated. Estimated limit of detection of such prepared layers was around 10³ CFU/ml. In order to further develop layers of phages deposited in the electric field, deeper understanding of the process was needed. Such analysis was the beginning of the work in this project within my PhD thesis.

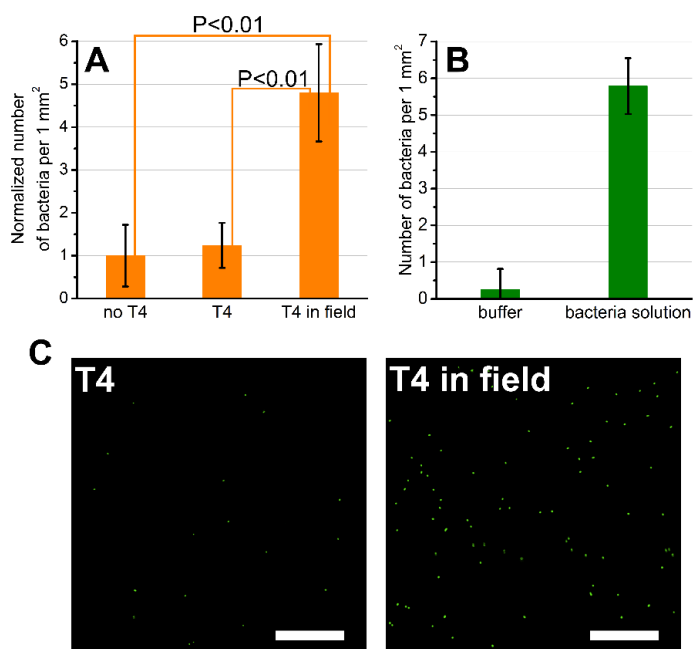


Figure 4.7 Presented results are taken from my Mater thesis and their only purpose here is to introduce to the project; **(A)** Averaged and normalized number of caught bacteria per 1 mm² of the biosensors: without any phages, with phages but without electric field, and with phages deposited upon application of the constant voltage; **(B)** Numbers of caught bacteria per 1 mm² of two sensors with phages deposited upon application of the field, immersed in physiological saline (blank) and solution of bacteria of a concentration of $2.60 \cdot 10^3$ CFU/ml. The sensing elements were prepared as sample “T4 in field”; **(C)** Representative confocal microscopy pictures were analyzed to calculate the sensitivity of sensing elements based on disordered and ordered layers of T4 phages. The scale bars correspond to 100 μ m.

In literature, the most common method of increasing sensitivity of phage sensing layers was direct increase of number of phages at the surface. Anany et al. showed the increase of the number of phages deposited onto positively charged surface when compared with neutral surface [47]. Han et al. gave example of electrophoretic deposition of phages [48]. To evaluate if such sensitivity to phage coverage relationship is also true in the case of my experiments, I performed atomic force microscopy (AFM) and scanning electron microscopy (SEM) imaging of prepared layers (Figure 4.8). Quantitative analysis of surface coverage was based on AFM imaging as it offered cleared view of phages comparing to SEM. I found that around 14.3 phages/ μm^2 were deposited upon application of the constant electric potential. This was only slightly more comparing to 13.4 phages/ μm^2 in case of samples prepared without the applied potential. This proved that the observed effect of increased sensitivity originated in more beneficial orientation of phages rather than increased phage surface coverage.

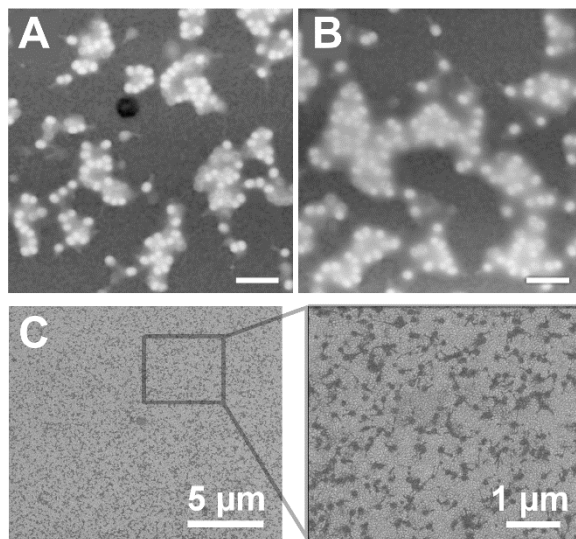


Figure 4.8 AFM images show surfaces of the sensors after phage deposition without (A) and with (B) electric potential applied. Numbers of deposited phages equal 13.4 phages/ μm^2 and 14.3 phages/ μm^2 , respectively. It confirms similar coverage of the sensor surface with bacteriophages in both experiments. Scale bars correspond to 500 nm. (C) SEM pictures of sensing layers from phages deposited upon constant applied voltage.

Calculated values were much higher than given in the literature data (less than 2 phages/ μm^2) and only slightly smaller than in case of chemically immobilized T4 virions (around 18 phages/ μm^2) [43]. Such high values of surface coverage can be explained by possible differences in purities of solutions of phages used by different authors. Naidoo et al. proved that the surface coverage might be increased to around 55 phages/ μm^2 by utilization of specially purified T4 suspension combined with chemical immobilization [54]. Additionally, the authors claimed that around 19 phages/ μm^2 gives the highest affinity to capture bacteria. Higher surface coverage results in clustering of virions, which ultimately limits the ability of immobilized phages to specifically capture its host bacteria. This

problem can be overcome by proper alignment of the phages in tail up position. This substantially increases the ability to capture bacteria, because (1) all RPBs are involved in the process and (2) number of phages per surface unit are limited only by dimensions of virions, giving theoretical value for the densest packing of capsids of T4 at the surface of around 100 phages/ μm^2 . Surface coverage obtained in my experiments was far from this maximum values, both practical, established by Naidoo et al. and theoretical resulting from size of phages. Therefore, in case of my sensing layers no clustering of virions was present.

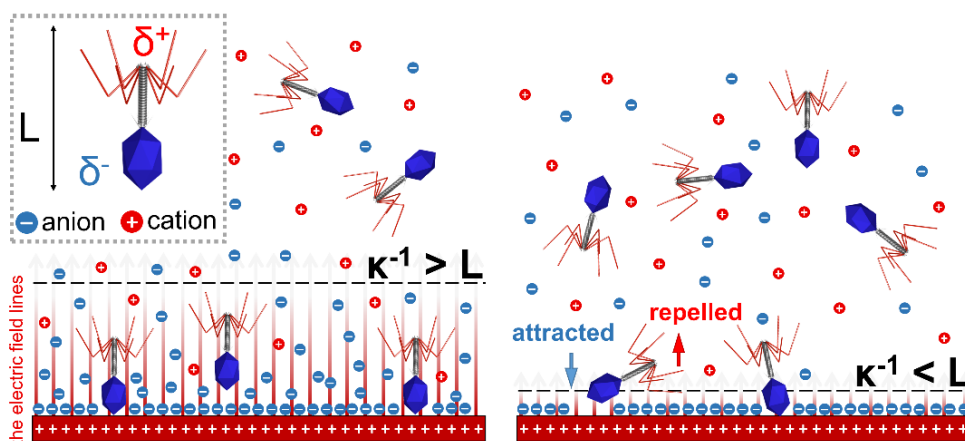


Figure 4.9 Two possible cases of influence of the electric field on phages upon application of the constant electric potential: **(left)** When Debye length κ^{-1} is larger than size of the phage (denoted as L) virions align along the lines of the electric field; **(right)** For κ^{-1} smaller than L the electrostatic interactions favor attachment with only one end of virion to the surface.

To understand the improved sensitivity of layers of phages deposited upon application of constant voltage, I analyzed presence of the electric field in the created system. As in cases described in previous chapters, also this system was a capacitor filled with the electrolyte and again creation of electrical double layer had crucial impact of behavior of the whole process. In my experiments phages were immersed in buffer TM, which is water solution with many different types of ions (e.g. magnesium, sulphate, hydrogen, hydroxide, TRIS). Such conditions were chosen to control pH and ionic strength – parameters crucial for phage survival. In such case, immediately after turning on the voltage, the electric field is created. Then, the ions move due to the electric field and create the electrical double layer (EDL) in the proximity of the gold surface. It resulted in fast decrease of the intensity of the electric field inside the solution. Therefore, after a short period of time the effective electric field is present only within thin electrical double layer. This suggested that overall orientation of phages could be possible only if length of virions (L) would be smaller than thickness of electrical double layer, which is comparable with Debye length (κ^{-1}). In such case virions align along the lines of the electric field only in the proximity of the gold surface, in the volume limited by the surface and the κ^{-1} (Figure 4.9(left)). However, the Debye length calculated for the studied system was few nanometers, i.e. much smaller than the size of the T4 phages (200 nm). Therefore, in my

case capsids (bearing negative partial charge) were much more energetically favored to attach to the gold surface (i.e. positively charged surface) resulting in more phages deposited in tail up orientation (Figure 4.9(right)). Orientation was possible not because of the virus rotation and alignment but due the local attraction and repulsion of head and fibers.

4.2.3. Deposition of phages in the alternating applied voltage

The aim was to further increase the sensitivity of phage-based biosensors. I wanted to facilitate the process of orientation of virions by limiting the screening of the applied field. There was only very limited possibility to increase the Debye length of studied system, as virions are unstable in low osmotic strength solutions [55]. Therefore, I decided to utilize alternating electric field, which allowed the EDL to spread during inter-pulse periods.

For my experiments the square alternating voltage was chosen. In case of such waveform in my setup at the beginning of each pulse the field spread across the whole suspension. Then the electrical double layer was formed and screened the external field. The specific time constant, which described the process of formation of electrical double layer and screening of the electric field by ions, is comparable with time in which ions travel through Debye length driven by electrophoretic forces. In my case the estimated time constant was 2.6 μs . This prediction was in a good agreement with other published results [56]. After this time the external electric field was screened and remained effective only within Debye length, which in studied system was few nanometers.

To be sure that the system relaxed completely (i.e. EDL spread) I assumed that the time between pulses (i.e. with applied 0 V) should be comparable with time of formation of EDL. On the other hand, the inter-pulses time cannot be too long as it should be much shorter than time constant of rotational diffusion of virions in order to avoid defocusing of phages. Rotational diffusion coefficient of T4 phages varies from 273 to 453 s^{-1} , depending on the conformation of the fibers of the virions. These values correspond to rotational time constant (i.e. time of defocusing) between 1.1 ms and 1.8 ms [57].

Higher frequencies (shorter pulses and less time between pulses) corresponded to more events of active orientation of phages by effective field and limited defocusing of phages. Lower frequencies allowed for exploitation of the whole length of each pulse in the most effective way to focus phages along the lines of the field but increased defocusing of phages. These contradicting time scales should be balanced. I judiciously chose 20 μs as duration time of each pulse as well as time between pulses, as it constituted good compromise between all the crucial factors.

In case of square voltage waveform, at the beginning of each pulse there was electric field spreading across the solution. However, the drop of the applied potential to zero at the end of the pulse also generated electric field, but directed oppositely (Figure 4.11). In contrast to analytes deposited on the SERS surface, described in chapter 3, in this case movement of particles (i.e. rotation of phages) was totally reversible. Thus, this symmetrical effect resulted in zero net virion rotation. To overcome this I designed voltage

waveform that allowed creating non-zero effect of orientation of phages. I exploited nonlinear electrophoretic effect, that was proved for number of different particles, e.g. polystyrene latex and aluminum oxide particles and even yeast cells [58]. This phenomenon was previously described in first chapter of this thesis. Due to isolation of one of the electrodes, the process is similar, as in case of application of asymmetrical AC electrophoretic deposition without net DC. When electric field is strong enough, i.e. 100 V/cm and higher, which was the case in my system, the dependence between electrophoretic velocity and applied electric field is non-linear [58]:

$$v_{eph} = \mu_{eph}E + \mu_{eph}^{(3)}E^3 \quad (4.1)$$

where v_{eph} is electrophoretic velocity, μ_{eph} is field-independent electrophoretic mobility coefficient, $\mu_{eph}^{(3)}$ is non-linear electrophoretic mobility coefficient and E is strength of the electric field. I designed trapezoidal voltage waveform, which allowed obtaining substantial difference between values of effective electric field between sharp increase and slow drop of the applied potential at the beginning and at the end of the pulse, respectively (Figure 4.11). Due to the non-linear electrophoretic effect, phages were oriented at the desired position along the lines of the electric field. To ensure proper difference in electric fields, I decided that slow drop of the potential at the end of the pulse should last 20 μ s. Together with 20 μ s of pulse of maximal applied potential and 20 μ s without any applied potential this resulted in 60 μ s period, which corresponded to frequency of 16.67 kHz. All exploited voltage waveforms and resulting electric fields are presented in Figure 4.11.

To produce and validate sensitivity of sensing layers I used procedure consisted of three steps. First clean glass plates with size 1 mm \times 8 mm \times 25 mm covered with gold layer were placed in the deposition cell. Then 160 μ l of phage solution of concentration of around $2 \cdot 10^{11}$ PFU/ml in TM buffer were applied into the deposition cell, the cell was closed and a given voltage was applied over the distance between electrodes of 1 mm. Positive potential was applied to the gold surface. Deposition of phages lasted for 30 min. Afterwards plates were removed from the deposition cell and excess of phages was rinsed. To avoid nonspecific binding of bacteria, the uncovered gold surface was blocked with 1% solution of skimmed milk powder in TM buffer for 1 hour. Casein, which was present in blocking solution, covered the gold surface unoccupied by bacteriophages. Afterwards, plates were rinsed once again. Figure 4.10 shows scheme of the procedure.

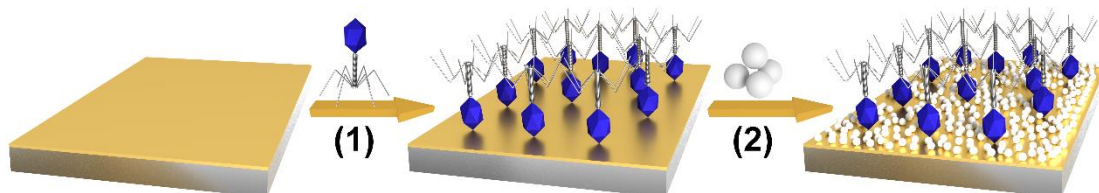


Figure 4.10 Procedure of creating biosensor: (1) deposition of phages on the gold surface upon application of voltage; (2) blockage of the uncovered surface of sensor with casein from skimmed milk.

To analyze sensitivity of prepared layers, they were immersed in bacteria solution for a given amount of time. As a final step, surface of the sensing layers were observed using confocal microscopy and number of caught bacteria (*E. coli* BL21(DE3) expressing GFP) per 1 mm² were determined and compared with control measurements.

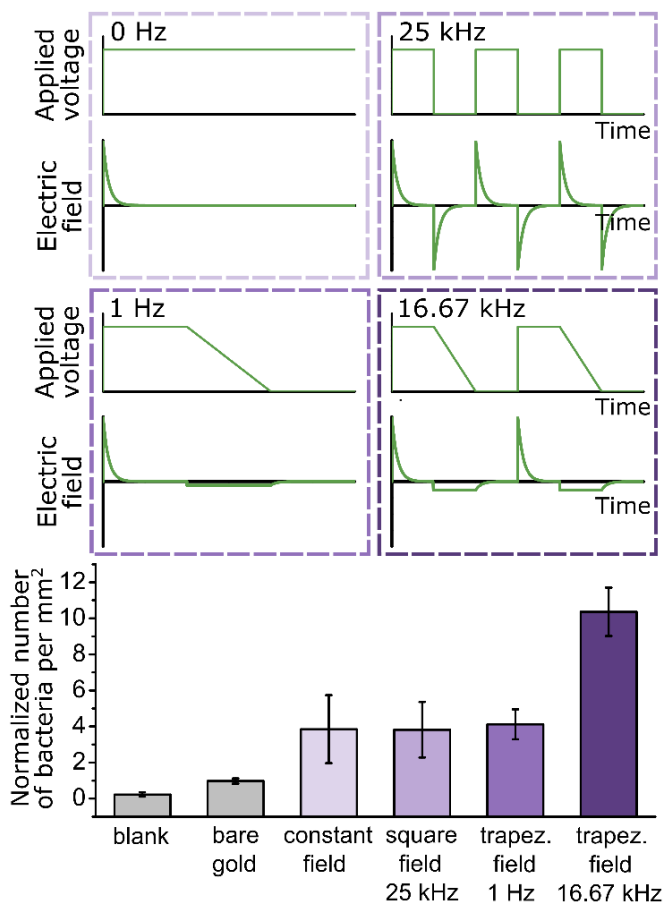


Figure 4.11 Comparison of sensitivity (normalized number of caught bacteria) of phage-based sensing layers prepared using various sets of parameters of the electric field. In all cases maximum applied voltage was 10 V. Upper panels present all the applied voltages and the resulting electric fields.

To check validity of my hypothesis I first prepared a set of sensing layers consisting of phages deposited with use of rectangular pulses of electric field (10 V, various frequencies) (Figure 4.12). I proved that utilization of square waveform didn't improve efficiency of bacteria capturing in comparison to constant voltage. The effect again was only due to electrostatic interactions with the surface. As another control I also tested trapezoidal waveform of frequency of 1 Hz, which allowed phages to defocus by rotational diffusion during inter-pulses periods (Figure 4.11). Again, no differences were observed in comparison to square waveform and constant voltage proving that mainly electrostatic interactions between surface (polarized positively) and capsids (negative pole of the dipole)

played role, when net focusing of phages in bulk was negligible. Utilization of designed (10 V, 16.67 kHz) trapezoidal voltage waveform resulted in 2.5-fold increase of sensitivity in comparison to square waveform and constant voltage applied. When compared to randomly oriented phages the increase upon application of trapezoidal waveform of properly adjusted frequency was around 10-fold (Figure 4.11).

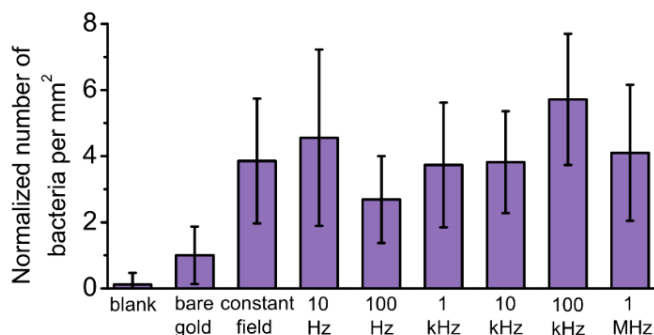


Figure 4.12 Sensitivity (normalized number of caught bacteria) of sensing layer prepared with application of the square voltage waveform (10 V) of different frequencies.

I also proved that 10 V was the most effective applied voltage for orientation of phages (Figure 4.13). This value seemed to balance the electrophoretic force, which oriented phages (higher potential was more favored), against unwanted phenomenon like deactivation of phages and increase of charge density of electrical double layer (higher potential was less favored).

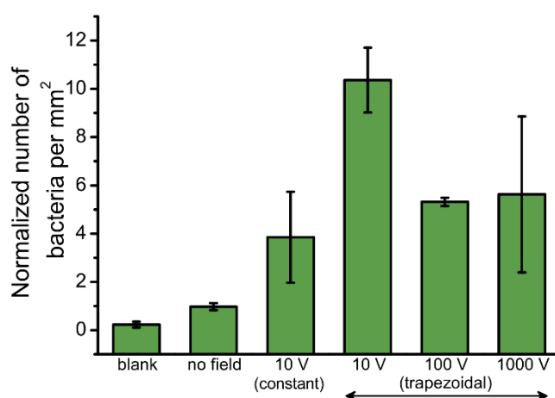


Figure 4.13 Normalized number of caught bacteria with sensing layers composed of phages deposited in different voltage waveforms. Different voltages applied in trapezoidal waveforms were compared with randomly oriented phages (“no field”) and phages oriented in constant field (“10 V (constant)”).

4.2.4. Preparation of the phage-based layers by combining chemical modification and the alternating electric field

In order to further increase sensitivity of prepared sensing layers, I combined chemical immobilization of phages with orientation using the electric field. For this purpose, I followed two protocols of surface modification. Singh et al. developed the method, in which

the gold surface is covered with cysteamine and then glutaraldehyde [43]. Arya et al. utilized self-assembly monolayers of dithiobis(succinimidyl propionate) (DTSP) [59]. The reported most effective surface coverages of T4 bacteriophages reached 18 phages/ μm^2 (method of Singh et al.) and around 20 phages/ μm^2 (method of Arya et al.; based on Figure 3c in ref. [59]). It should be noted that in case of DTSP less T4 phages (20 phages/ μm^2) performed better in capturing bacteria comparing to maximal obtained surface coverage of around 30 phages/ μm^2 (based on Figure 3d in ref. [59]). This confirmed a jamming due to clustering of the virions at high surface coverage.

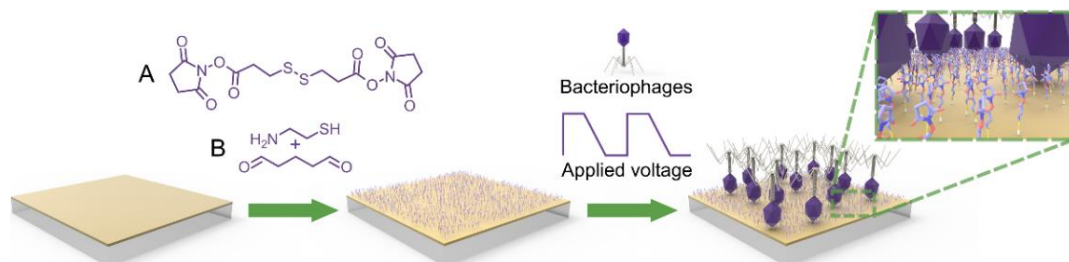


Figure 4.14 Scheme for fabricating dense sensing layers of ordered phages. At first gold surface was modified with (A) dithiobis(succinimidyl propionate) (DTSP) or (B) cysteamine and subsequently glutaraldehyde. Second step consisted of deposition of phages in the alternating electric field. As the third step of sensing element preparation protocol (not shown) the surface between virions was covered with inert protein, casein, to prevent unspecific binding of bacteria to the surface.

I expected to obtain synergistic effect of both procedures and thus to create densely packed layers of properly ordered phages, which were not sterically restricted. First I modified surfaces with (A) DTSP or (B) cysteamine and glutaraldehyde (CA+GA). Then I deposited phages in the alternating electric field of trapezoidal voltage waveform (10 V and 16.67 kHz). Finally the remaining uncovered surface of gold was blocked with casein (Figure 4.14). If not stated otherwise, all experimental details was the same as in case of deposition of phages in the alternating electric field. To check the effect of chemical modification itself, I also deposited phages on chemically modified surfaces without the applied voltage. As it is shown in Figure 4.15, I obtained 64-fold and 50-fold increase in number of captured bacteria (i.e. sensitivity) due to combination of alternating electric field (trapezoidal, 10 V and 16.67 kHz) and DTSP or CA+GA, respectively, when compared to randomly oriented phages on bare gold surface. Application of alternating electric potential alone resulted in around 10-fold increase (for both bare gold and chemically modified surfaces), whereas chemical immobilizations alone increased number of caught bacteria 4 to 5 times.

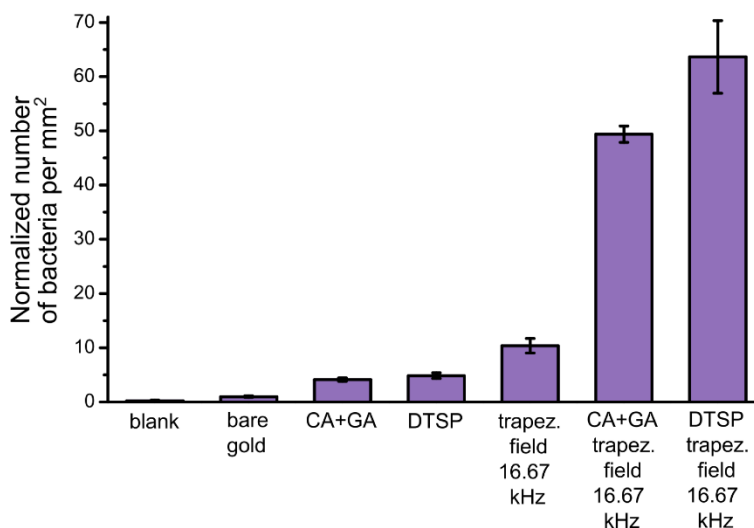


Figure 4.15 Sensitivity (normalized number of caught bacteria) of phage-based sensor prepared with chemical modifications of the surfaces and applied trapezoidal voltage waveform. Combined effect of both methods resulted in up to 64-fold increase in sensitivity.

To further investigate the combined effect of both studied factors I used atomic force microscopy (AFM) to analyze layers of phages after deposition process in various conditions. I also calculated surface coverage of phages within each layer (Figure 4.16). Both methods of chemical modifications significantly increased surface coverages of phages. Similarly as in case of constant voltage, the electric field caused only slight change in phage coverage. This proved that chemical modifications increased number of phages on surface and therefore increased number of caught bacteria, whereas the electric field increased number of caught bacteria only by proper orientation of phages. For comparison I showed representative images acquired by means of confocal microscopy of sensor surface with caught bacteria.

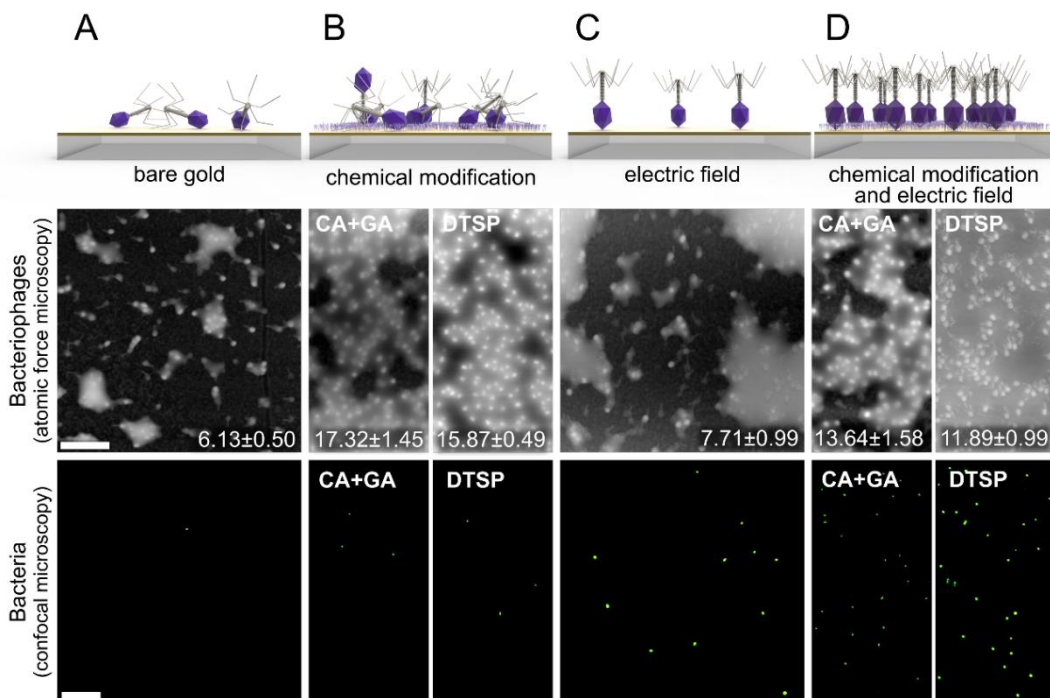


Figure 4.16 Schematic illustrations and corresponding atomic force microscopy (AFM) images of layers of phages deposited on (A) bare gold, or in various conditions: (B) with chemical modifications of the surface (with cysteamine and glutaraldehyde (CA+GA) or dithiobis(succinimidyl propionate) (DTSP)), (C) in electric field from trapezoidal voltage (16.67 kHz, 10 V) and (D) combination of thereof. Numbers on AFM images correspond to surface coverage of phages in each layer in phages/μm². The presented values are means obtained from analysis of at least three samples. Corresponding confocal microscopy images show surface of sensing layers with caught bacteria. Each green spot depicts single bacteria. Scale bars on AFM and confocal microscopy pictures correspond to 1 μm and 50 μm, respectively.

As a next step the selectivity of prepared phage-based sensing elements was analyzed. I prepared real sample contaminated with two different species of bacteria. Tap water was spiked with similar concentrations of *Escherichia coli* BL21(DE3) (host bacteria) and *Enterobacter aerogenes* PCM 1832 (non-specific bacteria). *E. aerogenes* bacterium was judiciously chosen for comparison, as it belongs to the same *Enterobacteriaceae* family as *E. coli*. To be able to distinguish signals coming from two different species, I stained bacteria *E. aerogenes* with red fluorescent dye SYTO RED 62. For experiments, layers with T4 phages deposited in the electric field generated by trapezoidal voltage waveform combined with chemical modifications of the surface were used. Concentration of *E. coli* was around $4 \cdot 10^5$ CFU/ml, whereas *E. aerogenes* was around $5 \cdot 10^5$ CFU/ml. High selectivity of phage-based biosensors and their usefulness in testing real samples was proved, what is in good agreement with other published studies (Figure 4.17A) [59]. Comparison of confocal microscopy images of prepared spiked tap water and representative images of sensing layer with caught bacteria are provided in Figure 4.17B.

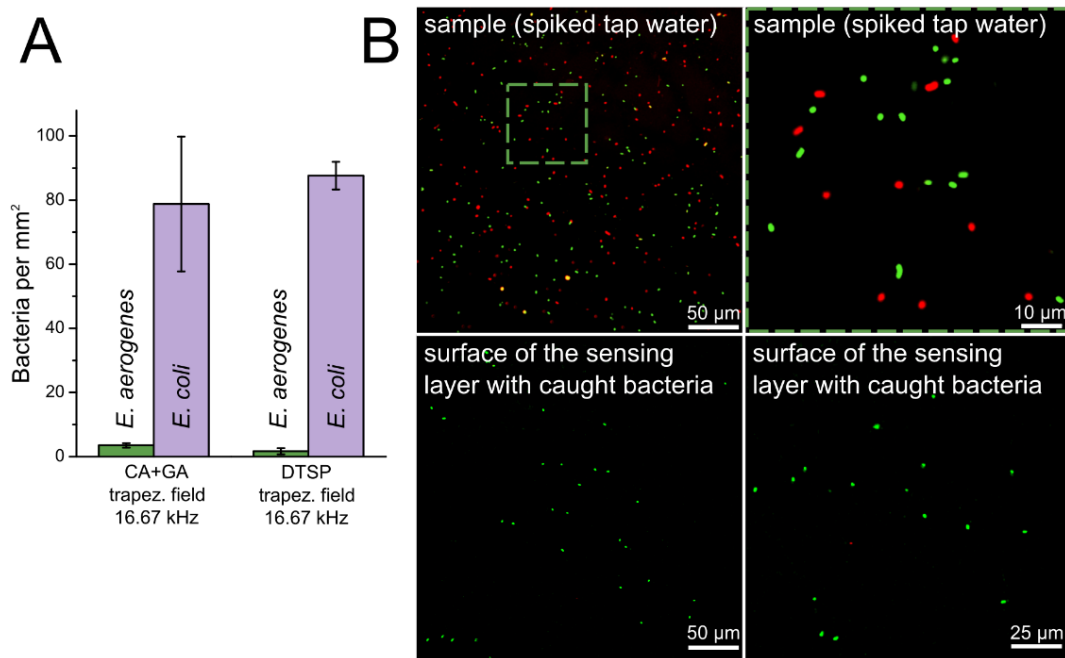


Figure 4.17 (A) Number of bacteria caught from tap water spiked with two species of bacteria: *E. coli* and *E. aerogenes*. Concentrations of bacteria were $4 \cdot 10^5$ CFU/ml and $5 \cdot 10^5$ CFU/ml, respectively. Great selectivity was assured by the natural properties of bacteriophages; (B) **top** – confocal microscopy images of prepared sample, i.e. tap water spiked with *E. coli* BL21(DE3) (green objects) and *E. aerogenes* PCM 1832 stained with SYTO RED 62 (red objects), **bottom** – representative confocal microscopy images of sensing layers with caught bacteria after detection from spiked tap water sample. Absence of red objects confirms high selectivity of prepared layers.

For evaluation of limit of detection I used only sensing layers with the highest sensitivity, i.e. phages chemically immobilized on DTSP-modified surface in trapezoidal electric field (10 V, 16.67 kHz). Number of bacteria caught from samples with different bacteria concentrations was analyzed. Obtained data are presented in Figure 4.18. Estimated limit of detection was around 100 CFU/ml.

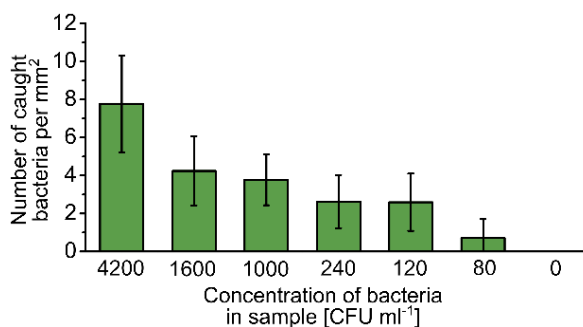


Figure 4.18 Analysis of limit of detection of prepared layers with the highest sensitivity, i.e. phages chemically immobilized on the DTSP modified surface in the trapezoidal electric field (10 V, 16.67 kHz). Estimated limit of detection was around 100 CFU/ml.

The number of reports on the effect of the electric field on activity of viruses is limited. Majority of recent reviews and books refer to work by Khadre and Yousef who showed that pulsed electric field has only marginal effect on the viral load of Rhinoviruses (Wa strain) [60]. However, there are some works indicating that the electric field might influence viruses. Therefore, I checked if experimental conditions utilized by me for orientation of the phages had impact on the virulence of T4 bacteriophages and if decrease of number of phages in the suspension was solely due to deposition of phages on solid substrate. I excluded possibility of deactivation of phages through faradaic currents by proper design of the deposition cell (PTFE separator of thickness of 200 μm), however the effect of the electric field still had to be checked. Thus, I estimated number of active bacteriophages in suspension before and after deposition process in different conditions (Figure 4.19). It was proved that application of the alternating electric field or utilization of the protocol of surface modification did not deactivate bacteriophages. The number of phages, which was present in the suspension after deposition process, was about 90% of initial value. This corresponded to around $1.76 \cdot 10^9 \pm 0.40 \cdot 10^9$ phages loss during deposition and it was observed in case of all samples, i.e. prepared with and without electric field, surface modification and combination of them. AFM imaging indicated that there were around $2.4 \cdot 10^9 \pm 0.8 \cdot 10^9$ virions in each sensing layer, which was estimated by multiplication of phage surface coverage and surface area of the sample. This proved that the decrease of number of phages in the suspension was solely due to deposition of phages and not deactivation.

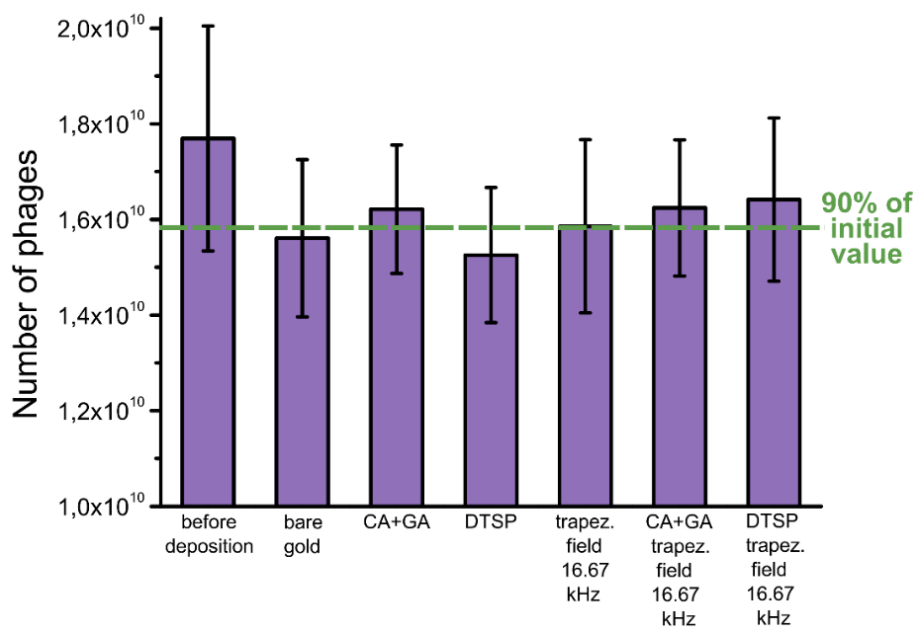


Figure 4.19 Number of phages in 160 μL (volume of phage suspension used for preparation of each sample) before and after deposition processes in different conditions. The decrease corresponded solely to phage deposition and not to deactivation of phages by the electric field.

4.3. Conclusions

Bacteriophages might supplement antibodies in the field of bioanalysis as phages are stable and resistant to external conditions. Up until now the research efforts were directed to increase of the number of virions at the surface of the sensing elements. This resulted in statistically higher number of receptors available for analyte. High surface coverage might be achieved by chemical immobilization of phages over physisorption [43] combined with proper adjustment of ionic strength and Debye radius [61], [62] and utilization of well purified phage suspensions [54]. In this chapter new approach for increasing the sensitivity of the phage-based sensors for bacteria detection was demonstrated. The increase in number of available receptors was achieved by the proper geometrical orientation of the virions. Ordering of phages at the surface of the sensors should also solve the problem of inactivation of phages upon increase of surface coverage [54].

I demonstrated the combined effect of increase in the number of T4 bacteriophages and their proper geometrical orientation on the sensitivity of the model sensing element for *E. coli* bacteria detection. Activation of the surface by utilization of CA+GA or DTSP resulted in 4-fold and 5-fold improvement of sensitivity, respectively. Separate experiments proved that proper arrangement of phages obtained by orientation of virions in properly designed alternating electric field gave 10-fold increase. Combined together these two approaches allowed for around 50- to 64-fold increase in number of captured *E. coli* cells by T4 bacteriophage-based sensing element depending on the method of surface modification. This synergetic effect arose from the fact, that ordering of phages at the chemically modified surface enabled to obtain dense layers of advantageously oriented phages. Introduced improvements resulted in 15 min detection with limit of detection of around 100 CFU/ml, i.e. in a range of best phage-based surface sensors described to time. This method can be used for preparation of phage-based biosensors for detection of almost every strain of bacteria, as T4 has the general structure that is common for majority of bacteriophages. The proposed procedure can be also exploited to form ordered structures of other colloidal particles, molecules, proteins or organisms with non-zero dipole moment.

4.4. Materials and methods

4.4.1. Materials

All chemicals were purchased from Sigma Aldrich (USA) and were used without further purification. Lysogeny broth (LB) medium and LB-agar medium were bought from Carl Roth (Germany) as an instant mixes ready to dissolve in deionized water. LB medium consisted of 10 g/l of tryptone, 5 g/l of yeast extract and 10 g/l of NaCl. LB-agar additionally contained 15 g/l of agar. Physiological saline was prepared by dissolving 9 g NaCl in 1 l of deionized water. TM buffer consisted of 10 mM TRIS (tris(hydroxymethyl)aminomethane) and 10 mM MgSO₄ dissolved in deionized water. pH of TM buffer was adjusted to 7.4 using hydrochloric acid. 5 μM CaCl₂ was added in order to allow activity of DNase I.

LB media, TM buffer and physiological saline were sterilized prior to use by autoclaving at 121 °C for 15 minutes.

4.4.2. Phage preparation and bacteria culturing

Phages were prepared according to Sambrook et al. [63]: T4 phage lysate was prepared by infection of early logarithmic culture of *Escherichia coli* MG1655. After lysis phages were precipitated by polyethylene glycol. After centrifugation of precipitate and resuspension in TM buffer with 1 M NaCl, phages were purified by ultracentrifugation in step CsCl gradient in Ti50 rotor using Beckman Optima XL70 ultracentrifuge. Phages formed a band, which was collected by aspiration using syringe and then phage solution was dialyzed against TM buffer. After completion of dialysis 0.2 µg/ml of DNase I was added in order to digest DNA released from capsids, which were damaged during dialysis. Number of viable phages was estimated by titration on bacteria *E. coli* BL21(DE3), i.e. the same strain, which was used as target analyte for phage-based sensing layers. I used plaque count method for determination of bacteriophage viability. Plaque forming units (PFU) can be directly correlated with number of active virions within the sample.

Escherichia coli BL21(DE3) (obtained from the Institute of Biochemistry and Biophysics in Warsaw, Poland) was used as a target analyte for T4 phages. The strain harbored a plasmids coding green fluorescence protein (GFP) and providing resistance to chloramphenicol and kanamycin. Bacteria were prepared according to the standard procedures. 25 mg of chloramphenicol and 50 mg of kanamycin were added to 1 L of LB media. Isopropyl β-D-1-thiogalactopyranoside (IPTG) was added to LB media to final concentration of 1 mM to induce the production of the GFP protein. At the beginning, the single colony from agar plate was inoculated into LB medium for overnight culturing (37 °C, 200 rpm). Next day the bacteria were diluted in fresh LB medium and cultured to obtain suspensions of OD₆₀₀ = 0.40. The culture was then centrifuged (4000 rpm, 4 min) and resuspended in greater amount of physiological saline. Dilutions ranged from 4 to 1000 times.

Enterobacter aerogenes PCM 1832 (purchased from Polish Collection of Microorganisms, Wrocław, Poland) was used as non-specific strain for T4 phage to evaluate selectivity of prepared sensing layers. First, the single colony from agar plate was inoculated into LB medium for culturing (37 °C, 200 rpm) to obtain suspensions of OD₆₀₀=0.40. The culture was then centrifuged (4000 rpm, 4 min), resuspended in equal amount of physiological saline. Next SYTO RED 62 (Thermo Fisher Scientific, USA) was added to bacteria solution to final concentration 20 µM. Bacteria were stained for 30 minutes (37 °C, 200 rpm), centrifuged (4000 rpm, 4 min) and resuspended in the same amount of physiological saline. Then solution was again centrifuged and again resuspended in physiological saline.

To determine exact value of bacteria concentrations colony count method was used. Colony forming units (CFU) can be directly correlated with number of bacteria within the sample.

To prepare spiked tap water, tap water was first filtered through filter with 0.22 μm pores. Then bacteria *E. aerogenes* PCM 1832 stained with SYTO RED 62 and bacteria *E. coli* BL21(DE3) was added to water to obtain final concentrations of bacteria around $5 \cdot 10^5$ CFU/ml.

4.4.3. Setup for deposition of phages in the electric field

The deposition cell consisted of two components: base and cover. The main part of the base consisted of three chambers, in which gold plates for phage deposition were placed. Above the deposition chambers the comb-shaped element was placed. It had two functions: 1) it pushed down and immobilized the plates on which phages were deposited and 2) its thickness determined volume of phage suspension, which could be applied into the chamber. In my design the comb-shape element could be easily replaced on demand. Two bolts on both sides of the base element provided proper alignment of cover and base. In the cover the electrical contacts were mounted. Three pins were pushed down by springs. This ensured electrical contact with the gold surfaces placed in the base of the cell. Three copper electrodes were covered with 200 μm PTFE separator. The whole cell was attached to heavy plate made of metal to assure stability.

The deposition cell was connected with voltage generation setup composed of function generator (DG1022, Rigol, China) and voltage amplifier (2210, Trek, USA). Signal provided by function generator was amplified by the factor of 100. Parallel connected oscilloscope (DS1052E, Rigol, China) with two probes for low (up to 250 V) and high (up to 1000 V) voltage enabled precise control of output voltage signal. The generated signal was applied to the deposition cell. Because of the PTFE separator, no electric current (measured with accuracy of nanoamperes) flowed through the system and thus no electrochemical reactions occurred.

The cell and voltage generation setup were connected with the distribution box that enabled full control over the setup, e.g. polarization of electrodes or even detaching channels (gold surface – copper electrode pair) in order to conduct control experiments (without electric field) in exactly the same geometrical configuration.

4.4.4. Solid substrates for sensing layers

1 \times 8 \times 25 mm glass plates covered first with 5 nm layer of titanium and subsequently with 150 nm layer of gold were used. The gold layer was hardened using argon canon. Substrates were obtained from the Institute of Electronic Materials Technology (Warsaw, Poland). Prior to use, substrates were gently wiped and washed thoroughly with water and ethanol. Afterwards the plates were sonicated sequentially in acetone, ethanol, isopropanol, and

twice in deionized water for 5 minutes in each solvent. Such substrates were used as support for T4 layers or were further subjected to chemical modifications.

4.4.5. Modifications with DTSP or with cysteamine and glutaraldehyde

Dithiobis(succinimidyl propionate) (DTSP) modification procedure was adapted from research of Arya et al. [59]. Clean solid substrates were immersed in 2 mg/ml solution of DTSP in acetone for 20 h at room temperature. Then modified substrates were washed with acetone and rocked for 15 min in acetone to get rid of unreacted substrate. Such modified plates were used for phage deposition within 1 h after modification (samples denoted as “DTSP”).

Second utilized procedure was inspired by Singh et al. [43]. Clean plates were exposed to 50 mM solution of cysteamine hydrochloride for 20 h at 40 °C. Afterwards substrates were rinsed thoroughly with acetone and water and activated by incubating in 2% (v/v) solution of glutaraldehyde in water for 1 h at room temperature. The substrates were then washed with large amount of water and used for phage deposition within 1 h afterwards (samples denoted as “CA+GA”).

4.4.6. Protocol for preparation of biosensors

Clean plates were placed in the deposition cell. 160 µl of phage solution in TM buffer were applied into the chamber of the deposition cell and onto the plate. Concentration of phages was around $2 \cdot 10^{11}$ PFU/ml. The cell was closed and voltage was applied over the distance between electrodes of 1 mm. Positive potential was applied to the gold surface of the glass plate. Deposition of phages lasted for 30 minutes. Afterwards plates were removed from the deposition cell. Excess of phages was rinsed from the surface of the plates with a large amount of TM buffer.

To avoid nonspecific binding of bacteria, the uncovered gold surface was blocked. 1% solution of skimmed milk powder in TM buffer was used as blocking agent. The sensing plates with deposited phages were immersed in saturated solution of milk for 1 hour. Casein, which was present in blocking solution, covered the gold surface unoccupied by bacteriophages. Afterwards, plates were rinsed with large amount of TM buffer.

4.4.7. Analysis of number of deposited phages and phage deactivation

To investigate the influence of the electric field and surface modification on activity of studied T4 bacteriophages plaque counting method was used. The concentration of phages before the experiment was $1.11 \cdot 10^{11} \pm 0.15 \cdot 10^{11}$ PFU/ml. 160 µl of suspension was placed in the deposition cell. The only difference between samples was whether electric field and/or surface modification were utilized. Influence on the phages of trapezoidal waveform of the electric field (10 V, 16.67 kHz) and chemical modification was evaluated. After deposition process, the phage suspension was carefully retrieved from the deposition cell. The concentration of phages for different samples was evaluated by plaque count method and

obtained results varied only in range from $0.95 \cdot 10^{11} \pm 0.09 \cdot 10^{11}$ PFU/ml to $1.03 \cdot 10^{11} \pm 0.11 \cdot 10^{11}$ PFU/ml. Taking into account volume of sample used for deposition it corresponded to around $1.76 \cdot 10^9 \pm 0.40 \cdot 10^9$ phages deposited on the surface.

4.4.8. Protocol for analysis of sensitivity of studied biosensors

Prepared biosensors were immersed and gently mixed in the 4 ml of bacteria solution for 15 min. Afterwards sensors were rinsed thoroughly in TM buffer to remove unbounded bacteria from the surface. Surface of the sensors were then observed using confocal microscopy. Obtained images were analyzed and number of bacteria per 1 mm^2 were determined.

For each set of phage deposition conditions were performed at least three independent experimental runs. In many cases precise determination of value of concentration of bacteria in prepared solution was not necessary. As control were always prepared two types of plates covered with: 1) randomly oriented phages and 2) only casein (to check the possibility of non-selective deposition of bacteria on casein). Corresponding error bars were provided. The results were normalized in respect to randomly oriented phages.

When I referred to limit of detection (LOD), LOD was considered as the lowest concentration of the analyte in the sample that generates response of the sensor equals three times the variability in the background signal added to the background signal [64].

4.4.9. Calculations of time constant τ in the system

Many specific time-scales of development of the electrical double layer were reported in the literature, as discussed in the first chapter of this thesis. Typically reported time constants spread from λ_D^2/D , through $\lambda_D L/D$, to L^2/D , where λ_D is Debye length, L is half of distance between electrodes, and D is diffusion coefficient of ions [65], [66], [67]. In the case presented here, consideration of different above-mentioned time scales resulted in values that vary from nanoseconds, through milliseconds, up to even hours. Thus, to better estimate dynamics of my system, I used another approach. Specific time constant is also comparable with time in which ions travel through Debye length driven by electrophoretic forces. This can be calculated as follows:

$$I = \frac{1}{2} \sum c_i z_i^2 \quad (4.2)$$

I – ionic strength, c_i – concentration of ion, z_i – charge of ion

$$\lambda^2 = \frac{\varepsilon RT}{2F^2 I} \quad (4.3)$$

λ – Debye length, ε – dielectric constant, R – gas constant, T – temperature, F – Faraday constant

$$\lambda = 1.43 \text{ nm}$$

$$\mu_i = \frac{z_i F}{RT} D_i \quad (4.4)$$

μ_i – electrical mobility, D_i – diffusion coefficient of ion

$$\epsilon_{\text{water}} = 6.9 \cdot 10^{-10} \text{ F/m}$$

$$R = 8.314 \text{ J/mol} \cdot \text{K}$$

$$T = 298.15 \text{ K}$$

$$F = 9.648 \cdot 10^4 \text{ C/mol}$$

Table 4.1. Detailed information about all ions in TM buffer.

Type of ion	Concentration [M]	Charge [-]	Diffusion coefficient [$10^{-9} \text{ m}^2/\text{s}$]	Electrophoretical mobility [$10^{-8} \text{ m}^2/\text{s} \cdot \text{V}$]
TRIS ⁺	10^{-2}	+1	0.90	3.5
Mg ²⁺	10^{-2}	+2	0.71	5.5
SO ₄ ²⁻	10^{-2}	-2	1.06	8.3
H ⁺	$10^{-7.4}$	+1	9.31	36.2
OH ⁻	$10^{-6.6}$	-1	5.28	20.6
Ca ²⁺	$5 \cdot 10^{-6}$	+2	0.79	6.1
Cl ⁻	$5 \cdot 10^{-6}$	-1	2.03	7.9

For further calculations I chose magnesium ions, as they were present at high concentration and have moderate mobility. All of the most common ions had similar mobility, so it is reasonable to consider mobility of magnesium ions.

$$\tau = \frac{\lambda}{\mu E} \quad (4.5)$$

E – strength of the electric field

$$E = 10^4 \text{ V/m}$$

$$\tau = 2.6 \text{ } \mu\text{s}$$

Obtained result of few microseconds is in agreement with other reported values. In very similar system time-dependent development of electrical double layer was calculated numerically [56]. All applied parameters were similar as in case of my system: voltage of 10 mV was applied over 1 μm distance, thus effective electric field was 10^4 V/m ; molarity of the solution was 10 mM, i.e. in range of TM buffer; considered ions Na⁺ and Cl⁻ had mobility of $7.9 \cdot 10^{-8} \text{ m}^2/\text{sV}$ and $5.19 \cdot 10^{-8} \text{ m}^2/\text{sV}$, respectively, which were similar to mobility

of magnesium ions. Time calculated numerically was 1.43 μs and thus it confirmed that my estimation is reasonable and can be used for subsequent analysis.

4.4.10. Additional instrumentation

Nikon Ti Eclipse with confocal system A1R was used for evaluation of sensitivity of prepared sensors. The system included ion laser IMA101040AL5 (Melles Griot, USA) emitting light of wavelength of 488 nm, objective CFI Plan Fluor 40x and NIS-Elements AR 4.13 software.

Atomic force microscopy (AFM) imaging was performed with a MultiMode Scanning Probe Microscope (Bruker, USA).

Scanning electron microscopy (SEM) images were taken with use of a NovaSEM (FEI, USA) scanning electron microscope.

4.5. References

- [1] A. Sulakvelidze, “Using lytic bacteriophages to eliminate or significantly reduce contamination of food by foodborne bacterial pathogens,” *J. Sci. Food Agric.*, vol. 93, no. 13, pp. 3137–3146, 2013.
- [2] D. H. Duckworth, “Who discovered bacteriophage?,” *Bacteriol. Rev.*, vol. 40, no. 4, pp. 793–802, 1976.
- [3] A. Cuervo and J. L. Carrascosa, “Bacteriophages: Structure,” in *eLS*, Chichester, UK: John Wiley & Sons, Ltd, 2012.
- [4] H. W. Ackermann, “5500 Phages examined in the electron microscope,” *Arch. Virol.*, vol. 152, no. 2, pp. 227–243, 2007.
- [5] J. Greve and J. Blok, “Transient electric birefringence of T-even bacteriophages. I. T4B in the absence of tryptophan and fiberless T4 particles,” *Biopolymers*, vol. 12, no. 11, pp. 2607–2622, 1973.
- [6] J. Greve and J. Blok, “Transient electric birefringence of T-even bacteriophages. II. T4B in the presence of tryptophan and T4D.,” *Biopolymers*, vol. 14, no. 1, pp. 139–54, 1975.
- [7] W. Boontje, J. Greve, and J. Blok, “Transient electric birefringence of T-even bacteriophages. III. T2L and T6 with retracted fibers compared with T4B,” *Biopolymers*, vol. 16, no. 3, pp. 551–572, 1977.
- [8] W. Boontje, J. Greve, and J. Blok, “Transient electric birefringence of T-even bacteriophages. IV. T2L0 and T6 with extended tail fibers,” *Biopolymers*, vol. 17, no. 11, pp. 2689–2702, 1978.
- [9] J. Bertozzi Silva, Z. Storms, and D. Sauvageau, “Host receptors for bacteriophage adsorption,” *FEMS Microbiol. Lett.*, vol. 363, no. 4, pp. 1–11, 2016.
- [10] D. R. Harper and E. Kutter, “Bacteriophage: Therapeutic Uses,” in *Encyclopedia of Life Sciences*, Chichester, UK: John Wiley & Sons, Ltd, 2003.
- [11] A. Parisien, B. Allain, J. Zhang, R. Mandeville, and C. Q. Lan, “Novel alternatives to antibiotics: Bacteriophages, bacterial cell wall hydrolases, and antimicrobial peptides,” *J. Appl. Microbiol.*, vol. 104, no. 1, pp. 1–13, 2008.
- [12] S. Matsuzaki, J. Uchiyama, I. Takemura-Uchiyama, and M. Daibata, “The age of the phage,” *Antibiot. Outlook*, vol. 509, no. 2004, p. 59, 2014.
- [13] J. Pirnay, G. Verbeken, T. Rose, S. Jennes, M. Zizi, I. Huys, R. Lavigne, M. Merabishvili, M. Vaneechoutte, A. Buckling, and D. De Vos, “Introducing yesterday’s phage therapy in today’s medicine,” *Future Virol.*, vol. 7, pp. 379–390, 2012.
- [14] P. Jault, T. Leclerc, S. Jennes, J. P. Pirnay, Y.-A. Que, G. Resch, A. F. Rousseau, F. Ravat, H. Carsin, R. Le Floch, J. V. Schaal, C. Soler, C. Fevre, I. Arnaud, L. Bretaudeau, and J. Gabard, “Efficacy and tolerability of a cocktail of bacteriophages to treat burn wounds infected by *Pseudomonas aeruginosa* (PhagoBurn): a randomised, controlled, double-blind phase 1/2 trial,” *Lancet Infect. Dis.*, vol. 19, no. 1, pp. 35–45, 2019.
- [15] C. H. Wu, I. J. Liu, R. M. Lu, and H. C. Wu, “Advancement and applications of peptide phage display technology in biomedical science,” *J. Biomed. Sci.*, vol. 23, no. 1, pp. 1–14, 2016.
- [16] George P. Smith, “Filamentous fusion phage: novel expression vectors that display cloned antigens on the virion surface,” *Science (80-)*, vol. 228, no. 4705, pp. 1315–

- 1317, 1985.
- [17] J. Pande, M. M. Szewczyk, and A. K. Grover, "Phage display: Concept, innovations, applications and future," *Biotechnol. Adv.*, vol. 28, no. 6, pp. 849–858, 2010.
- [18] L. K. Harada, E. C. Silva, W. F. Campos, F. S. Del Fiol, M. Vila, K. Dąbrowska, V. N. Krylov, and V. M. Balcão, "Biotechnological applications of bacteriophages: State of the art," *Microbiol. Res.*, vol. 212–213, pp. 38–58, 2018.
- [19] U. T. Bornscheuer, B. Hauer, K. E. Jaeger, and U. Schwaneberg, "Directed evolution empowered redesign of natural proteins for the sustainable production of chemicals and pharmaceuticals," *Angew. Chemie Int. Ed.*, pp. 36–40, 2018.
- [20] M. Kazi and U. S. Annapure, "Bacteriophage biocontrol of foodborne pathogens," *J. Food Sci. Technol.*, vol. 53, no. 3, pp. 1355–1362, 2016.
- [21] W. A. Sarhan and H. M. E. Azzazy, "Phage approved in food, why not as a therapeutic?," *Expert Rev. Anti. Infect. Ther.*, vol. 13, no. 1, pp. 91–101, 2015.
- [22] Z. D. Moye, J. Woolston, and A. Sulakvelidze, "Bacteriophage applications for food production and processing," *Viruses*, vol. 10, no. 4, pp. 1–22, 2018.
- [23] G. G. Greer, "Bacteriophage control of foodborne bacteria," *J. Food Prot.*, vol. 68, no. 5, pp. 1102–1111, 2005.
- [24] B. Balogh, J. B. Jones, M. T. Momol, S. M. Olson, A. Obradovic, P. King, and L. E. Jackson, "Improved efficacy of newly formulated bacteriophages for management of bacterial spot on tomato," *Plant Dis.*, vol. 87, no. 8, pp. 949–954, 2003.
- [25] E. L. Schnabel, W. G. D. Fernando, M. P. Meyer, A. L. Jones, and L. E. Jackson, "Bacteriophage of *Erwinia amylovora* and their potential for biocontrol," *Acta Hortic.*, vol. 13, no. 489, pp. 649–654, Jul. 1999.
- [26] H. W. Smith, M. B. Huggins, and K. M. Shaw, "The control of experimental *Escherichia coli* diarrhoea in calves by means of bacteriophages," *Microbiology*, vol. 133, no. 5, pp. 1111–1126, 1987.
- [27] H. W. Smith and M. B. Huggins, "Effectiveness of phages in treating experimental *Escherichia coli* diarrhoea in calves, piglets and lambs," *Microbiology*, vol. 129, no. 8, pp. 2659–2675, 1983.
- [28] H. Anany, Y. Chou, S. Cucic, R. Derda, S. Evoy, and M. W. Griffiths, "From bits and pieces to whole phage to nanomachines: Pathogen detection using bacteriophages," *Annu. Rev. Food Sci. Technol.*, vol. 8, no. 1, pp. 305–329, 2017.
- [29] M. Janczuk, J. Niedziółka-Jönsson, and K. Szot-Karpińska, "Bacteriophages in electrochemistry: A review," *J. Electroanal. Chem.*, vol. 779, pp. 207–219, 2016.
- [30] R. Peltomaa, I. López-Perolio, E. Benito-Peña, R. Barderas, and M. C. Moreno-Bondi, "Application of bacteriophages in sensor development," *Analytical and Bioanalytical Chemistry*, vol. 408, no. 7, pp. 1805–1828, 2016.
- [31] Z. Hosseinidoust, A. L. J. Olsson, and N. Tufenkji, "Going viral: Designing bioactive surfaces with bacteriophage," *Colloids Surfaces B Biointerfaces*, vol. 124, pp. 2–16, 2014.
- [32] I. Sorokulova, E. Olsen, and V. Vodyanoy, "Bacteriophage biosensors for antibiotic-resistant bacteria," *Expert Rev. Med. Devices*, vol. 11, no. 2, pp. 175–186, 2014.
- [33] R. G. van der Merwe, P. D. van Helden, R. M. Warren, S. L. Sampson, and N. C. Gey van Pittius, "Phage-based detection of bacterial pathogens," *Analyst*, vol. 139, no. 11, pp. 2617–26, 2014.
- [34] N. Tawil, E. Sacher, R. Mandeville, and M. Meunier, "Bacteriophages: biosensing tools for multi-drug resistant pathogens," *Analyst*, vol. 139, no. 6, p. 1224, 2014.

- [35] H. Anany, L. Brovko, N. K. El Dougdoug, J. Sohar, H. Fenn, N. Alasiri, T. Jabrane, P. Mangin, M. Monsur Ali, B. Kannan, C. D. M. Filipe, and M. W. Griffiths, "Print to detect: a rapid and ultrasensitive phage-based dipstick assay for foodborne pathogens," *Anal. Bioanal. Chem.*, 2017.
- [36] A. Martelet, G. Lhostis, M. C. Nevers, H. Volland, C. Junot, F. Becher, and B. H. Muller, "Phage amplification and immunomagnetic separation combined with targeted mass spectrometry for sensitive detection of viable bacteria in complex food matrices," *Anal. Chem.*, vol. 87, no. 11, pp. 5553–5560, 2015.
- [37] J. Chen, S. D. Alcaine, Z. Jiang, V. M. Rotello, and S. R. Nugen, "Detection of *Escherichia coli* in drinking water using T7 bacteriophage-conjugated magnetic probe," *Anal. Chem.*, vol. 87, no. 17, pp. 8977–8984, 2015.
- [38] D. Wang, J. Chen, and S. R. Nugen, "Electrochemical detection of *Escherichia coli* from aqueous samples using engineered phages," *Analytical Chemistry*, vol. 89, pp. 1650–1657, 2017.
- [39] A. Mortari, A. Adami, and L. Lorenzelli, "An unconventional approach to impedance microbiology: Detection of culture media conductivity variations due to bacteriophage generated lyses of host bacteria," *Biosens. Bioelectron.*, vol. 67, pp. 615–620, 2015.
- [40] Z. Wang, D. Wang, A. J. Kinchla, D. A. Sela, and S. R. Nugen, "Rapid screening of waterborne pathogens using phage-mediated separation coupled with real-time PCR detection," *Anal. Bioanal. Chem.*, vol. 408, no. 15, pp. 4169–4178, 2016.
- [41] Y. Zhang, C. Yan, H. Yang, J. Yu, and H. Wei, "Rapid and selective detection of *E. coli* O157:H7 combining phagomagnetic separation with enzymatic colorimetry," *Food Chem.*, vol. 234, pp. 332–338, 2017.
- [42] E. V. Olsen, I. B. Sorokulova, V. A. Petrenko, I.-H. Chen, J. M. Barbaree, and V. J. Vodyanoy, "Affinity-selected filamentous bacteriophage as a probe for acoustic wave biodetectors of *Salmonella typhimurium*," *Biosens. Bioelectron.*, vol. 21, no. 8, pp. 1434–1442, 2006.
- [43] A. Singh, N. Glass, M. Tolba, L. Brovko, M. Griffiths, and S. Evoy, "Immobilization of bacteriophages on gold surfaces for the specific capture of pathogens," *Biosens. Bioelectron.*, vol. 24, no. 12, pp. 3645–3651, 2009.
- [44] Christopher K Mathews, "Bacteriophage T4," in *Encyclopedia of Life Sciences*, Chichester, UK: Wiley, 2007.
- [45] N. Tawil, E. Sacher, R. Mandeville, and M. Meunier, "Surface plasmon resonance detection of *E. coli* and methicillin-resistant *S. aureus* using bacteriophages," *Biosens. Bioelectron.*, vol. 37, no. 1, pp. 24–29, 2012.
- [46] M. Tolba, O. Minikh, L. Brovko, S. Evoy, and M. Griffiths, "Oriented immobilization of bacteriophages for biosensor applications," *Appl. Environ. Microbiol.*, vol. 76, no. 2, pp. 528–535, 2010.
- [47] H. Anany, W. Chen, R. Pelton, and M. W. Griffiths, "Biocontrol of *Listeria monocytogenes* and *Escherichia coli* O157:H7 in meat by using phages immobilized on modified cellulose membranes," *Appl. Environ. Microbiol.*, vol. 77, no. 18, pp. 6379–6387, 2011.
- [48] J. H. Han, M. S. Wang, J. Das, L. Sudheendra, E. Vonasek, N. Nitin, and I. M. Kennedy, "Capture and detection of T7 bacteriophages on a nanostructured interface," *ACS Appl. Mater. Interfaces*, vol. 6, no. 7, pp. 4758–4765, 2014.
- [49] N. K. Abuladze, M. Gingery, J. Tsai, and F. A. Eiserling, "Tail length determination

- in bacteriophage T4,” *Virology*, vol. 199, no. 2, pp. 301–310, 1994.
- [50] A. M. Comeau, C. Bertrand, A. Letarov, F. Tétart, and H. M. Krisch, “Modular architecture of the T4 phage superfamily: A conserved core genome and a plastic periphery,” *Virology*, vol. 362, no. 2, pp. 384–396, 2007.
- [51] B. Keller, J. Dubochet, M. Adrian, M. Maeder, M. Wurtz, and E. Kellenberger, “Length and shape variants of the bacteriophage T4 head: mutations in the scaffolding core genes 68 and 22,” *J Virol*, vol. 62, no. 8, pp. 2960–2969, 1988.
- [52] G. J. Baran and V. A. Bloomfield, “Tail-fiber attachment in bacteriophage T4D studied by quasielastic light scattering-band electrophoresis,” *Biopolymers*, vol. 17, no. 8, pp. 2015–2028, 1978.
- [53] K. P. Drees, M. Abbaszadegan, and R. M. Maier, “Comparative electrochemical inactivation of bacteria and bacteriophage,” *Water Res.*, vol. 37, no. 10, pp. 2291–2300, 2003.
- [54] R. Naidoo, A. Singh, S. K. Arya, B. Beadle, N. Glass, J. Tanha, C. M. Szymanski, and S. Evoy, “Surface-immobilization of chromatographically purified bacteriophages for the optimized capture of bacteria,” *Bacteriophage*, vol. 2, no. 1, pp. 15–24, 2012.
- [55] S. P. Leibo and P. Mazur, “Effect of osmotic shock and low salt concentration on survival and density of bacteriophages T4B and T4Bo1,” *Biophys. J.*, vol. 6, no. 6, pp. 747–772, 1966.
- [56] R. Morrow, D. McKenzie, and M. M. M. Bilek, “The time-dependent development of electric double-layers in saline solutions,” *J. Phys. D. Appl. Phys.*, vol. 39, no. 5, pp. 937–943, 2006.
- [57] J. G. De La Torre and V. A. Bloomfield, “Hydrodynamics of macromolecular complexes. III. Bacterial viruses,” *Biopolymers*, vol. 16, no. 8, pp. 1779–1793, 1977.
- [58] S. Barany, F. Madai, and V. Shilov, “Study of nonlinear electrophoresis,” *Prog. Colloid Polym. Sci.*, vol. 128, pp. 14–20, 2004.
- [59] S. K. Arya, A. Singh, R. Naidoo, P. Wu, M. T. McDermott, and S. Evoy, “Chemically immobilized T4-bacteriophage for specific Escherichia coli detection using surface plasmon resonance,” *Analyst*, vol. 136, no. 3, pp. 486–92, 2011.
- [60] M. A. Khadre and A. E. Yousef, “Susceptibility of human rotavirus to ozone, high pressure, and pulsed electric field,” *J. Food Prot.*, vol. 65, no. 9, pp. 1441–6, 2002.
- [61] M. J. Archer and J. L. Liu, “Bacteriophage T4 nanoparticles as materials in sensor applications: Variables that influence their organization and assembly on surfaces,” *Sensors*, vol. 9, no. 8, pp. 6298–6311, 2009.
- [62] K. Winkler, M. Paszewski, T. Kalwarczyk, E. Kalwarczyk, T. Wojciechowski, E. Gorecka, D. Pocięcha, R. Holyst, and M. Fialkowski, “Ionic strength-controlled deposition of charged nanoparticles on a solid substrate,” *J. Phys. Chem. C*, vol. 115, no. 39, pp. 19096–19103, 2011.
- [63] J. Sambrook, E. F. Fritsch, and T. Maniatis, *Molecular Cloning – A Laboratory Manual, 2nd ed.* Cold Spring Harbor: Cold Spring Harbor Press, 1989.
- [64] D. MacDougall and W. B. Crummett, “Guidelines for data acquisition and data quality evaluation in environmental chemistry,” *Anal. Chem.*, vol. 52, no. 14, pp. 2242–2249, 1980.
- [65] M. Mittal, P. P. Lele, E. W. Kaler, and E. M. Furst, “Polarization and interactions of colloidal particles in ac electric fields,” *J. Chem. Phys.*, vol. 129, no. 6, p. 064513, 2008.

- [66] M. Z. Bazant, K. Thornton, and A. Ajdari, “Diffuse-charge dynamics in electrochemical systems,” *Phys. Rev. E*, vol. 70, no. 2, p. 021506, 2004.
- [67] T. M. Squires and M. Z. Bazant, “Induced-charge electro-osmosis,” *J. Fluid Mech.*, vol. 509, no. 509, pp. 217–252, 2004.

Chapter 5

Magnetic-fluorescent bacteriophage-based bioconjugates for bacteria detection

Parts of this chapter are published as:

M. Janczuk*, L. Richter*, G. Hoser, J. Kawiak, M. Łoś, J. Niedziółka-Jönsson, J. Paczesny, R. Hołyst, “Bacteriophage-Based Bioconjugates as a Flow Cytometry Probe for Fast Bacteria Detection”, *Bioconjugate Chemistry* 2017, 28, 419-425

*equal contribution

Reproduced in part with permission from M. Janczuk, L. Richter et al., Bioconjugate Chemistry 2017, 28, 419-425. Copyright 2019 American Chemical Society.

5.1. Introduction

Previous chapters describe the utilization of the electric field in sensing and biosensing. However, the electrostatic field is not the only possibility to manipulate particles in order to improve detection methods. In this chapter the method of detection of bacteria based on the magnetic field is described. Plenty of applications of the magnetic field in bacteria detection have been widely described over last 20 years [1]–[3]. Magnetic properties have been mostly used to separate and concentrate detected particles or organisms. Utilization of magnetic properties was combined with surface enhanced Raman spectroscopy (SERS) [4], matrix-assisted laser desorption/ionization mass spectrometry (MALDI-MS) [5], electrochemical impedance spectroscopy [6], and polymerase chain reaction (PCR) [7]. Also magnetic resonance was utilized for this purpose [8]. One of the most promising recently developed application seems to be combination of the magnetic field and phage-based methods for bacteria detection. Phages are cheaper and more robust than antibodies. Large quantities of phages can be easily obtained by amplification inside bacteria. Moreover, for every species of bacteria there is a specific type of phage. In fact, there are plenty of different bacteriophages that share the same host. Thus, it is possible to tailor a developed method to detect desired species of bacteria.

One of the first reported attempts of using phages and magnetism for bacteria detection was described by Goodridge et al. [9]. They used fluorescently labeled phages to capture and provide bacteria a fluorescent “halolike” appearance, which was visible in epifluorescent microscopy. Flow cytometry was applied to quantify the results. In this research immunomagnetic particles (magnetic beads modified with specific antibodies) were used for bacteria separation. It was later proved that phages can also serve as such capturing elements bonding bacteria and magnetic particles.

Phagomagnetic separation utilizes phages as sensing elements to capture bacteria, whereas magnetic particles enable fast and simple separation of bacteria even from complex samples (Figure 5.1). Phagomagnetic separation does not require additional filtration or centrifugation, which can disrupt bacterial cells. There are a number of approaches allowing for realization of phagomagnetic separation. One possibility to combine phages with magnetic particles is utilization of genetic modifications. For instance, Chen et al. biotinylated T7 bacteriophages *in vivo* [10]. Such modified phages were further conjugated with streptavidin-coated magnetic particles. Utilization of phage-coated magnetic nanoparticles resulted in capture efficiency of *E. coli* cells ranging from 50% to 90%. Concentration of detected bacteria ranged from 10^2 to 10^7 CFU/ml. Later that year the same research group showed that similarly prepared bioconjugates can be combined with phage-mediated lysis. Again, the first step was capturing and separation of bacteria with bacteriophage-conjugated magnetic beads. Then, phages caused lysis of captured cells and release of endogenous β -galactosidase was detected in a colorimetric assay [11]. Another example of such an approach was proposed by He et al. [12]. In this work authors also

combined phagomagnetic separation with phage-mediated release of bacterial content. However, this time released adenosine triphosphate was detected.

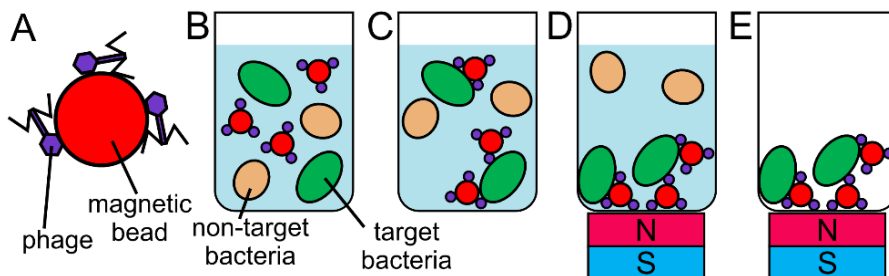


Figure 5.1 (A) Phagomagnetic separation is based on bioconjugates composed of bacteriophages attached to a magnetic particles. Steps of separation procedure: (B) bioconjugates are added to analyzed sample, (C) bioconjugates capture target bacteria, (D) upon application of the external magnetic field created bioconjugates-bacteria complexes are dragged down, (E) remaining solution is removed and replaced.

Another technique that can be coupled with magnetic separation is PCR. Wang et al. prepared bioconjugates composed of biotinylated phages and streptavidin-coated magnetic particles and used them to capture 86.2% of *E. coli* cells from broth within 20 min. PCR amplification performed on captured cells enabled detection of 10^2 CFU/ml within 3 h without any pre-enrichment step [13]. The same group combined PCR and yet another type of bioconjugates. Carboxylic acid-functionalized magnetic beads were conjugated with phages and used to separate and concentrate *E. coli* bacteria. Resulting bioconjugate-bacteria complexes were then detected by real-time quantitative PCR [14].

Phage-based magnetoseparation was also combined with electrochemical magnetosensing [15]. Combining this two approaches allowed for limit of detection as low as 3 CFU/ml for 3 hour-long analysis. However, this approach was very complicated and required many laborious steps, such as magnetic bacteria separation, PCR, enzymatic labeling of DNA and electrochemical measurement. Much simpler electrochemical approach was proposed by Shabani et al [16]. The authors coated both carbon-based impedimetric sensor and magnetic beads with phages. Such prepared magnetically-assisted impedimetric method enabled to detect 10^3 CFU/ml of *E. coli*. Phages and magnetic field were also coupled with immunoassays. Laube et al. used for that purpose two types of magnetic carriers: carboxyl-activated magnetic nanoparticles and tosyl-activated magnetic microparticles [17]. Bacteria were captured and detected by antibodies conjugated to horseradish peroxidase as an optical reporter. Similar approach was proposed by Yan et al. [18]. Authors covered magnetic beads with lytic phages P-*S.aureus*-9 via EDC-NHS reaction. Bacteria *Staphylococcus aureus* captured with these bioconjugates were then detected by horseradish peroxidase-labeled immunoglobulin (IgG) antibodies.

Immunoassay can be also combined with the utilization of bacteriophages in different way. Recently, it was proved that immunomagnetic separation coupled with phage amplification can be an useful method for bacteria detection. In approach proposed by

Martelet et al. T4 phages amplified in detected bacteria were first separated on immunobeads and then detected by liquid chromatography coupled to targeted mass spectrometry [19]. Similar approach was proposed by Mido et al. In their research phage MS2 amplification-coupled immunoassay on the Luminex® MAGPIX instrument was performed for detection of bacteria *E. coli* [20]. In very recent work, unusual combination of magnetic separation and reporter phages was described. First, bacteria were captured by magnetic beads covered with cell wall-binding phage domains and then detection by the bioluminescent reporter phage assay was performed [21].

Despite many examples of the utilization of different phage-based bioconjugates, there are hardly any reports of easy and simple protocols to prepare them. Additionally, in most cases phages have to be genetically or chemically modified, which introduces costs and laborious procedures. The aim of study presented in this chapter was to create cheap and simple method for both separation and fast detection of bacteria. For this purpose bioconjugates composed of magneto-fluorescent particles and bacteriophages were prepared. Flow cytometry was used as a detection technique. Flow cytometry is widely available in bioanalytical laboratories (also in hospitals) and routinely used in molecular biology, medicine and pathology. The goal was to create the method that can be easily introduced in such facilities and that can broaden the range of possible microbiological tests. For this purpose, native phages which can be isolated from the environment and do not require expensive and laborious genetic modifications, were used. As a second component, commercially available sub-micron particles, that are both fluorescent and magnetic, were utilized. T4 phages were attached to the surface of the particles and allowed for specific capture of *E. coli* bacteria. Magnetic core of particles enabled separation of created bioconjugates-bacteria complexes and fluorescent properties were crucial for flow cytometry detection. The proposed design of the phage-based probes is advantageous, as it combines cheap and accessible components, simple method of preparation and easy but efficient method of bacteria detection that can be performed with commonly available equipment.

5.2. Results and discussion

Most phage types belong to *Myoviridae*, *Siphoviridae*, or *Podoviridae* family [22]. They share a common design of icosahedral head in which genetic information is stored and tail ended with fibers which is responsible for detection and attachment to the host bacteria. As in previously described methods, well-studied model pair T4 bacteriophage and its host bacteria *Escherichia coli* was used.

5.2.1. Preparation and characterization of phage-based bioconjugates

Bacteriophages T4 were covalently attached to magnetic-fluorescent particles (with size of ~0.5 μm in diameter) to create multifunctional probes for separation and detection of bacteria. Scheme of synthesis of bioconjugates is provided in Figure 5.2. Used particles had

maghemite core and silica shell terminated with carboxylic groups. Size of the particles was carefully adjusted. Particles should be small enough to detect significant shift in size upon binding between bioconjugates and bacterium. On the other hand too small size of magnetic core would cause too weak magnetic drag force, which could prevent effective separation.

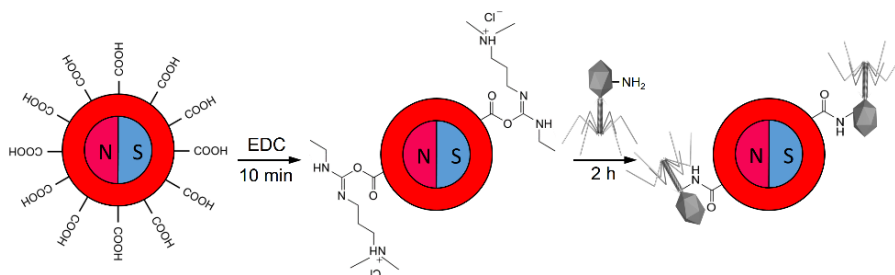


Figure 5.2 Schematic presentation of preparation of phage-based bioconjugates. First, carboxylic groups on the surface of beads are activated with EDC. Then, phages are added and bind covalently to activated beads.

Procedure of preparation of phage-based bioconjugates was performed in room temperature and took 2.5 h. Carboxylic groups on the surface of beads was first activated with EDC (1-ethyl-3-(3-dimethylaminopropyl)carbodiimide) and then conjugated with amine groups on the surface of bacteriophages. Phages are composed of proteins, thus primary amines are common groups at the virion surface. Important aspect was to use beads coated with carboxylic groups and not primary amines (which are more common and more straightforward to prepare). In case of beads coated with primary amines, there would be a need to activate carboxylic groups on the surface of phages, which immediately would react with amine groups of other phages. As a result phages would aggregate and sediment. Effect of other parameters of the procedure, such as time, phages to beads ratio and type of mixing, was analyzed. All used sets of parameters are presented in Table 5.1.

Table 5.1 Sets of parameters used in preparation of phage-based bioconjugates.

No	Phages to beads ratio	Time of incubation	Mixing	Additional data
1	80x	4 h	Intensive	
2	80x	3 h	Intensive	
3	80x	2 h	Intensive	
4	20x	3 h	Intensive	
5	20x	2 h	Intensive	
6	20x	2 h	Intensive	Reaction solution diluted twice
7	20x	2 h	Gentle	

In order to evaluate effectiveness of the procedure and quality of created bioconjugates, phages labeled with green fluorescent dye were used. Confocal microscopy images of beads and dyed phages as well as bioconjugates prepared according to all sets of parameters are presented in Figure 5.3. Beads are visible as red objects, whereas phages are represented by small green dots. Results from different sets of parameters showed that only 5th set resulted in obtaining desired product. In all other cases phages and beads merged in big aggregates. Thus, in all further experiments, bioconjugates were synthesized with parameters described in set number 5. Expected bioconjugates should be composed of single bead and few attached virions. As presented in Figure 5.4B, confocal microscope analysis confirmed that at least one virion is attached in case of vast majority of particles.

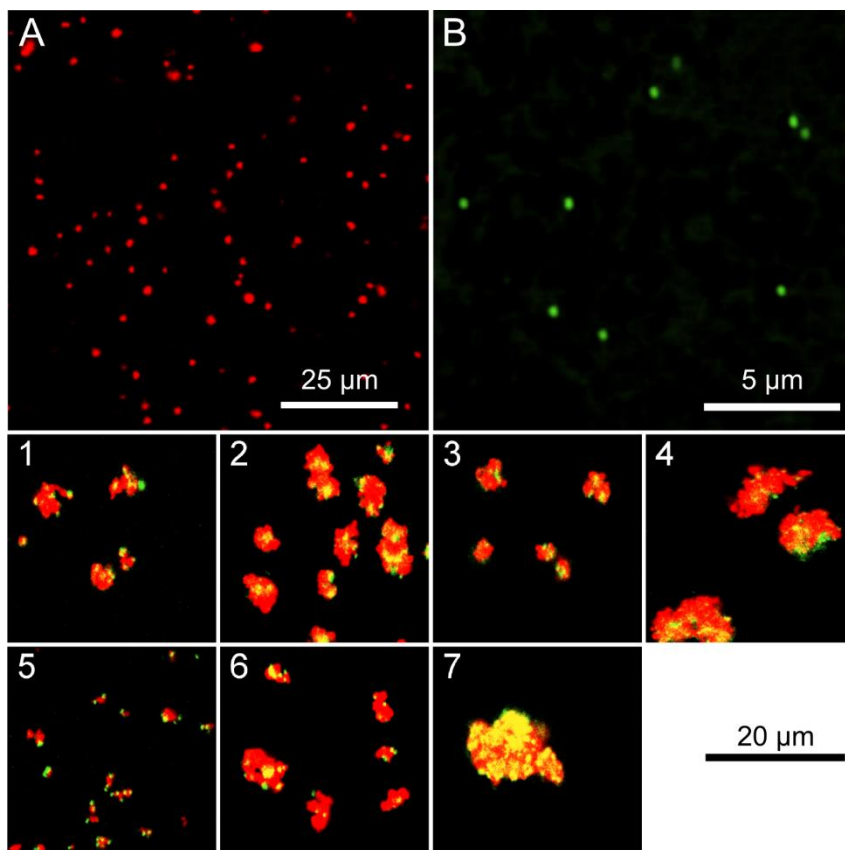


Figure 5.3 Confocal microscopy images of (A) magneto-fluorescent beads; (B) bacteriophages T4 stained with SYBR Green dye and (1-7) bioconjugates prepared in different sets of parameters described in Table 5.1.

Although successful binding of phages to beads was confirmed by confocal microscopy, there was still a need to check if phages remained infective and were able to capture bacteria. Covalent attachment of phages could create a risk of losing infectivity due to unfavorable orientation of virions on the surface of the particles (tail oriented towards the bead) or loss of activity of structural proteins of bacteriophage. For evaluation of infectivity

of phage-based bioconjugates, the plaque count method was used, similarly to typical phage viability test. However, in this case, every single plaque that is visible on layer of bacteria corresponds to single active bioconjugate, no matter how many phages are attached to the particle. As presented in Figure 5.4C, prepared bioconjugates were able to capture and infect bacteria and created plaques similar to pristine T4 phage. Estimated concentration of bioconjugates was around 10^8 PFU/ml. This value was confirmed by measurement with flow cytometer, where measured concentration was $3.33 \cdot 10^7$ bioconjugates/ml. Confocal microscopy showed that every particle had at least one phage attached to it. Therefore, obtained values suggested that the protocol of preparation did not affect infectivity of phages and that number of free phages remained in the solution was negligible.

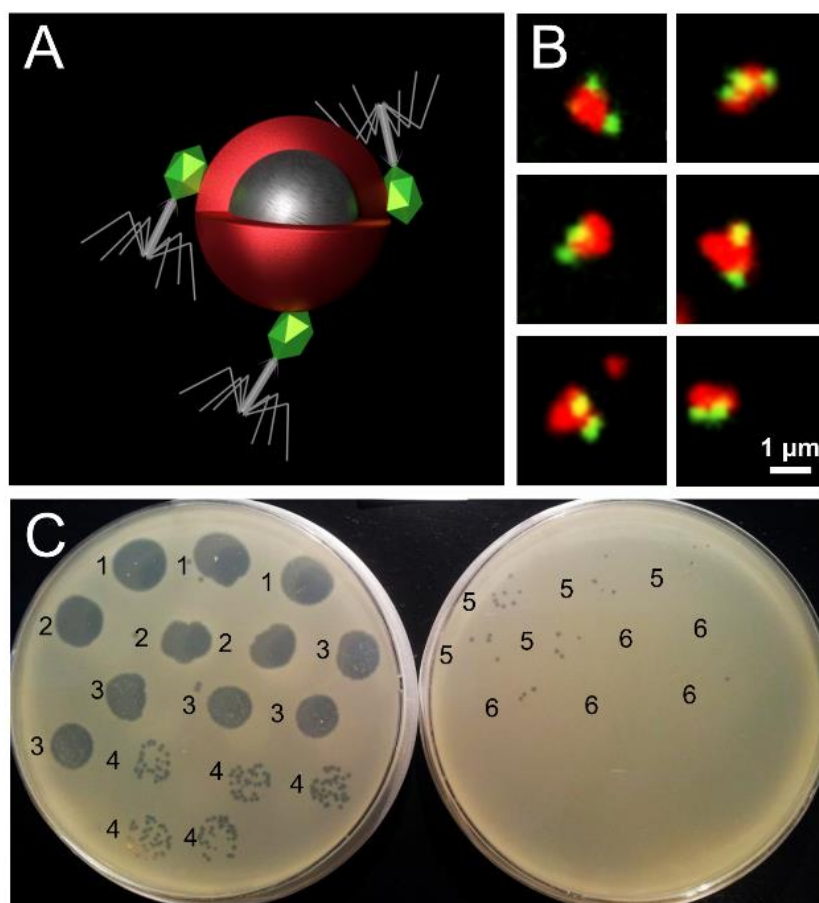


Figure 5.4 (A) Schematic representation of desired bioconjugate. Bacteriophages T4 were covalently attached to the surface of magnetic-fluorescence particle. To check effectiveness of immobilization, phages were stained with SYBR Green; (B) Confocal microscope images presenting bioconjugates composed of beads (red fluorescence) and attached phages (green fluorescence); (C) Images of layers of bacteria grown on agar plates after titration of the bioconjugates by the plaque count method. The numbers corresponded to consecutive 10-fold dilutions. Presence of typical for T4 bacteriophage plaques confirmed that bacteriophages coupled with beads were infective and active. The estimated concentration of bioconjugates was around 10^8 PFU/ml.

5.2.2. Analysis of capture efficiency of prepared bioconjugates

To analyze the efficiency of magnetic separation, bioconjugates prepared from non-stained phages were incubated in solutions of target *E. coli* bacteria of concentrations ranging from 33 to $3.3 \cdot 10^5$ CFU/ml. Time of incubation was 15 min. This value was judiciously chosen. Too short time could result in not efficient capture of bacteria, but too long time could cause lysis of captured and infected bacterial cells. After incubation, bacteria-bioconjugates complexes were separated with a magnet and the amount of bacteria remained in the supernatant was evaluated by colony count method (Figure 5.5). The capture efficiency (CE) was calculated according to the equation:

$$CE(\%) = \left(1 - \frac{N_1}{N_0}\right) \times 100\% \quad (5.1)$$

where N_0 is the number of bacteria in the initial sample (CFU/ml), N_1 is the amount of remained unbound bacteria after capturing procedure (CFU/ml).

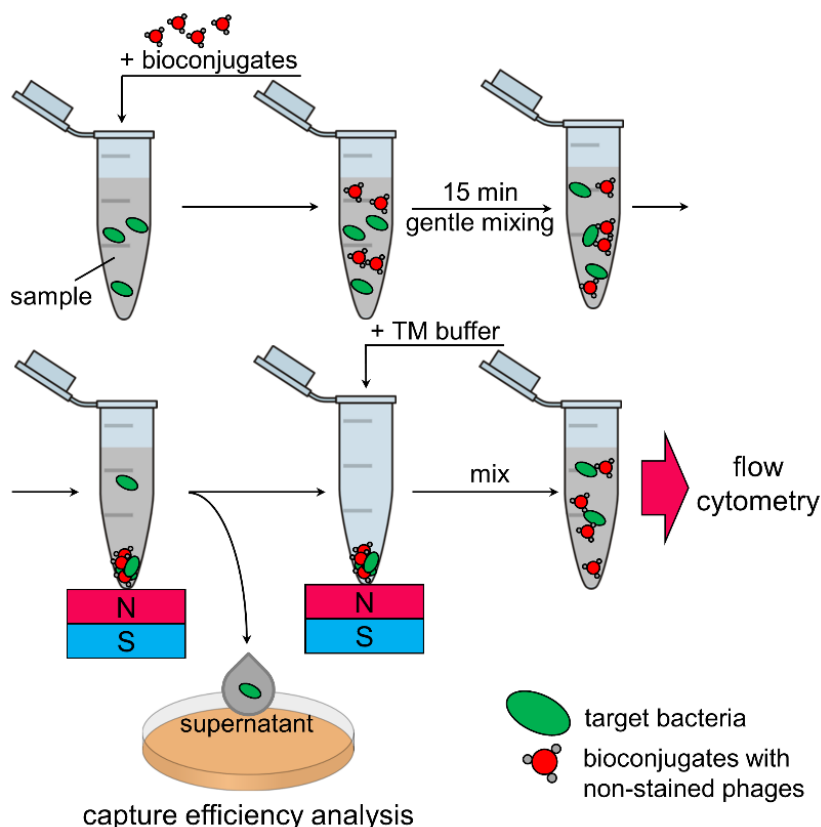


Figure 5.5 Schematic representation of sample preparation for capture efficiency measurement and flow cytometry. Bioconjugates were incubated for 15 min with bacteria and then bacteria-bioconjugates complexes were separated with a magnet. Supernatant was removed and replaced with fresh TM buffer. Such prepared solution was analyzed by means of flow cytometry to evaluate number of target bacteria in the sample. Number of bacteria remained in the removed supernatant was determined by colony count method.

Prepared bioconjugates were able to capture more than 90% of bacteria in wide range of initial bacterial concentrations (Figure 5.6A). For the most diluted samples number of caught bacteria reached almost 100%. For higher concentrations of bacteria (around $3.3 \cdot 10^5$ CFU/ml) capture efficiency decreased, which is typical for magnetic separation due to decrease of number of bioconjugates per bacterium [10], [13]. In comparison with previously reported methods, prepared bioconjugates showed very high capture efficiency, especially in higher concentrations of bacteria [10], [16].

Additionally, I performed experiment in which *E. coli* bacteria stained with blue fluorescent dye was captured with bioconjugates consisted of magnetic-fluorescent beads and phages stained with green fluorescent dye. As usual, after incubation for 15 min bacteria-bioconjugates complexes were separated with magnet and resuspended in fresh TM buffer. Such prepared samples were analyzed with confocal microscope (Figure 5.6B). I observed expected complexes and proved additionally that bioconjugates are attached to the bacteria via bacteriophages (green dots), as it was designed and expected.

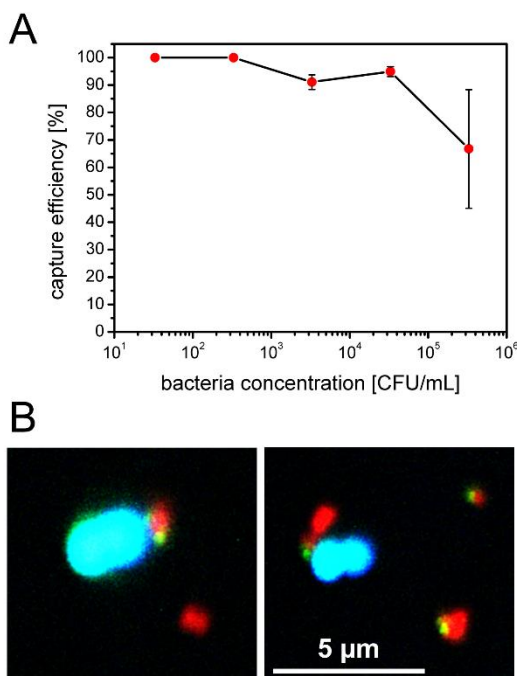


Figure 5.6 Utilization of phage-based bioconjugates to separate bacteria. **(A)** Analysis of efficiency of bacteria capturing for different initial concentrations of bacteria. High efficiency (over 90%) was obtained even for concentrated samples (10^4 - 10^5 CFU/ml); **(B)** Confocal microscopy images of bacteria-bioconjugate complexes. Bacteria (blue fluorescence) are captured by bioconjugates composed of magnetic bead (red fluorescence) and bacteriophage (green fluorescence).

5.2.3. Detection of bacteria *E. coli* with phage-based bioconjugates

As a method for detection of target bacteria flow cytometry was chosen. This technique is routinely used in medial and biochemical analyses, thus is very good choice for further

practical implementations. Samples were prepared similarly as for the capture efficiency analysis. Immediately after resuspension in fresh TM buffer, they were analyzed in triplicates in flow cytometer (Figure 5.5). As control sample, the bioconjugates were incubated with physiological saline without any bacteria. The rest of the procedure remained the same. Measured values were: side scattering (which can be correlated with size of the objects) and red fluorescence (coming from particles within bioconjugates). The obtained results were organized as two-parameter dot plots showing both analyzed values. Bioconjugates were small and had red fluorescence, therefore in prepared plots they should create population of fluorescent, weakly scattering objects (Figure 5.7A). This result allowed for determining the gate in the region of higher fluorescence and side scattering where complexes of bacteria and bioconjugates were expected and where signal coming from single bioconjugates was negligible.

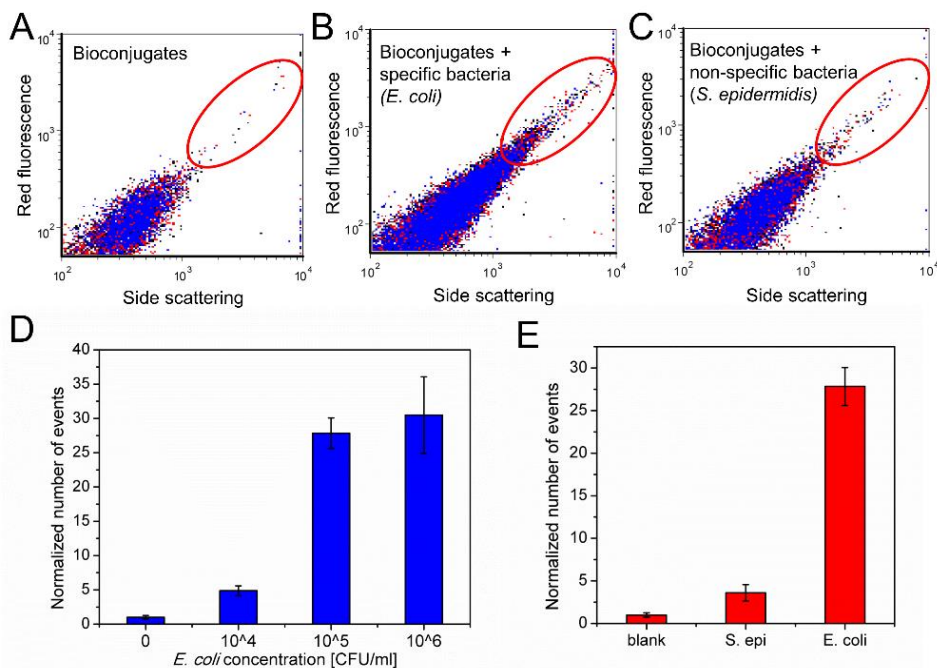


Figure 5.7 Flow cytometry measurements of bacteria detection. Two-parameter dot plots of red fluorescence and side scattering present the results obtained for (A) bioconjugates without any bacteria; (B) bioconjugates with target bacteria *E. coli* and (C) bioconjugates with nonspecific bacteria *S. epidermidis*. The red gate border was judiciously chosen to detect signal coming only from bacteria with attached bioconjugates. Three repetitions represented by black, red and blue dots were plotted on each graph. (D) Analysis of sensitivity of bacteria detection. Results from chosen gate obtained for different initial concentrations of target bacteria *E. coli* are shown. (E) Selectivity evaluation of bioconjugate-based method was performed by comparison of results from target (*E. coli*) and nonspecific bacteria (*S. epidermidis*). In both cases the initial concentration of bacteria was 10^5 CFU/ml.

For analysis of sensitivity, samples with concentration of bacteria ranging from 10^4 to 10^6 CFU/ml were analyzed with developed protocol of magnetic separation followed by

subsequent flow cytometry analysis. As presented in Figure 5.7B increased number of events in selected gate indicated the presence of big objects with high red fluorescence. This was expected result since bacteria-bioconjugates complexes usually consist of single bacterium (which size was bigger than single bioconjugate) and many bioconjugates (which combined fluorescence is higher than in case of one particle). Moreover, strong signal in region of single bioconjugates suggested that many bioconjugates remained free and didn't attached to any bacteria. Results obtained for different concentrations of bacteria were summarized in Figure 5.7D. The signal from 10^4 CFU/ml of *E. coli* was still distinguishable, however for lower concentrations signal was comparable with blank measurement. Possible explanation can be weak initial monodispersity of used magnetic-fluorescent particles. As presented in Figure 5.7A, both signals (fluorescence and scattering) from bioconjugates spread over order of magnitude. Thus, in case of bioconjugates with smaller size and resultant weaker fluorescence, attachment to the bacteria might cause change of signal that was insufficient to be included in analytical gate. In fact, in Figure 5.7B it is visible that there was additional population located between chosen gate and initial position of bioconjugates on the plot.

For further analysis the specificity test was performed. Two measurements with (a) target bacteria *E. coli* and (b) nonspecific bacteria *S. epidermidis* in similar concentrations of 10^5 CFU/ml were performed. In Figure 5.7C the two-parameter dot plot for nonspecific bacteria is presented. Only few additional events were recorded in designed gate. Quantitative comparison is provided in Figure 5.7E. The signal obtained for *S. epidermidis* bacteria was similar to the negative control and significantly lower than the result for *E. coli*. Such result was expected, due to the fact that utilized phages T4 ensure high selectivity against *E. coli* bacteria.

5.3. Conclusions

Number of reports describing methods based on bacteriophages for bacteria detection can be found in the literature [23], [24]. However, there are many issues that still need to be addressed: (1) simple preparation process, (2) lack of expensive and complicated genetic modifications, (3) single-step detection method and (4) available and cheap probes. Within this chapter, a method that meets all this requirement was described. Protocol for preparation of multifunctional bioconjugates for bacteria detection was designed and optimized. Bacteriophages were used as highly specific and selective bioreceptors. Phages were attached via EDC reaction to the surface of magnetic-fluorescent beads. All used components were inexpensive and easily accessible. Additionally, developed protocol of bacteria detection using prepared bioconjugates as flow cytometry probes was straightforward and at the same time efficient, specific and selective. All of these features enables utilization of developed technique in all facilities using flow cytometry on a daily basis. Developed procedures are easily adaptable to all bacteriophages, and thus can be adjusted to any target bacteria. The method does not require any genetic or chemical

modification of phages, therefore wild types or even libraries of phages can be used as sensing elements.

Bioconjugates that offer capture efficiency close to 100% in wide range of bacteria concentrations spreading from 10^1 up to 10^5 CFU/ml were developed. Resulting limit of detection in case of flow cytometry detection was in range of 10^4 CFU/ml and was mostly limited by broad distribution of sizes of used magnetic-fluorescent particles. Nonetheless, prepared bioconjugates can be useful in screening test for fast (15 min) determination of bacterial species in samples that are already heavily infected. Additionally, to improve limit of detection even more, created method can be further combined with preincubation step. In such approach, the time of assay and limit of detection can be balanced depending on the specific need.

Within this chapter it was proved that not only electric field can aid detection methods. Magnetic field also greatly improves detection techniques and can be used for easy and simple separation and concentration of captured bacteria from the complex sample.

5.4. Materials and methods

5.4.1. Materials

Carboxyl-terminated superparamagnetic-fluorescent particles were purchased from the Chemicell (Germany). Hydrodynamic size of particles was 0.5 μm and they were saturated with red fluorescent dye (maximum excitation in 633 nm and maximum emission in 672 nm). All chemicals were purchased from Sigma-Aldrich (USA). Instant mixes of LB medium and LB-agar were purchased from Carl Roth (Germany). LB medium was composed of 10 g/l of NaCl, 10 g/l of tryptone and 5 g/l of yeast extract. LB-agar additionally contained 15 g/l of agar. Top LB-agar contained 5 g/l of agar. TM buffer consisted of 10 mM TRIS (tris(hydroxymethyl)aminomethane), 10 mM MgSO_4 , 5 μM CaCl_2 . pH of the TM buffer was adjusted at 7.4. Buffer MES consisted of 0.1 M of 2-(N-morpholino)ethanesulfonic acid. pH of the buffer MES was adjusted at 4.5.

LB media, buffers and all other solutions were autoclaved prior to use.

5.4.2. Phage preparation and bacteria culturing

Preparation of lysate of T4 phages was already described in chapter 4. Briefly, phages were amplified inside bacteria *Escherichia coli* MG1655. Then, the phages were precipitated and purified by ultracentrifugation. Finally, bacteriophages were dialyzed against TM buffer and 0.2 $\mu\text{g/ml}$ of DNase I was added to the solution.

The standard protocol was used to culture the bacteria. As target (specific) bacterial cells *E. coli* MG1655 were used. Bacteria *Staphylococcus epidermidis* WT (received from the Faculty of Biology, Warsaw University, Poland) were used as non-specific control. At the beginning, a single colony from agar plate was inoculated and incubated overnight into

LB medium (37 °C, 200 rpm). Then, small volume of overnight culture was diluted into new portion of LB medium and cultured to obtain suspension with given OD₆₀₀.

5.4.3. Determination of number of active phages and bacteria

To determine number of active phages, the plaque count method was used. Plaque forming units (PFU) can be directly correlated with a number of active phages in the sample. In this approach, 20 ml LB-agar medium was poured into Petri dish. Then 4 ml of top LB-agar mixed with 0.2 ml of overnight culture of *E. coli* MG1655 and poured onto agar plate. Tenfold dilutions of phages were prepared and droplets (5 µl each) of every dilution were spotted on prepared Petri dish with bacteria. Plates were then incubated at 37 °C overnight. Finally, created plaques were counted.

To evaluate viability of bacteria, the colony count method was applied. Colony forming units (CFU) can be directly correlated with number of viable bacteria. In this method, series of tenfold dilutions of bacteria solution were prepared. Then, 25 µl of every dilution was spread over separate agar plate (i.e. Petri dish with 20 ml of LB-agar). Next, agar plates were incubated overnight at 37 °C. Finally, grown colonies were counted.

5.4.4. Preparation of fluorescently labeled phages and bacteria

Bacteria and phages were stained with fluorescent dyes to observe and adjust the processes of bioconjugation and attachment to the bacteria.

The purified phages T4 were labeled with SYBR Green dye (ThermoFisher Scientific, USA, excitation max 497 nm, emission max 520 nm) at 4 °C for 24 h. Concentration of phages was $5 \cdot 10^{11}$ PFU/ml. Stock solution of SYBR Green was diluted 1000 times. The stained phages were purified from remained dye by dialysis against TM buffer at 4 °C for 48 h. The plaque count method was applied to assess activity of phages.

The bacteria *E. coli* MG1655 were labeled with SYTO Blue dye (ThermoFisher Scientific, USA, excitation max 420 nm, emission max 441 nm). For this purpose, overnight culture was diluted to obtain OD₆₀₀=0.4, then centrifuged (5000 rpm, 5 min) and resuspended in physiological saline (0.9% NaCl). Next, 500 µl of bacteria suspension was mixed and incubated with 5 µl of stock solution of SYTO Blue dye for 80 min at 37 °C with rotation 250 rpm. To remove free dye, stained bacteria were centrifuged (5000 rpm, 5 min) and resuspended in fresh physiological saline.

5.4.5. Preparation of phage-based bioconjugates

Carboxyl-terminated magnetic-fluorescent beads were coated with T4 bacteriophages by EDC (1-ethyl-3-(3-dimethylaminopropyl)carbodiimide) reaction. The solution of the magnetic beads (66.7 µl, $7.5 \cdot 10^9$ particles/ml) was washed two times with MES buffer on the hand-made separator with neodymium magnet. The particles were resuspended in 5 mM ECD solution in MES buffer and were mixed 300 rpm on the orbital shaker at 25 °C for 10 min to activate carboxyl groups. Then, the particles were again washed two times with MES

buffer and once with TM buffer. Next, the phage T4 solution (200 μ l, $5 \cdot 10^{11}$ PFU/ml) was added to the beads and incubated with mixing at 25 °C for 2 h in the dark. During that time amide bonds between carboxyl groups presented on magnetic particles and amine groups of bacteriophages were created. The phage-based bioconjugates were washed three times with TM buffer and resuspended in 100 μ l of storage solution (0.1% of bovine serum albumin in buffer TM). The bioconjugates were stored at 4 °C in the dark.

The bioconjugates were prepared in two versions: with non-stained and with labeled bacteriophages. SYBR Green-stained phages were used to assess effectiveness of synthesis. The non-stained phages were used to prepare proper bioconjugates used for final detection of bacteria with flow cytometry. A number of active bioconjugates were evaluated by applying plaque count method described in previous section.

5.4.6. Efficiency of bacteria capture

Overnight culture of bacteria *E. coli* MG1655 was centrifuged (5000 rpm, 5 min) and pellet was resuspended in physiological saline. Tenfold dilutions of bacteria solution were prepared to obtain concentrations from $3.3 \cdot 10^1$ to $3.3 \cdot 10^5$ CFU/ml. Exact values of concentrations were analyzed by the colony count method. The bacteria solutions were then mixed with solution of phage-based bioconjugates (10^8 PFU/ml) in the ratio 5:1 and incubated at 25 °C for 15 min. Next, the bacteria-bioconjugates complexes were separated by hand-made separator with neodymium magnet and the supernatant was collected. A number of bacteria remaining in the solution was determined by the colony count method.

5.4.7. Flow cytometry

The bioconjugates with non-labeled phages were mixed with bacteria solution in volume ratio 2:1 and incubated at 25 °C for 15 min. Concentrations of prepared solutions of *E. coli* ranged from 10^4 to 10^6 CFU/ml. Concentration of solution of *S. epidermidis* was 10^5 CFU/ml. After incubation, bacteria-bioconjugates complexes were separated on hand-made separator with neodymium magnet and resuspended in 50 times bigger volume of fresh TM buffer. Finally, the solution was analyzed with flow cytometry in three separate measurements. As control measurement, solution of bacteria was replaced with physiological saline without bacteria. The rest of the procedure remained the same.

5.4.8. Additional instrumentation

Nikon Ti Eclipse with confocal system A1R was applied for analysis of quality of prepared bioconjugates and for evaluation of bacteria catching process. The system included lasers 488nm, 405 nm, 635 nm, objective CFI Plan Fluor 40 \times and NIS-Elements AR 4.13 software.

Detection of bacteria was performed by using Becton Dickinson FACS CantoII cytometer (Becton Dickinson, USA) equipped with argon, red and violet laser and Diva software.

5.5. References

- [1] Y. W. Chu, D. A. Engebretson, and J. R. Carey, “Bioconjugated magnetic nanoparticles for the detection of bacteria,” *J. Biomed. Nanotechnol.*, vol. 9, no. 12, pp. 1951–1961, 2013.
- [2] R. A. Bohara and S. H. Pawar, “Innovative developments in bacterial detection with magnetic nanoparticles,” *Appl. Biochem. Biotechnol.*, vol. 176, no. 4, pp. 1044–1058, 2015.
- [3] K. Niemirowicz, K. H. Markiewicz, A. Z. Wilczewska, and H. Car, “Magnetic nanoparticles as new diagnostic tools in medicine,” *Adv. Med. Sci.*, vol. 57, no. 2, pp. 196–207, 2012.
- [4] C. Wang, J. Wang, M. Li, X. Qu, K. Zhang, Z. Rong, R. Xiao, and S. Wang, “A rapid SERS method for label-free bacteria detection using polyethylenimine-modified Au-coated magnetic microspheres and Au@Ag nanoparticles,” *Analyst*, vol. 141, no. 22, pp. 6226–6238, 2016.
- [5] H. N. Abdelhamid and H. F. Wu, “Multifunctional graphene magnetic nanosheet decorated with chitosan for highly sensitive detection of pathogenic bacteria,” *J. Mater. Chem. B*, vol. 1, no. 32, pp. 3950–3961, 2013.
- [6] Q. Chen, D. Wang, G. Cai, Y. Xiong, Y. Li, M. Wang, H. Huo, and J. Lin, “Fast and sensitive detection of foodborne pathogen using electrochemical impedance analysis, urease catalysis and microfluidics,” *Biosens. Bioelectron.*, vol. 86, pp. 770–776, 2016.
- [7] H. Zhang, F. Huang, G. Cai, Y. Li, and J. Lin, “Rapid and sensitive detection of *Escherichia coli* O157:H7 using coaxial channel-based DNA extraction and microfluidic PCR,” *J. Dairy Sci.*, vol. 101, no. 11, pp. 9736–9746, 2018.
- [8] Y. Li, H. Yu, Y. Qian, J. Hu, and S. Liu, “Amphiphilic star copolymer-based bimodal fluorogenic/magnetic resonance probes for concomitant bacteria detection and inhibition,” *Adv. Mater.*, vol. 26, no. 39, pp. 6734–6741, 2014.
- [9] L. Goodridge, J. Chen, and M. Griffiths, “Development and characterization of a fluorescent-bacteriophage assay for detection of *Escherichia coli* O157:H7,” *Appl. Environ. Microbiol.*, vol. 65, no. 4, pp. 1397–1404, 1999.
- [10] J. Chen, B. Duncan, Z. Wang, L.-S. Wang, V. M. Rotello, and S. R. Nugen, “Bacteriophage-based nanoprobe for rapid bacteria separation,” *Nanoscale*, vol. 7, no. 39, pp. 16230–16236, 2015.
- [11] J. Chen, S. D. Alcaine, Z. Jiang, V. M. Rotello, and S. R. Nugen, “Detection of *Escherichia coli* in drinking water using T7 bacteriophage-conjugated magnetic probe,” *Anal. Chem.*, vol. 87, no. 17, pp. 8977–8984, 2015.
- [12] Y. He, M. Wang, E. Fan, H. Ouyang, H. Yue, X. Su, G. Liao, L. Wang, S. Lu, and Z. Fu, “Highly specific bacteriophage-affinity strategy for rapid separation and sensitive detection of viable *Pseudomonas aeruginosa*,” *Anal. Chem.*, vol. 89, no. 3, pp. 1916–1921, 2017.
- [13] Z. Wang, D. Wang, J. Chen, D. A. Sela, and S. R. Nugen, “Development of a novel bacteriophage based biomagnetic separation method as an aid for sensitive detection of viable *Escherichia coli*,” *Analyst*, vol. 141, no. 3, pp. 1009–1016, 2016.
- [14] Z. Wang, D. Wang, A. J. Kinchla, D. A. Sela, and S. R. Nugen, “Rapid screening of waterborne pathogens using phage-mediated separation coupled with real-time PCR detection,” *Anal. Bioanal. Chem.*, vol. 408, no. 15, pp. 4169–4178, 2016.

- [15] S. Liébana, D. A. Spricigo, M. P. Cortés, J. Barbé, M. Llagostera, S. Alegret, and M. I. Pividori, “Phagomagnetic separation and electrochemical magnetogenosensing of pathogenic bacteria,” *Anal. Chem.*, vol. 85, no. 6, pp. 3079–3086, 2013.
- [16] A. Shabani, C. A. Marquette, R. Mandeville, and M. F. Lawrence, “Magnetically-assisted impedimetric detection of bacteria using phage-modified carbon microarrays,” *Talanta*, vol. 116, pp. 1047–1053, 2013.
- [17] T. Laube, P. Cortés, M. Llagostera, S. Alegret, and M. I. Pividori, “Phagomagnetic immunoassay for the rapid detection of Salmonella,” *Appl. Microbiol. Biotechnol.*, vol. 98, no. 4, pp. 1795–1805, 2014.
- [18] C. Yan, Y. Zhang, H. Yang, J. Yu, and H. Wei, “Combining phagomagnetic separation with immunoassay for specific, fast and sensitive detection of *Staphylococcus aureus*,” *Talanta*, vol. 170, pp. 291–297, 2017.
- [19] A. Martelet, G. Lhostis, M. C. Nevers, H. Volland, C. Junot, F. Becher, and B. H. Muller, “Phage amplification and immunomagnetic separation combined with targeted mass spectrometry for sensitive detection of viable bacteria in complex food matrices,” *Anal. Chem.*, vol. 87, no. 11, pp. 5553–5560, 2015.
- [20] T. Mido, E. M. Schaffer, R. W. Dorsey, S. Sozhamannan, and E. R. Hofmann, “Sensitive detection of live *Escherichia coli* by bacteriophage amplification-coupled immunoassay on the Luminex® MAGPIX instrument,” *J. Microbiol. Methods*, vol. 152, no. July, pp. 143–147, 2018.
- [21] J. W. Kretzer, M. Schmelcher, and M. J. Loessner, “Ultrasensitive and fast diagnostics of viable *Listeria* cells by CBD magnetic separation combined with A511::luxAB detection,” *Viruses*, vol. 10, no. 11, 2018.
- [22] H. W. Ackermann, “5500 Phages examined in the electron microscope,” *Arch. Virol.*, vol. 152, no. 2, pp. 227–243, 2007.
- [23] A. Singh, S. Poshtiban, and S. Evoy, “Recent advances in bacteriophage based biosensors for food-borne pathogen detection,” *Sensors*, vol. 13, no. 2, pp. 1763–1786, Jan. 2013.
- [24] Ł. Richter, M. Janczuk-Richter, J. Niedziółka-Jönsson, J. Paczesny, and R. Hołyst, “Recent advances in bacteriophage-based methods for bacteria detection,” *Drug Discov. Today*, vol. 23, no. 2, pp. 448–455, 2018.

Chapter 6

Conclusions and future perspectives

6.1. Summary

The electric and magnetic fields are phenomena that intrigued and inspired scientific community for many centuries. Their utilization initiated and accelerated wide range of applications in both science and industry. Main goal of this work is to make a contribution in this field and create important solutions that aid sensing and biosensing. Moreover, to increase the comprehensiveness of prepared thesis, practical applications are supplemented with fundamental research that aim to expand understanding of electrokinetic phenomena.

First chapter consists of general introduction to electrokinetics. At the beginning, core concept of classical theory of the electrical double layer and its characterization are described. Then, to fully present potential of the field, most commonly utilized electrophoretic phenomena are discussed. Second part of this chapter summarizes two applications of the electric field, which are relevant in context of research described in this thesis: 1) improvement of biodetection methods and 2) deposition of objects in the electric field.

Although theoretical and experimental analysis of electrokinetics creates complete and comprehensive picture, it is still dynamically developing field and unexpected phenomena are constantly reported [1]–[3]. **Second chapter** of this thesis provides insight into novel electrokinetic phenomenon of non-trivial characteristics. Namely, long-range repulsion between oppositely charged surfaces is described. Studied surface forces apparatus (SFA) setup was in fact a capacitor filled with the electrolyte consisting of ions of unequal electrophoretic mobilities. Range, strength, and time scale of the observed effect exceeded all previously reported electrokinetic phenomena [4]–[6]. Detailed analysis of influence of numerous parameters was performed. As a result, explanation that matches observed relationships and measured values was proposed.

Third chapter focuses on first practical utilization of the electric field described in this thesis. Deposition of analyte on solid substrates in the alternating electric field was developed to improve surface-enhancement Raman spectroscopy (SERS). Such electrokinetic preconcentration was previously reported in the literature [7]–[9]. However, technology described in this chapter omits many drawbacks that hindered broad implementation of this approach. Created deposition step was independent from final SERS analysis, which increased flexibility of prepared design. Moreover, isolation of one electrode was combined with application of the alternating electric field. This enabled to avoid destructive Faradaic currents, redox reactions and at the same time omitted the problem of screening of the electric field with the electrical double layers. Time of deposition was shortened from 20 hours to 5 min. At the same time, needed volume of tested sample was reduced roughly 40 times. Also homogeneity of recorded SERS spectra was improved, due to more dense occupation of hot spots by deposited molecules. Wide range of analytes was successfully deposited in the electric field, which confirmed robustness of developed technology. Frequency was identified as crucial parameter that had to be adjusted

separately for each compound to be deposited. Above all, to increase usefulness of developed method, dependency between applied frequency and electrophoretic mobility of deposited molecule was determined.

Also detection of bigger objects, such as bacteria was improved by methods developed within this thesis. **Fourth chapter** describes utilization of alternating electric field to create layers of properly oriented phages for fast and sensitive bacteria detection. In typical layers of randomly orientated phages, receptor binding proteins are sterically blocked and thus sensitivity of such layers is drastically decreased. Application of the alternating electric field enables favorable orientation of phages. Although similar approaches were utilized in the past [10], [11], to the best of my knowledge this was the first time that provided direct comparison of ordered and unordered layers of bacteriophages. Moreover, additional combination of such prepared layers with chemical modification of the surfaces resulted in densely packed layers of properly ordered phages. Sensitivity increased 50 to 64 times compared to randomly oriented phages deposited on bare gold. Detection step took only 15 min and resulting limit of detection was lower than 100 CFU/ml, which was in range of the best-performing phage-based sensors described so far.

During development of phage-based method for bacteria detection, it turned out that also magnetic field is a powerful tool to improve techniques of biodetection. Thus, **fifth chapter** presents development of phage-based bioconjugates for bacteria detection. Created bioconjugates consisted of fluorescent and magnetic sub-micron particles coated with bacteriophages. Magnetic properties allowed for effective separation and concentration of detected bacteria from the sample. Fluorescent properties enabled simple detection. Finally, bacteriophages ensured proper selectivity of given bacteria species. In the literature, similar approaches can be found, however all of them require complicated and expensive preparation [12], [13] or specialized method of detection, rarely available in hospitals and diagnostic laboratories [14]–[16]. Main goal of this project was to create method that would be easily accessible not only in highly-equipped research laboratories. Thus, utilized compounds were accessible and inexpensive. Moreover, selected method of detection (flow cytometer) is commonly used in hospitals and bioanalytical laboratories, which additionally increased versatility of developed solution.

Sixth chapter is the summary of all described advances and discoveries. This part puts them in perspective of present and future research, and allow to understand their input in the field of practical applications.

6.2. Future perspectives

Each part of this thesis contains research that can be further utilized in broader context for improvement of detection methods and utilization of electric and magnetic fields in sensing and biosensing.

Research presented in chapter two resulted in discovery of intriguing electrokinetic phenomena. Although influence of various parameters on studied effect was measured and well characterized, additional calculations would be beneficial for further in-depth quantitative analysis. In fact, as a follow up studies, cooperation with mathematicians and theoretical physicists has been already established. Discoveries and experiments performed using surface forces apparatus will be complemented with analytical calculations of observed effect. This will provide deeper understanding of the electrokinetic processes involved in the observed phenomenon and enable even better control over designed system. Moreover, reported effect can potentially open new paths in numerous applications based on controlled movement of ions and surfaces, such as desalination of water, permselective channels, ionic valves, macroscopic separation of charges and tunable capacitors.

Also developed method of deposition of analytes on solid surfaces has a great potential for further development. Although developed method was proven to be effective in SERS improvement, practical application can be hindered by laborious preparation of some components (wires, counterelectrode, deposition cell) and utilization of external power source. Thus, next step should be development of prototype of the device that would combine improved deposition cell and miniaturized system generating desired voltage. First step towards this goal was already made. Together with researchers that developed *SERSitive* substrates, I have already started working on the prototype of commercial device for deposition of analytes on SERS substrates in the electric field.

Moreover, described method was independent from final SERS analysis and the only limitation was that solid surface, on which analyte was deposited, needs to be conductive. Research presented in this thesis already showed, that deposition of analytes can improve also fluorescence signal. Thus, developed solution can potentially aid also other analytical techniques that require presence of detected molecules at the sensing layer. Few examples of such technologies are surface plasmon resonance [17], optical fiber sensors [18], electrochemistry [19], and surface enhanced luminescence [20].

Different approach should be applied for further development of phage-based sensing layers. One of the biggest drawbacks of currently developed sensors for bacteria detection that hinders their wide practical implementation is poor sensitivity. Typically applied microbiological and biochemical tests can detect few CFU/l, which is regime inaccessible for phage-based sensing layers developed to this day [21]. Proposed solution of improving sensitivity of sensing layers for bacteria detection is a step towards removing these limitations. Therefore, further studies should focus on combination of oriented sensing layers with proper transducers. Moreover, obtained technology can be applied to improve sensitivity of already developed phage-based biosensors. Wide range of such sensors, utilizing various transducers, such as surface plasmon resonance [22], long-period fiber gratings [23], and electrochemical impedance spectroscopy [24], was reported in the literature. Proper orientation of phages will increase their sensitivity and bring them one step closer to real-world implementation.

In case of development of created bioconjugates, further advancement should be divided into two aspects. First one is improvement of the provided technology. To upgrade performance of bioconjugates, experiments with more homogenous particles and other types of phages should be performed. Also, particles with fluorescence of other wavelengths should be utilized to allow for simultaneous detection of many bacteria species. Second aspect is implementation of developed solution in real process of diagnosis. Disease that seems to be ideal for this case is sepsis. In many cases of heavily infected patients, number of bacteria in body fluids is very high [25] and rapid identification of infecting pathogens is required. This seems to be proper application for phage-based bioconjugates. Detection procedure takes only few tens of minutes and the flow cytometer used in this approach is common equipment in hospitals and diagnostic laboratories.

As it was evidenced with this thesis, the electric and magnetic fields are useful tools for improvement of sensing and biosensing methods. I am looking forward to witness further development of this field and observe the breakthrough research it will bring in the future.

6.3. References

- [1] B. Balu and A. S. Khair, “Role of Stefan-Maxwell fluxes in the dynamics of concentrated electrolytes,” *Soft Matter*, vol. 14, no. 41, pp. 8267–8275, 2018.
- [2] R. Tivony, S. Safran, P. Pincus, G. Silbert, and J. Klein, “Charging dynamics of an individual nanopore,” *Nat. Commun.*, vol. 9, no. 1, pp. 1–8, 2018.
- [3] S. M. H. M. H. Hashemi Amrei, S. C. Bukosky, S. P. Rader, W. D. Ristenpart, and G. H. Miller, “Oscillating electric fields in liquids create a long-range steady field,” *Phys. Rev. Lett.*, vol. 121, no. 18, p. 185504, 2018.
- [4] V. A. Parsegian and D. Gingell, “On the electrostatic interaction across a salt solution between two bodies bearing unequal charges,” *Biophys. J.*, vol. 12, no. 9, pp. 1192–1204, 1972.
- [5] M. A. Gebbie, A. M. Smith, H. A. Dobbs, A. A. Lee, G. G. Warr, X. Banquy, M. Valtiner, M. W. Rutland, J. N. Israelachvili, S. Perkin, and R. Atkin, “Long range electrostatic forces in ionic liquids,” *Chem. Commun.*, vol. 53, no. 7, pp. 1214–1224, 2017.
- [6] M. Z. Bazant, K. Thornton, and A. Ajdari, “Diffuse-charge dynamics in electrochemical systems,” *Phys. Rev. E*, vol. 70, no. 2, p. 021506, 2004.
- [7] P. D. Lacharmoise, E. C. Le Ru, and P. G. Etchegoin, “Guiding molecules with electrostatic forces in surface enhanced raman spectroscopy,” *ACS Nano*, vol. 3, no. 1, pp. 66–72, 2009.
- [8] H. Cho, B. Lee, G. L. Liu, A. Agarwal, and L. P. Lee, “Label-free and highly sensitive biomolecular detection using SERS and electrokinetic preconcentration,” *Lab Chip*, vol. 9, no. 23, pp. 3360–3363, 2009.
- [9] M. Park, Y. J. Oh, S. G. Park, S. B. Yang, and K. H. Jeong, “Electrokinetic preconcentration of small molecules within volumetric electromagnetic hotspots in surface enhanced Raman scattering,” *Small*, vol. 11, no. 21, pp. 2487–2492, 2015.
- [10] H. Anany, W. Chen, R. Pelton, and M. W. Griffiths, “Biocontrol of *Listeria monocytogenes* and *Escherichia coli* O157:H7 in meat by using phages immobilized on modified cellulose membranes,” *Appl. Environ. Microbiol.*, vol. 77, no. 18, pp. 6379–6387, 2011.
- [11] J. H. Han, M. S. Wang, J. Das, L. Sudheendra, E. Vonasek, N. Nitin, and I. M. Kennedy, “Capture and detection of T7 bacteriophages on a nanostructured interface,” *ACS Appl. Mater. Interfaces*, vol. 6, no. 7, pp. 4758–4765, 2014.
- [12] Z. Wang, D. Wang, J. Chen, D. A. Sela, and S. R. Nugen, “Development of a novel bacteriophage based biomagnetic separation method as an aid for sensitive detection of viable *Escherichia coli*,” *Analyst*, vol. 141, no. 3, pp. 1009–1016, 2016.
- [13] J. Chen, B. Duncan, Z. Wang, L.-S. Wang, V. M. Rotello, and S. R. Nugen, “Bacteriophage-based nanoprobe for rapid bacteria separation,” *Nanoscale*, vol. 7, no. 39, pp. 16230–16236, 2015.
- [14] S. Liébana, D. A. Spricigo, M. P. Cortés, J. Barbé, M. Llagostera, S. Alegret, and M. I. Pividori, “Phagomagnetic separation and electrochemical magnetogenosensing of pathogenic bacteria,” *Anal. Chem.*, vol. 85, no. 6, pp. 3079–3086, 2013.
- [15] Z. Wang, D. Wang, A. J. Kinchla, D. A. Sela, and S. R. Nugen, “Rapid screening of waterborne pathogens using phage-mediated separation coupled with real-time PCR detection,” *Anal. Bioanal. Chem.*, vol. 408, no. 15, pp. 4169–4178, 2016.

- [16] A. Martelet, G. Lhostis, M. C. Nevers, H. Volland, C. Junot, F. Becher, and B. H. Muller, "Phage amplification and immunomagnetic separation combined with targeted mass spectrometry for sensitive detection of viable bacteria in complex food matrices," *Anal. Chem.*, vol. 87, no. 11, pp. 5553–5560, 2015.
- [17] J. Homola, S. S. Yee, and G. Gauglitz, "Surface plasmon resonance sensors: review," *Sensors Actuators B Chem.*, vol. 54, no. 1–2, pp. 3–15, 1999.
- [18] M. El-Sherif, L. Bansal, and J. Yuan, "Fiber optic sensors for detection of toxic and biological threats," *Sensors*, vol. 7, no. 12, pp. 3100–3118, 2007.
- [19] C. C. Wu, W. C. Huang, and C. C. Hu, "An ultrasensitive label-free electrochemical impedimetric DNA biosensing chip integrated with a DC-biased AC electroosmotic vortex," *Sensors Actuators, B Chem.*, vol. 209, pp. 61–68, 2015.
- [20] A. Wokaun, H. P. Lutz, A. P. King, U. P. Wild, and R. R. Ernst, "Energy transfer in surface enhanced luminescence," *J. Chem. Phys.*, vol. 79, no. 1, pp. 509–514, 1983.
- [21] T. Neufeld, A. Schwartz-Mittelmann, D. Biran, E. Z. Ron, and J. Rishpon, "Combined phage typing and amperometric detection of released enzymatic activity for the specific identification and quantification of bacteria," *Anal. Chem.*, vol. 75, pp. 580–585, 2003.
- [22] N. Tawil, E. Sacher, R. Mandeville, and M. Meunier, "Surface plasmon resonance detection of *E. coli* and methicillin-resistant *S. aureus* using bacteriophages," *Biosens. Bioelectron.*, vol. 37, no. 1, pp. 24–29, 2012.
- [23] M. Smietana, W. J. Bock, P. Mikulic, A. Ng, R. Chinnappan, and M. Zourob, "Detection of bacteria using bacteriophages as recognition elements immobilized on long-period fiber gratings," *Opt. Express*, vol. 19, no. 9, p. 7971, 2011.
- [24] M. Janczuk, J. Niedziółka-Jönsson, and K. Szot-Karpińska, "Bacteriophages in electrochemistry: A review," *J. Electroanal. Chem.*, vol. 779, pp. 207–219, 2016.
- [25] J. L. Shenep and K. A. Mogan, "Kinetics of endotoxin release during antibiotic therapy for experimental gram-negative bacterial sepsis," *J. Infect. Dis.*, vol. 150, no. 3, pp. 380–388, 1984.



B. 510/19

F-B.510/19



5000000202584



Audaces fortuna iuvat

<http://rcin.org.pl>